UNIVERSITY OF CALIFORNIA, SAN DIEGO

Energy-resolved positron-molecule annihilation: Vibrational Feshbach resonances and bound states

A dissertation submitted in partial satisfaction of the requirements for the degree of Doctor of Philosophy in Physics

by

Levi Daniel Barnes

Committee in charge:

Clifford M. Surko, Chair
Lu Sham
Dmitri Basov
Charles Perrin
Robert Continetti

2005

The dissertation of Levi Daniel Barnes is approved and it is acceptable in quality and form for publication on microfilm.

_____

_____

_____

_____

_____

_____

Chairman

University of California, San Diego

2005

Contents

Signature Page . . . iii
Table of Contents . . . iv
List of Figures . . . viii
List of Tables . . . xi
Acknowledgments . . . xii
Vita, Publications and Fields of Study . . . xiii
Abstract . . . xvi

1 Introduction **1**
1.1 Early positron research . . . 1
1.2 Technological applications of positrons . . . 2
1.3 Interaction of positrons with gas phase atoms and molecules . . . 3
1.4 Outline of the dissertation . . . 4

2 Previous Positron Annihilation Measurements **7**
2.1 Challenges in measuring direct annihilation . . . 7
2.2 The meaning of Z_{eff} . . . 8
2.3 Early measurements of Z_{eff} . . . 8
2.4 Models of positron annihilation . . . 9
2.5 Further investigation of positron annihilation rates . . . 10
2.6 Measurements of Z_{eff} using Penning traps . . . 11
2.7 Fluorine substitution and its effect on Z_{eff} . . . 12
2.8 Doppler-broadening studies of positron annihilation . . . 14

3 Description of the Experiment **17**
3.1 Source and moderator . . . 19
3.2 Buffer gas trapping and cooling . . . 19
3.3 Positron beam production and characterization . . . 22
3.4 Test gas delivery and measurement . . . 26
3.5 Adjusting beam energy . . . 27

3.6 Radiation detection . . . 28
3.7 Reducing background counts . . . 29
3.8 Computation of Z_{eff} . . . 31
3.9 Verifications . . . 31
3.10 Error analysis . . . 32
3.10.1 Error in the magnitude of Z_{eff} . . . 32
3.10.2 Error in positron energy . . . 33

4 Vibrational Feshbach Resonances in the Z_{eff} Spectra for Alkane Molecules 35
4.1 Energy-resolved Z_{eff} for butane: an example of resonant enhancement of annihilation . . . 35
4.2 Comparison with capture resonances in electron scattering . . . 39
4.3 The Feshbach resonance picture for positron annihilation . . . 41
4.4 Feshbach resonance analysis of the butane spectrum . . . 42
4.5 Increasing binding energy for large alkanes . . . 46
4.6 Additional deuterated alkanes . . . 51
4.7 Shape of the CH stretch resonance peak . . . 53
4.8 Factors affecting the magnitude of resonance features in Z_{eff} . . . 55
4.8.1 Estimating Γ_{cap} . . . 56
4.9 Z_{eff} below 50 meV . . . 61
4.10 Effects of fluorine substitution on Z_{eff} . . . 63
4.10.1 Energy-resolved Z_{eff} spectra for fluoro-alkanes . . . 64
4.10.2 Doppler-broadening of annihilation radiation for fluoro-alkanes . . . 67
4.11 Effects of double and triple bonds on Z_{eff} . . . 67
4.12 Molecular isomers . . . 69
4.13 Z_{eff} for ring hydrocarbons . . . 69

5 Annihilation for Smaller Molecules 75
5.1 Z_{eff} for methane . . . 75
5.2 Z_{eff} at very low positron energy . . . 77
5.3 Fluoromethanes . . . 79
5.4 Ammonia . . . 81
5.5 Vibrational modes of the positron-molecule complex . . . 83
5.6 Z_{eff} at higher positron energies . . . 86
5.7 Z_{eff} for noble gases . . . 87

6 Progress in the Theory of Positron Annihilation on Molecules 89
6.1 Basic vibrational Feshbach resonance theory 89
6.2 Static calculations 90
6.2.1 Configuration interaction ground state calculations 90
6.2.2 Density functional models 92
6.2.3 Schwinger multichannel method 92
6.3 Incorporating nuclear motion 94
6.4 Direct annihilation near the positronium threshold 97

7 Additional Observations 101
7.1 Annihilation for very large alkanes–second positron bound state? 101
7.2 Incorporating positron escape by
de-excitation of thermally excited vibrations 104

8 Summary and Concluding Remarks 107
8.1 Summary of results 107
8.2 Future Work 108

References 112

List of Figures

2.1 Z_{eff} compared with Z for thermal positron distributions 13

3.1 Drawing of the positron source and moderator 18
3.2 Drawing of the buffer-gas trap 20
3.3 Extracting a beam of cold positrons 23
3.4 Analyzing the energy distribution of the positron beam 24
3.5 Drawing of gas region, detector and shielding 25
3.6 Detection efficiency of CsI detector 28

4.1 Z_{eff} for butane (C_4H_{10}) 36
4.2 Pressure dependence of the annihilation signal 37
4.3 Z_{eff} for butane-d_{10}(C_4D_{10}) 38
4.4 Feshbach resonance in dissociative attachment of CH_3I by electron impact 40
4.5 Potential energy space picture of a Feshbach resonance 43
4.6 Comparison of the Z_{eff} spectrum and vibrational modes for butane 45
4.7 Z_{eff} for the alkane molecules I 47
4.7 Z_{eff} for the alkane molecules II 48
4.7 Z_{eff} for the alkane molecules III 49
4.8 Positron affinity for the alkane molecules 50
4.9 Z_{eff} for nonane-d_{20} (C_9D_{20}) 52
4.10 Comparison of the shape of the resonance peaks for propane (C_3H_8) and heptane (C_7H_{16}) 54
4.11 Comparison of the Z_{eff} and IR absorption spectra for propane . 59
4.12 Comparison of energy-resolved Z_{eff} to Z_{eff} for thermal distributions of positrons 62
4.13 Z_{eff} for fluorohexane ($C_6H_{13}F$) and fluorononane ($C_9H_{19}F$) . . . 65
4.14 Infrared absorption spectra for hexane and 1-fluorohexane 66
4.15 Z_{eff} for ethane, ethylene and acetylene 68
4.16 Z_{eff} for 2-methylbutane (isopentane) and pentane 70

4.17 Z_{eff} for benzene (C_6H_6) and cyclohexane (C_6H_{12}) 71
4.18 Computed infrared spectrum for hexane, cyclohexane and benzene 73
4.19 Three-dimensional rendering of benzene, cyclohexane and hexane molecules 74

5.1 Z_{eff} for methane (CH_4) 76
5.2 Z_{eff} for methane (CH_4) and carbon tetrafluoride (CF_4) 78
5.3 Z_{eff} for fluorine-substituted methane molecules 80
5.4 Z_{eff} for ammonia (NH_3) 82
5.5 Z_{eff} spectrum for ethane (C_2H_6). 84
5.6 Z_{eff} and IR absorption for methyl fluoride (CH_3F) 85
5.7 Energy-resolved Z_{eff} for argon and xenon. 88

6.1 Density of vibrational modes in the alkanes 91
6.2 Z_{eff} for acetylene as a function of CH bond length (calculation) . 93
6.3 Z_{eff} for ethylene as a function incident positron energy (calculation) 95
6.4 Z_{eff} for Kr_2 (calculation) 96
6.5 Annihilation cross section near positronium threshold (calculation) 98

7.1 Z_{eff} for dodecane ($C_{12}H_{26}$) 102
7.2 Z_{eff} for tetradecane ($C_{14}H_{30}$) 103
7.3 Magnitude of resonances in alkanes compared with positron binding energy 105

List of Tables

4.1 Vibrational mode energies of butane 44
4.2 Thermal Z_{eff} for fluorinated hydrocarbons. 63

5.1 Z_{eff} for higher energy positrons 86

Acknowledgments

I would like to thank my advisor, Cliff Surko. As both a scientist and as a leader of people, he is an absolute marvel. His incisive scientific analysis, his love of discovery and his care for individuals has made this journey both challenging and enjoyable.

Steve Gilbert (and to a lesser degree Rod Greaves) gave me a running start in the form of a working positron trap and excellent scientific guidance. Effusive thanks, also, to the Gene Jerzewski, who assures me that when I'm his age, I'll know everything, too. By my calculation, he's earned about nine Ph.D.'s by now.

I always appreciated discussing experimental troubles and interpretation of results (and books and religion) with Joan Marler. Jason Young was a wonderful co-worker and has a brilliant career ahead.

I also acknowledge shared scientific wisdom on a variety of topics from Gleb Gribakin, Lu Sham, Jay Schrader, Bob Continetti, Steve Buckman, Jay Siegel and Koji Iwata (to whose dissertation I refer on an almost daily basis). Peter Langhoff and Jeff Mills were invaluable in guiding me through the wilderness of computational chemistry. Thanks also to Charles Perrin, John Crowell and Emmanuel Theodorakis for the use of their infrared spectrometry equipment.

Financial support of this work was provided by the Office of Naval Research and the U. S. National Science Foundation.

Finally, without my patient and supportive wife, Liberty Walther, neither graduate school, nor life to this point would have been the joy that they have been. What a blessing to have fallen in with such brilliant and big-hearted people. Thank you all.

Vita

June 19, 1975	Born, Provo, Utah, U. S. A..
2000	B.A., Physics, Brigham Young University.
2002	M.S., Physics, University of California, San Diego.
2005	Ph.D., Physics, University of California, San Diego.

Publications

ARTICLES

1. L. D. Barnes, J. P. Marler, J. P. Sullivan, and C. M. Surko "Positron Scattering and Annihilation Studies Using a Trap-Based Beam," *Physica Scripta*, **T110**, 280-5 (2004).

2. J. P. Marler, L. D. Barnes, S. J. Gilbert, J. P. Sullivan, J. A. Young, and C. M. Surko "Experimental Studies of the interaction of low-energy positrons with atoms and molecules," *Nuclear Instruments and Methods in Physics Research B*, **221**, 84 (2004).

3. L. D. Barnes, S. J. Gilbert, and C. M. Surko, "Energy-resolved positron annihilation for molecules," *Physical Review A* **67**, 032706 (2003).

4. S. J. Gilbert, L. D. Barnes, J. P. Sullivan, and C. M. Surko, "Vibrational-Resonance Enhancement of Positron Annihilation in Molecules," *Physical Review Letters* **88**, 043201 (2002).

5. J. P. Sullivan, S. J. Gilbert, J. P. Marler, L. D. Barnes, S. J. Buckman, and C. M. Surko, "Low energy scattering and annihilation studies using a high resolution trap-based beam," *Nuclear Instruments and Methods in Physics Research B* **192**, 3-16 (2002).

6. S. J. Gilbert, J. P. Sullivan, J. P. Marler, L. D. Barnes, P. Schmidt, S. J. Buckman, C. M. Surko, "Low energy positron-matter interactions using trap-based beams," *American Institute of Physics Conference Proceedings* **606**, 24-34 (2002).

INVITED TALKS

- Levi Barnes, "Energy-resolved positron annihilation studies of molecules - resonant annihilation and bound states," XII International Workshop on Positron and Positronium Physics, Sandbjerg, Denmark (2003).
- L. Barnes, "Energy-resolved Measurements of Positron Annihilation on Large Molecules," Joint Japan-US Workshop of Resonances in Physics, Chemistry and Biology, Hayama, Japan (2002).
- Levi Barnes, "Energy-resolved Measurement of Positron Annihilation on Large Molecules," 7th International Conference on Positron and Positronium Chemistry, Knoxville, Tennessee (2002).

Fields of Study

Major Field: Physics

Studies in Biophysics
Professor Herbert Levine

Studies in Group Theoretical Methods
Professor Aneesh Manohar

Studies in Electron Materials
Professor Francis Hellman

Studies in Nonlinear Dynamics
Professor Henry Abarbanel

Studies in Plasma Physics
Professor Vitaly Shapiro

ABSTRACT OF THE DISSERTATION

Energy-resolved positron-molecule annihilation: Vibrational Feshbach resonances and bound states

by

Levi Daniel Barnes

Doctor of Philosophy in Physics

University of California, San Diego, 2005

Professor Clifford M. Surko, Chair

This thesis describes a new technique for the measurement of positron annihilation rates for positrons incident on atoms and molecules. Positrons from a radioactive source are collected and cooled in a Penning-Malmberg trap and formed into a magnetically guided beam. The beam is then guided through a cell filled with the molecule to be studied while the gamma ray signal from annihilation events is recorded. As distinguished from previous work, these experiments allow tuning of the positron energy over the range between 50 meV and the threshold for positronium formation. The energy resolution of the beam is 25 meV. A key result in these measurements is the discovery of resonances in the annihilation rates for selected molecules, associated with the vibrations of the target. We attribute these resonances (in accordance with a model proposed by Gribakin [28]) to the presence of a Feshbach resonant state consisting of a positron bound to a vibrationally excited target molecule. The annihilation spectra for a number of molecules are presented including alkane molecules, fluoroalkanes, deuterated alkanes, ring hydrocarbons, noble gases, alkenes and alkynes. The goals of these measurements are to investigate the dependence of these resonant processes on the size, composition and shape of the target molecules, and to provide benchmarks for theoretical descriptions of this process.

Chapter 1

Introduction

The positron, the anti-particle of the ubiquitous electron, is becoming more widely used in laboratories, hospitals and industrial research facilities. Positrons have contributed greatly to medical technologies, surface studies of condensed matter and interpretation of astrophysical gamma-ray spectra [71]. Also, as the most available form of anti-matter, positrons are important in the search for answers to some of the most fundamental questions in physics.

The development of new techniques for creating and manipulating positron beams have expanded the availability of positrons in the laboratory and enabled fruitful study of the scattering of positrons from ordinary matter.

1.1 Early positron research

In 1930, P. A. M. Dirac sought a Lorentz invariant formulation of electron dynamics. Among the results of his analysis was a prediction of the existence of an "anti-electron." This new particle was to have a charge of +e and so Dirac assumed it was a proton [13]. The theory also predicted that an electron and anti-electron could annihilate one another, converting their mass into the energy of photons [14]. For an electron-antielectron pair in an antisymmetric spin state, the decay is dominated by two-photon emission. In the symmetric spin state, two-photon emission is forbidden by conservation of spin angular momentum and three-photon emission is dominant.

Dirac's antielectron was first observed by C. D. Anderson in 1932 [2, 3] in the cloud-chamber tracks of cosmic radiation. Anderson noticed a particle with charge opposite the electron but lighter than either of the known positive particles at the time, the proton and the alpha particle. Subsequent experiments confirmed that this was the anti-electron predicted by Dirac. It was Anderson

who gave the positron its name.

1.2 Technological applications of positrons

Today, several areas of science and technology take advantage of the uniqueness of positrons. The most well known application is Positron Emission Tomography (PET). PET is a common medical imaging technique which involves tagging of a sample with a positron emitter, commonly ^{19}F. The sample can then be given to a patient orally or intravenously and tracked as it moves through the body by detecting the radiation from the annihilation of emitted positrons. By tagging a glucose sample, PET can be used to investigate the metabolism of sugars in the brain.

Positrons have also recently become important in material science for measuring both defect fraction and porosity of manufactured materials [48, 79]. The presence of lattice defects or large pores in a metal increases the lifetime of positrons in the bulk of the material. Positrons can therefore be useful in producing low dielectric constant materials or ultra-pure metals both of which are important in microchip fabrication.

Positrons are also of particular interest in studying the surfaces of materials. For example, the lifetime of positrons in silicon is highly sensitive to the thickness of a gold surface layer [47]. Two factors contribute to this increased sensitivity compared with similar electron experiments. First, positrons with very low kinetic energy can create holes in the electron valence band since the mechanism for hole creation is annihilation instead of ionization. Annihilation can occur at any energy while ionization or electron-hole pair creation each have an energy threshold. A lower initial kinetic energy allows the positrons to thermalize closer to the surface of the material making positrons a sensitive probe of surface effects [84].

On another level, positrons can become trapped in a shallow surface state between the repulsive bulk metal and the attractive image potential. Positrons in these states are extraordinarily sensitive to the composition of the very top layer of the metal [60].

As positron sources improve and positrons become more readily available, they may find use in many more areas. Since the bound state of a positron and an electron, called positronium, is much lighter than atoms, it may be useful in matter interferometry or Bose-Einstein condensates. Also, pair annihilation may one day be an important source of gamma-ray radiation for gamma-ray lasers [61].

In the near future, positron studies may provide an important test of fundamental theories. Already, the prediction of the lifetime of positronium has been an impressive achievement of quantum electrodynamics [22]. In the future, the optical spectroscopy of anti-hydrogen, the bound state of the positron and antiproton, is expected to provide a sensitive test of CPT invariance, an important feature of the Standard Model as well as many other field theories.

1.3 Interaction of positrons with gas phase atoms and molecules

Positrons can interact in several ways with atoms and molecules in the gas phase. As in electron scattering, positrons can cause electronic, vibrational or rotational excitations of target atoms and molecules or collide elastically leaving the target in its original electronic and vibrational state. The cross sections for these processes are typically measured as in electron scattering experiments, although the challenges involved in building a high-flux positron source are considerable.

Beyond those processes which have an analog in electron scattering, positron scattering can involve two additional channels. The positron can annihilate one of the electrons in the target, changing the charge of the target by +e and emitting either two or three gamma-ray photons.

$$A + e^+ \longrightarrow A^+ + 2\gamma \ (3\gamma) \tag{1.1}$$

This process is called direct annihilation. It is dominated by two-photon decay since the target typically contains electrons of several spin orientations and the rate of two-photon decay is much faster than the three-photon rate. Direct annihilation is allowed at all energies.

The other process unique to positron scattering is the formation of a positron-electron bound state. This state is called positronium, represented by Ps. Positronium atoms have different properties depending on the spin state of the electron and positron. A Ps atom with positron and electron in a symmetric spin state is called ortho-positronium (o-Ps). It decays into three photons of combined energy 1.022 MeV. The lifetime for this process is 142.0 ns. Para-positronium (p-Ps) with the positron and electron in an antisymmetric spin state decays into two 511 keV photons with a much shorter lifetime of 125.1 ps. The process of p-Ps (o-Ps) formation can be written in this way:

$$A + e^+ \longrightarrow A^+ + \text{p-Ps (o-Ps)} \longrightarrow A^+ + 2\gamma(3\gamma). \tag{1.2}$$

Because Ps formation involves ionization of the target, it is not allowed for all positron energies in all targets. Since the binding energy of positronium is 6.8

eV, the condition on the incident positron energy, ϵ, for formation of Ps is

$$\epsilon > E_i - 6.8\text{eV}. \tag{1.3}$$

where E_i is the ionization energy of the target. For targets with ionization energy greater than 6.8 eV, Ps formation is forbidden for positrons with energy less than the threshold.

In all positron-matter interactions, there are some fundamental differences from electron-matter interactions. Since the positron is distinguishable from the electrons in various targets, the full wave function is not required to be antisymmetric with respect to exchange of the positron and the target electrons. In some computational approaches, this eliminates the exchange interaction between the positron and the target.

Additionally, because both the positron and the target electrons have very small mass compared with the target nuclei, it is possible to form short-lived, highly correlated positron-electron states even below the threshold for positronium formation. This is often referred to as "virtual positronium" formation and can have a large effect on positron scattering from all types of matter.

Positrons thus present a great challenge to our theoretical understanding of atomic and molecular scattering and interact with matter in different and often useful ways.

1.4 Outline of the dissertation

Chapter 2 will discuss previous measurements of the rate of direct annihilation for positrons incident on gas phase targets below the positronium formation threshold. These results pointed to interesting trends in the annihilation rates for different molecules. However, many theoretical explanations of these trends predicted features in the annihilation rate that would be masked by the broad distribution of positron energies typical of positron annihilation measurements.

Improvements in positron sources and a new technique for collecting and cooling positrons have increased energy resolution and allowed positron energy to be tuned from 0.05 V to 90 V. This thesis presents the first successful measurement of direct annihilation resolved as a function of incident positron energy. These experiments establish the existence of vibrational Feshbach resonances (VFRs) in the energy-resolved annihilation rates for some molecules. We have used a tunable positron beam to investigate these resonances in a variety of molecules.

Chapter 3 discusses the specifics of the apparatus that we use to make measurements of annihilation rate as a function of incident positron energy. We

use positrons collected and cooled in a Penning trap to generate a cold positron beam and record annihilation events as the beam interacts with various test gases.

Chapter 4 presents and discusses the annihilation rates for alkanes resolved as a function of incident positron energy. Much of this dissertation will focus on resonances in these energy-resolved spectra. These resonances are due to temporary trapping of positrons into quasi-bound states. These resonances are the first experimental evidence of positrons binding to individual molecules.

Chapter 5 presents and discusses annihilation rates for smaller molecules. Resonances of the type introduced in Chap. 4 are less prevalent in these smaller molecules. This gives us opportunities to examine energy-resolved annihilation in the absence of resonances. This chapter also presents annihilation data for noble gases.

Chapter 6 reviews some of the theory of positron annihilation. Much progress has been made recently, but matching theory with experiment remains challenging.

Chapter 7 presents a few more speculative hypotheses about positron annihilation. And finally, Chapter 8 draws some conclusions about the present state of low-energy positron annihilation measurement and points to some future directions for research in this area.

Chapter 2

Previous Positron Annihilation Measurements

Unexpectedly large annihilation rates for some molecules were first observed in the 1950's and 60's by Deutsch [12] and by Paul and Saint-Pierre [70]. These large rate were studied subsequently by many authors [35, 41, 42, 44, 56, 77, 81] leading up to the present. Mainly due to experimental limitations, the mechanism behind these large rates has remained unexplained for nearly four decades. However, previous experiments helped establish important chemical and energetic trends in annihilation rates. Also, several theoretical models of positron-molecule interactions have been forwarded and were important in motivating the work in this thesis.

2.1 Challenges in measuring direct annihilation

Since both positronium formation and direct annihilation end in the same products (an ionized target and γ-ray photons) they can be difficult to distinguish experimentally. Positronium formation cross sections are typically on the order of the cross sections for elastic and inelastic processes while cross sections for direct annihilation are several orders of magnitude smaller. For example, for Argon the positronium formation cross-section is $\sim 1a_0^2$ where a_0 is the bohr radius, while the direct annihilation cross section is $\sim 10^{-5}a_0^2$. For this reason, above the threshold for positronium formation, it is difficult to measure direct annihilation.

Below the threshold for positronium formation, direct annihilation is the only allowed process which produces either ions or gamma radiation and so it can be measured more easily. However, in low-pressure experiments the probability of

direct annihilation is very small. To compensate, the target pressure can be increased, but this leads to a dominance of other scattering processes and to rapid thermalization of the positrons with the test gas itself. Historically, test gas pressures were sufficiently high that positrons were in thermal equilibrium with the target gas.

2.2 The meaning of Z_{eff}

The rate of direct annihilation of positrons with matter has historically been expressed in terms of the dimensionless parameter, Z_{eff}. Z_{eff} is the time annihilation rate normalized to the rate for a free electron gas defined by [20]

$$Z_{\mathit{eff}} \equiv \frac{\Gamma}{\pi r_0^2 c n_m}, \tag{2.1}$$

where Γ is the annihilation rate for positrons in a gas of number density n_m, r_0 is the classical electron radius, and c is the speed of light. The Dirac annihilation rate for positrons in a free electron gas of density n_e is $\Gamma_{FE} = \pi r_0^2 c n_e$ [13]. If the correlations between positrons and molecular electrons are weak, Z_{eff} is expected to be close to Z, the actual number of electrons per molecule. Defined in this way, Z_{eff} can be thought of as the effective number of electrons per molecule participating in the interaction assuming negligible electron-positron correlation (as in a free electron gas). Even for cases in which electron-positron correlations are large, the notation is retained for historic reasons.

2.3 Early measurements of Z_{eff}

In the 1950's and 60's positron annihilation rates were measured by introducing positrons from a radioactive source into a high density ($\sim$ 100 torr) molecular gas and measuring the annihilation lifetime. In these experiments, the time between the emission of the positron (as determined, for example, by the detection of the accompanying 1.28 MeV γ photon) and the annihilation of the positron (determined by the detection of the 511 keV annihilation photon) was recorded for several thousand events. Positrons that annihilated quickly before reaching thermal equilibrium with the test gas were ignored. The decay rate of thermal positrons can be deduced by fitting the lifetime data to an exponential decay curve and Z_{eff} can be calculated using equation 2.1.

Studies of this type were performed with oxygen, helium, nitrogen, methane and freon by Deutsch and collaborators [11,12,75]. Oxygen, helium and nitrogen fit exhibit annihilation rates close to that expected for a free electron gas of the

same electron density ($Z_{eff} \simeq Z$). In the case of methane, these measurements indicated annihilation rates a factor of two or three larger than the expected rate for the free electron gas ($Z_{eff}/Z \simeq 3$). These enhancements were attributed to the attraction of the positron due to polarization of the neutral molecules. A much larger annihilation rate was noticed for freon (CCl_2F_2). The freon rate was attributed to a large "positron attachment coefficient," the mechanism behind which was not explained.

In similar experiments a few years later, Paul and Saint-Pierre found that the annihilation rates for hydrocarbon molecules such as propane (C_3H_8) and n-butane (C_4H_{10}) were 20 to 200 times larger than the expected free electron rate, indicating very strong electron-positron correlations [70]. In addition, they noticed a rapid increase in the annihilation rate as a function of molecular size. They and others proposed the formation of positron-molecular ions to explain these findings [24, 70, 77].

2.4 Models of positron annihilation

Accepting the Dirac model of pair annihilation, the annihilation parameter, Z_{eff}, for a system is exactly the overlap of the positron and electron wave-functions given by

$$Z_{eff} = \sum_{i=1}^{n} \int \Psi(\mathbf{r}_1, \mathbf{r}_2, ...\mathbf{r}_n, \mathbf{r}_p)\Psi^*(\mathbf{r}_1, \mathbf{r}_2, ...\mathbf{r}_n, \mathbf{r}_p)\delta(\mathbf{r}_i - \mathbf{r}_p)\mathbf{dr}_1\mathbf{dr}_2...\mathbf{dr}_n\mathbf{dr}_p \tag{2.2}$$

for an n-electron system where $\mathbf{r_i}$ are the electron positions, $\mathbf{r_p}$ is the position of the positron, $\delta(\mathbf{r})$ is the Dirac delta function, and $\Psi(\mathbf{r}_1, \mathbf{r}_2, ...\mathbf{r}_n, \mathbf{r}_p)$ is the ground state solution (with appropriate scattering boundary conditions) of the Schrödinger equation incorporating the Coulomb interactions of all particles. Explanations of the large annihilation rates have focussed on models which lead to unusually high overlap of positron and electron wave functions.

Several theoretical models were proposed to account for this increased overlap. Paul and Saint-Pierre suggested the formation of positron-molecular ions was responsible for the large observed values of Z_{eff}. However, they did not discuss a mechanism for the trapping of free positrons into such a state [70]. Later, Smith and Paul [77] made the suggestion that the positron-molecular ions were formed in vibrationally or rotationally excited states which were unstable to reemission of the positron. Expansions on this concept were proposed involving stabilization of positron-molecular ions by collisions with other molecules [6, 59] and the formation of bound states between positrons and clusters of several

target molecules [59].

Goldanskii and Sayasov were the first to propose that an increased positron-electron overlap might be due to quasi-stable positron-target states with energy very close to zero [24]. Such states are predicted to enhance annihilation rates by two or three orders of magnitude over the Dirac rate for positrons of very low energy. Surko *et al.* invoked this idea to explain large annihilation rates for alkanes in 1988 [81]. This idea has been expanded on recently by Gribakin [28]. Aspects of this model and a comparison with present data will be discussed in Chap. 5.

Finally, it has been proposed that the large annihilation rates could be explained by the temporary formation of positronium atoms bound to the target molecules [50]. Since, in the case of most target molecules for which measurements have been made, positrons do not have enough energy to form free positronium, these states are limited in lifetime by the uncertainty principle. For this reason, this type of highly correlated positron-electron state is referred to as "virtual positronium." Section 6.4 discusses this and other models of positron annihilation near the threshold for positronium.

Although not directly applicable to Z_{eff} for molecules, calculations of positron interactions with atoms provide useful insights. Recent calculations by Dzuba *et al.* suggested that alkaline earth metals such as Mg, Zn, Cd and Hg could stably bind positrons [16]. Ryzhikh and Mitroy rigorously investigated bound states for a positron and a lithium atom [72]. Their model predicted bound positron-atom complexes with binding energies on the order of 60 meV. Subsequent calculations also predicted positron binding to Be, Na, Mg, Ca, Cu, Zn, Ag and Cd (see ref [64] for a review). In these cases, the positron wave function is either a nebulous and extended cloud far outside the electron density or, for easily ionized targets, a Ps atom bound to a positive ion by polarization of the Ps [64].

Further discussion of the current state of low energy positron annihilation theory follows in Chap. 6.

2.5 Further investigation of positron annihilation rates

Following the early measurements by Shearer and Deutsch, Paul and Saint-Pierre and others, a number of experiments were performed to quantify the dependence of Z_{eff} on pressure and positron energy. In order to investigate the dependence of annihilation rates on positron energy, measurements were made for varying test gas temperatures and for positrons under the influence of a static electric field of varying magnitude [10, 34, 59]. For targets with weak or absent

inelastic scattering at low positron energies, the addition of an electric field spreads the energy of positrons upward. An increase in temperature does the same by increasing the temperature of the Maxwellian distribution of positron energies.

The annihilation rate was found, almost invariably, to decrease with increasing electric field or temperature [10, 56], lending credibility to theories involving enhancements for positrons with very low energy.

Measurements of the dependence of Z_{eff} on test gas pressure were suggestive of three-body effects [59]. However, it has long been clear that, even in situations where the interactions are exclusively two-body, the annihilation rates for many molecules are unusually large.

2.6 Measurements of Z_{eff} using Penning traps

More recent experiments measured Z_{eff} by introducing low pressure ($\sim 10^{-7}$ torr) gases into thermal positrons in a Penning-Malmberg magnetic trap [41, 43, 49, 66, 81]. The annihilation parameter, Z_{eff}, can be deduced from the decay rate of the annihilation signal. This scheme requires the trapping and cooling of large numbers of positrons ($\sim 10^6$), but has several advantages over previous high pressure experiments. The low test gas pressure in these trapped positron experiments effectively eliminates the possibility of three-body interactions. Also, this new setup enabled the study of gases with much larger values of Z_{eff}. In previous experiments, for gases with very large values of Z_{eff}, the majority of the positrons were lost before thermalization. In the trap experiment, the test-gas pressure could be adjusted to, in turn, adjust the positron lifetime to a conveniently measurable level.

Experiments using the magnetic traps established several important facts about positron annihilation on molecules. For example, these measurements determined that large annihilation rates are observed even when interaction of the positron with two or more target molecules is precluded. Mechanisms which depend on three-body interactions, such as collisional stabilization of positron-molecule complexes and positron binding to clusters of target molecules, while not eliminated from the discussion, were shown to be unnecessary in explaining large annihilation rates at low test-gas pressures.

The advent of the magnetic positron trap also dramatically expanded the range of molecules which could be studied. A systematic study was made of the effects of dipole moment, polarizability, ionization energy and other parameters on Z_{eff} for a variety of carbon-based molecules [66]. The molecules studied

included ring molecules, double- and triple-bonded hydrocarbons and halogen-substituted hydrocarbons.

One important result of these studies was the dependence of the thermal Z_{eff} on ionization energy. This dependence is described by this equation

$$\ln(Z_{eff}) \approx \frac{A}{E_i - 6.8 \text{ eV}} + B. \tag{2.3}$$

In this expression, E_i is the ionization energy of the target and A and B are constants independent of the target. This relation holds remarkably well for the diatomic molecules (except O_2), the noble gases, the alkanes and the substituted alkanes, although it fits poorly with the data for ring molecules or molecules with double or triple bonds. The mechanism behind this dependence is unclear, but a model which reproduces this dependence will be discussed in Chap. 6.

Also in the studies of Z_{eff} using magnetic positron traps, it was also concluded that ring hydrocarbons have smaller values of Z_{eff} than linear hydrocarbons of comparable size and that full halogen substitution in hydrocarbons also reduces Z_{eff} compared with the analogous hydrogenated compounds. For the molecules studied, dipole moment and polarizability showed poor correlations with Z_{eff} [66].

The trapped-positron technique was used to study the dependence of the annihilation rate on positron temperature [44, 49]. Trapped positrons were heated using broadband RF noise applied to one of the confinement electrodes. Then, the test gas was introduced and the decay rate of positrons was measured as discussed above. For methane (CH_4), deuteromethane (CD_4) and butane (C_4H_{10}) the annihilation rate was found to depend on temperature, T, approximately as [44]

$$Z_{eff} \propto \frac{1}{\sqrt{T}}, \tag{2.4}$$

which is consistent with a theory that predicts a $1/k$ dependence of Z_{eff} at lower energies (where k is the positron wave number) [28]. At higher temperatures, the temperature dependence of annihilation is much weaker [44].

2.7 Fluorine substitution and its effect on Z_{eff}

Studies of the effect of halogen-substitutions in hydrocarbons gave perplexing results. As shown in Fig. 2.1, the alkanes (linear hydrocarbons with the chemical formula C_nH_{2n+2}) have very large values of Z_{eff}/Z, meaning that electron-positron correlations are very strong. Also, Z_{eff} increases very rapidly with molecular size. The alkenes (i. e., alkanes with some double carbon-carbon bonds) show

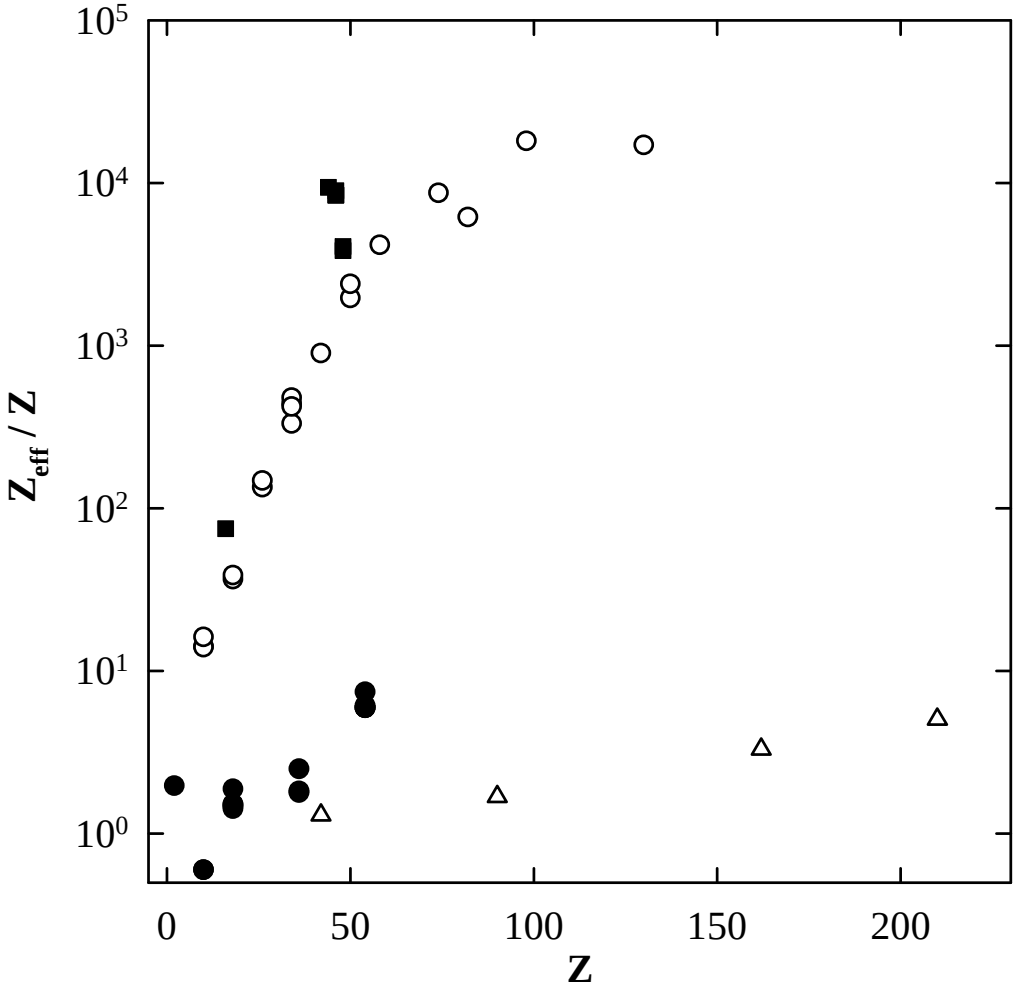

Figure 2.1: The annihilation parameter, Z_{eff}, measured using thermal distributions of positrons as a function of Z, the actual number of electrons. Data is shown for the alkanes (○), the alkenes (■), the noble gases (●) and the perfluorinated alkanes (△). This figure was previously published by Iwata in ref. [39].

a similar pattern. By contrast, for the noble gases, Z_{eff}/Z is only moderately larger than unity. Most surprisingly, the perfluorinated alkanes (i. e. alkanes with all hydrogen atoms replaced with fluorine atoms with the chemical formulae C_nF_{2n+2}) have some of the lowest Z_{eff}/Z values measured.

Later experiments by Iwata *et al.* [41,44] with partially-fluorinated hydrocarbons revealed some general patterns in the effect of fluorine substitution on Z_{eff} for hydrocarbons. The substitution of one fluorine atom for a hydrogen atom in hydrocarbons typically increases Z_{eff} often quite dramatically. This is true in the case of methyl fluoride (CH_3F), fluoroethane (C_2H_5F), 1-fluorohexane ($C_6H_{13}F$) and fluorobenzene (C_6H_5F). This increase in Z_{eff} can be as large as a factor of 10, as in methane, or as small as a factor of two, as in hexane. The effect is typically less dramatic for larger molecules.

Further fluorine substitution reduces Z_{eff} compared with the singly fluorinated molecule. Each additional substitution causes Z_{eff} to decrease further. As mentioned, fully fluorinated molecules have a smaller Z_{eff} than their hydrogenated counterparts for all molecules studied.

One explanation of this behavior was propsed by Gribakin [28]. He postulated that the large Z_{eff} for the fluoromethanes is caused by coupling to a virtual or bound state with energy very close to zero, similar to the enhancement proposed by Goldanskii and Sayasov [24]. If methane is assumed to have a bound state with a positron, the observed behavior could then be explained by an increase in the energy of the bound state with fluorine substitution. One fluorine substitution increases the energy of the state, moving it closer to zero. Further substitution, however, moves the state beyond and away from zero. The comparison of this theory with more recent experimental results will be discussed in Chap. 5.

2.8 Doppler-broadening studies of positron annihilation

Following an annihilation event, the distribution of energy of the annihilation photons gives information about the states of the particles before annihilation. In the rest frame of the positron-electron pair, two photons are emitted each with 511 keV. If the pair have momentum in the lab frame, the energies of these photons, as measured by the detector, are Doppler shifted.

Experiments at the University of California-San Diego used the doppler-broadened annihilation radiation spectrum from positrons interacting with gaseous molecules to obtain information about the momentum of annihilating pairs

[43,83]. In these experiments, positrons were trapped and cooled in a buffer-gas Penning trap before low-pressure test gas was introduced as described above. To measure the Doppler width of the annihilation radiation, the gamma-ray signal was measured using a high-purity liquid-nitrogen-cooled germanium detector which responds to gamma radiation with pulses of visible light the size of which vary with the energy of the gamma photon.

For the positron energies considered, the Doppler width of the annihilation radiation is dominated by the momentum of the electron being annihilated. Since electrons occupying different molecular orbitals generally have very different momenta, the Doppler width can be used to determine which molecular electron orbitals are responsible for the annihilation events or equivalently, which orbitals have the most overlap with the positron wave function.

A simple analysis of this data led to several important conclusions. The first is that, for low energy positrons, annihilation occurs primarily with valence electrons [45]. This seems reasonable since the electrostatic repulsion of the nuclei is expected to become very strong as positrons penetrate the electron cloud.

Further, these Doppler-broadening studies indicate that annihilation occurs with roughly equal probability on all valence electrons. This is established by observing the changes in the width of the annihilation radiation for molecules with subtle chemical differences. In one case, the hydrogens in an alkane molecule were gradually substituted with fluorine. Since electrons attached to a fluorine atom have a larger average momentum than those attached to hydrogen, the Doppler width is expected to increase. The evidence that all valence electrons are involved approximately equally comes from observing that the Doppler width increases linearly as a function of the fraction of valence electrons attached primarily to a fluorine [45]. Similar observations were made concerning electrons attached to carbon and hydrogen atoms for the alkane molecules.

All of the experiments described in this chapter used positrons in thermal equilibrium with either the test gas or, as in the case of the magnetic trap based experiments, with another background gas. The dependence of the annihilation rate on positron energy could be investigated only by increasing the temperature of the gas or by the introduction of an electric field. The next chapter will describe a method for measuring Z_{eff} resolved as a function of positron energy which is the key experimental technique for the results presented in this thesis.

Chapter 3

Description of the Experiment

Prior to the experiments in this thesis, positron experiments were performed with positrons in thermal equilibrium either with the test gas itself or with a surface by radiative exchange. The thermal spread of positron energies in these experiments masks many effects key to our understanding of positron annihilation rates.

Positron beam production based on a buffer gas trap like the one in the experiments in this thesis has advantages over other methods both in positron flux and in energy-resolution. This enables studies of positrons interacting with low pressure gases and allows the energy of the positrons to be tuned independent of the test gas temperature. This thesis presents the first successful measurement of direct annihilation resolved as a function of incident positron energy.

The data presented here was taken using a beam extracted from a three-stage nitrogen buffer gas trap. This setup uses a ^{22}Na source with a solid neon moderator. Positrons from the moderator are collected in a three-stage Penning-Malmberg trap by interaction with a molecular nitrogen buffer gas. The positrons are then pushed out of the trap and guided through a test gas region. A cesium iodide detector and associated electronics detect radiation from single annihilation events.

The apparatus described here produces pulses of $\sim 4 \times 10^4$ positrons at a repetition rate of 3 Hz. The energy spread of the positrons is ~ 25 meV, and the mean energy is tunable from 50 meV to several tens of eV. The annihilation apparatus has measured values of Z_{eff} from 10 to 10^7. For the work presented here, the positron energy is kept below the threshold for positronium formation.

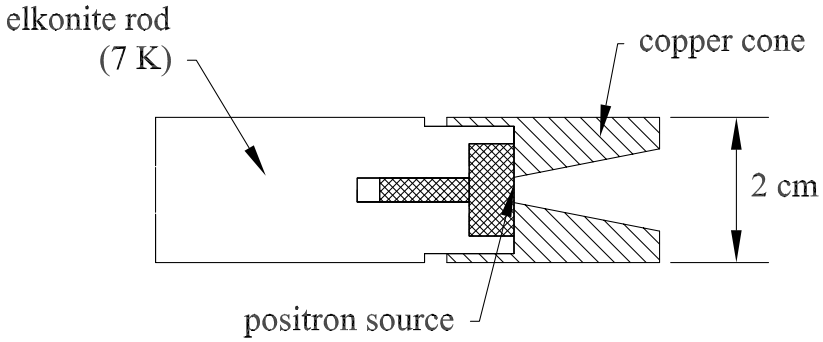

Figure 3.1: Diagram of the positron source and moderator cone. Positrons from the source impinge on a layer of neon grown on the cold cone. They thermalize with the neon and are reemitted with much lower energy.

3.1 Source and moderator

The positrons originate from a ^{22}Na source. Positrons are emitted from ^{22}Na in the reaction

$$^{22}\mathrm{Na} \longrightarrow ^{22}\mathrm{Ne} + \beta^+ + \nu_e + \gamma \tag{3.1}$$

with a branching ratio of 90.5%. The half-life for this process is 2.6 years. The simultaneously emitted 1.28 MeV photon (γ) can be used as a start pulse for positron lifetime measurements. The long half-life of ^{22}Na allows the system to run for years without replacement or replenishment of the radioactive source.

The source for these experiments was purchased from DuPont Pharma. At the time of purchase in 1997, the activity was measured to be 150 mCi. During the time of the experiments in this thesis (2000-2004), the activity fell from 70 to 25 mCi. The source is mounted to an elkonite rod of length 10 cm for radiation shielding and surrounded by a copper cone. This is shown in Fig. 3.1. The elkonite rod is attached to the second stage of a two-stage He refrigerator which maintains a temperature of about 7 K.

A film of solid neon can be grown on the copper cone by exposing the vacuum system to low pressures (10^{-4} torr) of neon for several hours. The neon is then evacuated. The neon crystal serves to slow the highly energetic (10-500 keV) positrons from the source to energies of a few electron Volts. On entering the Ne crystal, positrons thermalize with the material first by ionization or electron-hole pair production, then by phonon production. Since solid neon has a negative positron work function, thermalized positrons that diffuse to the surface can be emitted into the vacuum with energies of a few electron Volts [62].

Rare gas moderators convert fast positron to slow positrons with much greater efficiency (2.6×10^{-2}) than metal moderators such as tungsten (10^{-4}). Rare gas moderators have the disadvantage of a broader distribution of emission energies (1 eV compared with 0.6 eV for tungsten) [25]. For a trap-based beam like the one used for these experiments, the width at this level is unimportant since the positrons will be trapped and undergo a second cooling phase. The moderator and source at the time of the experiments described here produced between one and two million slow positrons per second. The rare gas moderator was discovered by Mills and Gullikson [62] and the technique used in these experiments was developed by Greaves and Surko [25].

3.2 Buffer gas trapping and cooling

The collection and cooling of positrons for these experiments was done using the nitrogen buffer gas trapping scheme developed by C. M. Surko and coworkers

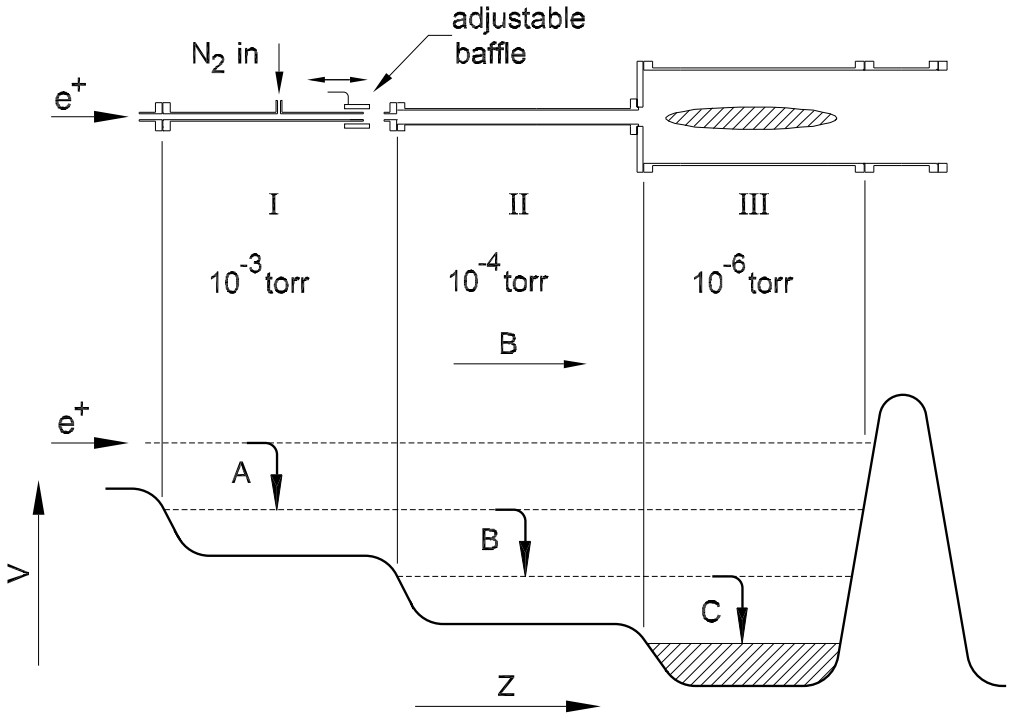

Figure 3.2: (above) Schematic diagram of the electrodes in the three-stage buffer-gas trap used in the experiments. Differential pumping from both ends of the electrodes maintains the nitrogen pressures indicated. (below) The electrostatic potential profile due to biases on the electrodes. Steps A, B and C indicate loss of energy by collision with the buffer gas.

[80]. Positrons from the source and moderator described in Sec. 3.1 are guided magnetically into a set of cylindrically symmetric electrodes shown in Fig. 3.2. A constant axial magnetic field of approximately 1.5 kGauss confines the positrons radially into cyclotron orbits of radius 3 μm.

For axial confinement, the electrodes at the top of Fig. 3.2 are individually biased to create the electrostatic potential profile shown at the bottom of the figure. The potential steps between the three stages can be varied to optimize trapping but are of order 10 eV in magnitude. Positrons with insufficient energy to surmount the potential barriers at each end of the trap are confined with lifetimes on the order of minutes.

Positrons from the source are loaded into the trap by interaction with a nitrogen buffer gas. A steady pressure of nitrogen is introduced through an inlet in the first electrode. Cryogenic pumps on either side of the electrode structure serve both to limit leakage of nitrogen into other parts of the system and to create the varying pressures indicated in Fig. 3.2. A lower pressure of carbon tetrafluoride (CF_4) is introduced into the third stage of the trap (III) for more rapid cooling [26].

In such a system, positrons enter the trap region with energy of about 30 eV relative to the potential in stage III which is sufficient to pass through the potential barrier on the inlet side of the trap. In trap stage I, the positrons inelastically collide with the nitrogen ("A") and lose sufficient energy to become trapped between the potential walls at either end of the trap. The bias on the electrode surrounding stage I sets the kinetic energy of the positrons in that region so as to maximize the probability of interaction with the nitrogen. By subsequent collisions with the nitrogen ("B" and "C"), the positrons become trapped in the third stage of the trap. The nitrogen pressure in this stage is smallest to allow long confinement time. Positrons are allowed to accumulate in this way for between 0.1 and 0.4 seconds.

Following the accumulation phase, the bias on the electrodes surrounding trap stages I and II are increased to prevent positrons from the source and moderator from entering stage III. Positrons already in stage III are allowed to fully thermalize with the nitrogen and carbon tetrafluoride. Positrons cool in this way for 0.1 seconds during which time they come into thermal equilibrium with the walls of the vacuum chamber.

This method for trapping and cooling of positrons accumulates approximately 40,000 positrons in 0.3 seconds including cooling time. The system is fully automated to run without supervision.

3.3 Positron beam production and characterization

From this reservoir of room temperature positrons, a positron beam can be extracted for use in a variety of positron scattering experiments [78]. The beam is produced by increasing the potential of the electrode in the accumulator as shown in Fig. 3.3. This increases the total energy of the positrons in the reservoir. The potential is raised on a time scale much longer than the transit time for positrons in the reservoir so that positrons leave the trap as soon as they have enough energy to surmount the potential barrier on the far side. The difference between the barrier potential and the potential in the rest of the apparatus determines the kinetic energy of the beam. This energy can be adjusted from about 0.05 eV to 90 eV.

The positrons in this beam are confined radially by an axial magnetic field. This field is sufficient to effectively confine the room temperature positrons to the magnetic field lines. The energy distribution of positrons in the beam can be measured using the retarding potential analyzer (RPA) shown in Fig. 3.3. The positrons are guided into a cylindrical electrode (the RPA), the bias on which can be varied. Positrons that have enough velocity in the axial direction to pass through the electrode continue along the magnetic field lines and strike a metal collector on the other side of the RPA. The radiation from the positrons annihilating with electrons in the collector can be measured with a sodium iodide scintillator and photomultiplier tube. The intensity of radiation detected gives a measure of the number of positrons with energy in the axial direction greater than the bias on the electrode. Repeating this measurement for varying RPA potential gives a curve similar to that in Fig. 3.4. The derivative of this curve provides a measure of the energy distribution of the positrons in the beam. For the data in this thesis, the width of the energy distribution is 25-35 meV (full width at half maximum).

The total number of positrons in a pulse is measured using a charge-sensitive amplifier attached to the collector. This amplifier was calibrated by applying a known voltage to a capacitor of precisely known capacitance, then using the amplifier to measure the charge on the capacitor. To eliminate effects from the capacitive coupling of the collector to other changing potentials, the amplifier is used to measure the charge delivered to the collector with the positrons blocked at the source and this signal is subtracted. This pickup was typically 3 orders of magnitude smaller than the signal from the positron pulse.

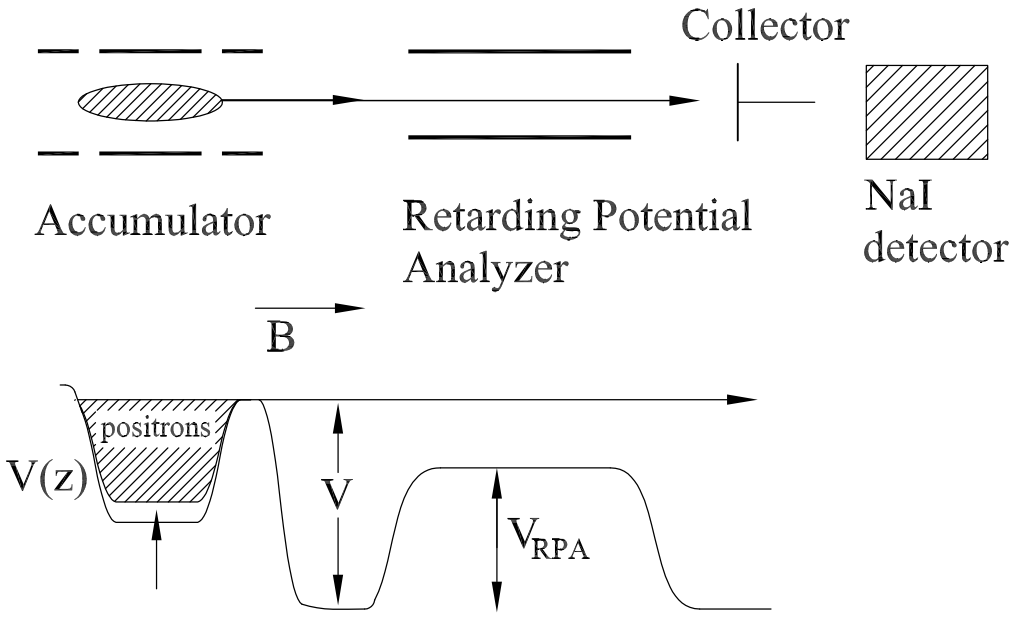

Figure 3.3: Illustration of the extraction of a beam of positrons and analysis of the energy distribution using a retarding potential analyzer (see Fig. 3.4). Positrons collected in the accumulator are forced out of this region by increasing the bias on the stage III trap electrode. Positrons that have enough energy to surmount the potential barrier formed by the retarding potential analyzer annihilate on the collector and the radiation is detected by the sodium iodide detector.

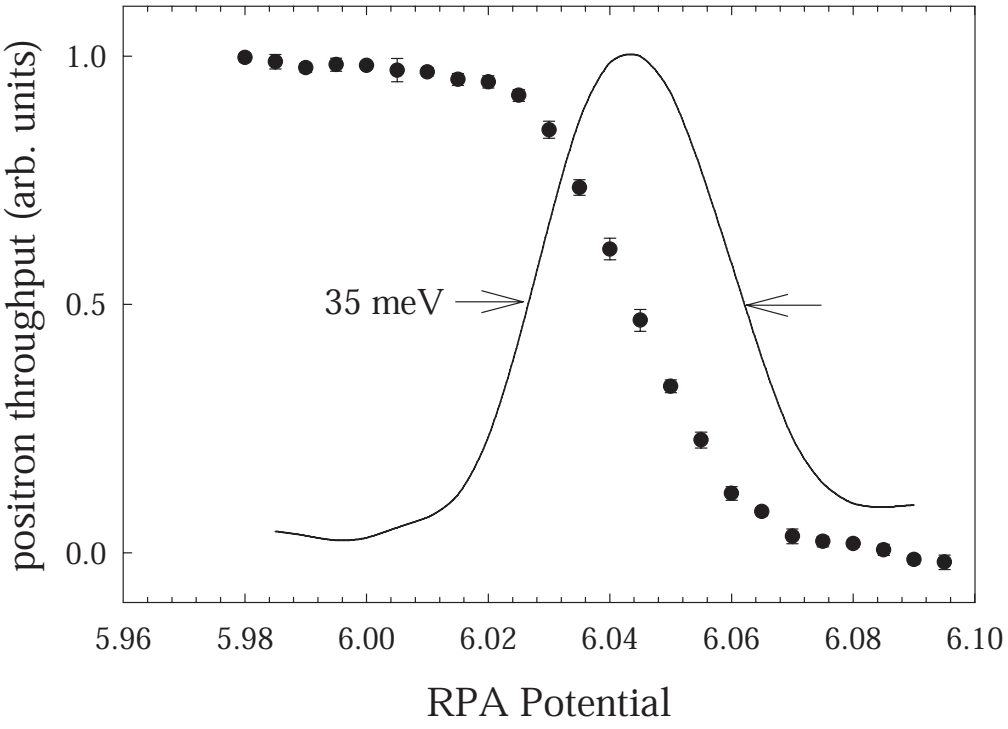

Figure 3.4: The positron throughput as a function of the potential on the retarding potential analyzer for the setup shown in Fig. 3.3 (see text). The solid curve shows the negative derivative of the data. This is the energy distribution of positrons in the beam. In this case, the width of the distribution is $\sim$ 35 meV (FWHM).

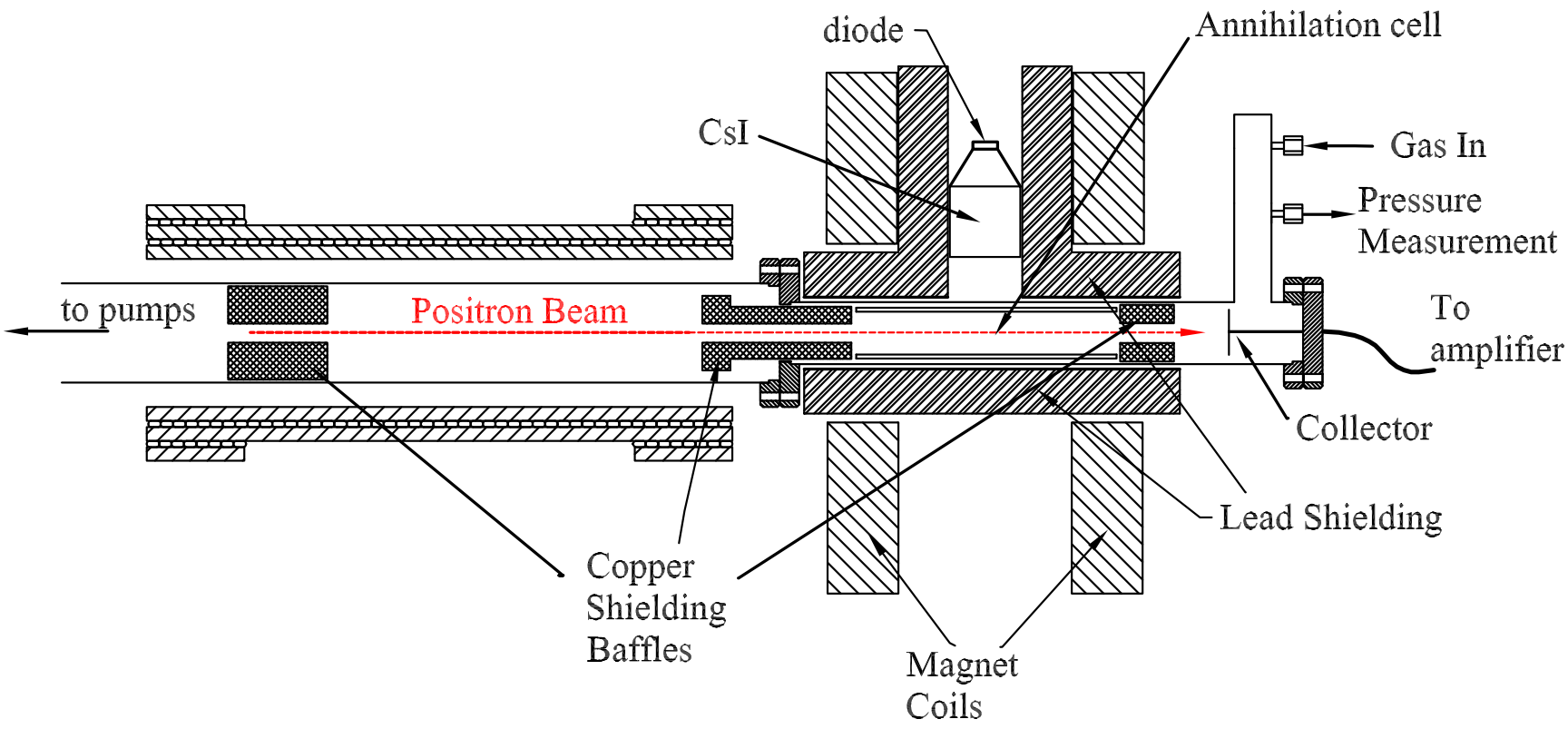

Figure 3.5: Schematic drawing of the annihilation cell, radiation detector and shielding.

3.4 Test gas delivery and measurement

In order to measure annihilation rates, the beam thus produced is magnetically guided through a region filled with the target gas to be studied. A diagram of this section of the apparatus is shown in Fig. 3.5. The positrons entering from the left are confined radially by a magnetic field of magnitude $\simeq 800$ Gauss produced by the two magnet coils. The coils are separated to allow access to the vacuum chamber for detection of annihilation radiation.

The test gas is introduced where indicated in the diagram. The pressure is measured by a capacitance manometer. This allows measurement of the pressure directly without calibration for different gases as is necessary for an ion gauge. However, drift in the absolute calibration of the device on long time scales ($\sim$ hour) contributes some uncertainty to the measurement. Also, the device cannot reliably measure pressure below 10^{-5} torr.

In early experiments, pressure was measured near the gas inlet and the known conductances of the various sections of the apparatus were used to calculate the pressure in the region visible to the detector. More recently, the pressure in the interaction region was directly measured by inserting a hollow tube (not shown in Fig. 3.5) into the baffle at the end of this region.

For compounds that are gaseous at room temperature, a constant test gas pressure was maintained by adjusting the voltage on a piezoelectric needle valve. A digital proportional-integral-differential (PID) device was responsible for controlling the test gas pressure.

A manual needle valve was used to adjust the flow of compounds that are liquid at room temperature. In this case, the technique was similar to that developed by Iwata [39]. A small amount of the liquid was placed in a test tube submerged in a water-ethanol mixture. The temperature of this mixture was controlled by a digital PID controller and thermoelectric cooling device. The temperature of this bath, once stabilized, is constant to within 1°. The manual needle valve between the test tube and the gas feed line allows the pressure in the inlet line to be adjusted. To remove impurities dissolved in the liquid, it was frozen by immersion in liquid nitrogen, then allowed to thaw while being pumped by a molecular drag pump. The gas pressure in this setup varies on slow time scales ($\sim$ hour). To compensate for this, the pressure was constantly recorded and an average pressure was used to calculate Z_{eff}.

3.5 Adjusting beam energy

The mean kinetic energy of positrons in the interaction region can be adjusted by a potential applied to the electrode surrounding the gas-filled region. To eliminate the effects of contact potentials or other offsets in the electrode potential, the mean kinetic energy of the positron beam is calculated relative to the electrode potential required to reflect the positron beam, the "cutoff potential." This is found by using the gas region electrode as a retarding potential analyzer as described in Sec. 3.3. This process gives the cutoff potential, V_C, for the electrode. The kinetic energy of the beam in the cell, ϵ, is related to the bias on the cell, V_B, by $\epsilon = e(V_C - V_B)$. Adjustment of this bias allows measurements to be taken for positron energies ranging from 50 meV to 90 eV while maintaining an energy resolution of 25 meV.

Since ϵ as computed above is the energy of the positron from motion only in the direction of the magnetic field, the energy from motion perpendicular to the magnetic field must be found and added to find the total positron kinetic energy. The energy in the perpendicular motion (cyclotron motion) in the region of interaction with the test gas is given by

$$\epsilon_\perp = \epsilon_\perp^{(t)} \frac{B_\mathrm{c}}{B_\mathrm{t}} \tag{3.2}$$

where $\epsilon_\perp^{(t)}$ is the perpendicular energy in the trap region and B_c and B_t are the magnitudes of the magnetic fields in the gas cell and trap regions. In the buffer gas trap, the positrons are in thermal equilibrium with the buffer gas, and so they have $1/2\ k_B T$ energy in each of the two perpendicular directions. The ratio of the field in the trap to that in the cell is ~ 1.5 so the perpendicular energy in the gas cell is 16 meV. This energy is added to the parallel energy to give the total positron kinetic energy.

Other elements of the apparatus can also be electrostatically biased. A sufficiently large potential applied to an electrode on the far side of the cell can cause the positron beam to be reflected axially and travel back through the gas-filled region. This reflector electrode (see Fig. 3.5) substantially increases the signal-to-noise. We will discuss this further in Sec. 3.7.

When the reflector electrode is biased high, it is important to know the number of times the positrons pass through the cell in a given amount of time. This can be computed since the velocity of the positrons in the direction of the magnetic field is known both in the gas cell region and in the remainder of the apparatus. Since the delay associated with positrons transiting the gas cell itself depends on the kinetic energy of the positrons in the cell, this number of passes

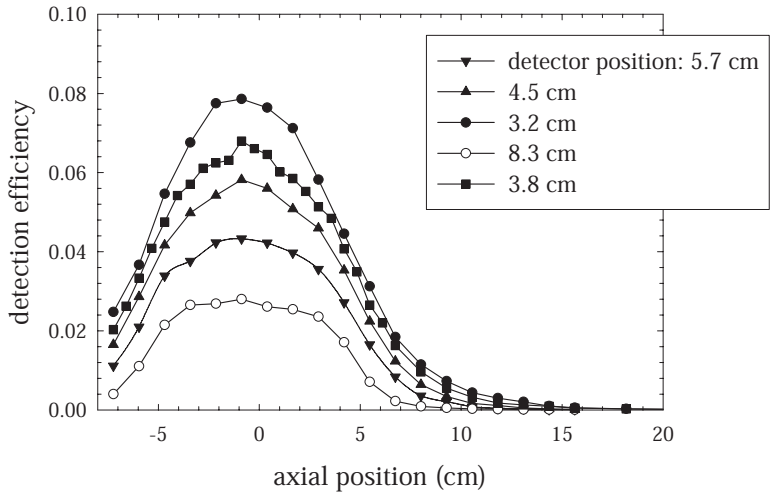

Figure 3.6: The detection efficiency of the annihilation radiation detector for a source at the axial position indicated. Axial position zero is directly in front of the detector. Data is shown for a detector in several radial positions. The detector position indicated is the distance between the closest face of the crystal and the radial center of the vacuum chamber.

must be recomputed for each positron energy. The frequency of these passes is on the order of 3 μs and can be crudely verified by the induced charge pickup on the electrode itself due to the positron pulse.

3.6 Radiation detection

Radiation due to the annihilation of positrons with electrons in the test gas was detected using a thallium-doped cesium iodide crystal and accompanying photodiode. It was purchased from Scionix Holland. The device is sufficiently sensitive to detect single gamma-ray photons, which result in a pulse of width $\sim 5\mu$s and height proportional to the energy of the photon. A photon of energy 511 keV corresponds to a pulse height of 0.70 V.

The signal from the detector is sent to a single channel analyzer that outputs a square pulse when the input receives a pulse of height between 0.5 and 1.0 V. This eliminates photons with energy significantly higher or lower than 511 keV including erroneous counts due to detector dark noise. Annihilation photons which arrive within a microsecond of one another can result in pulses of height

greater than 1.0 V into the window element. For this reason, signal levels must be kept low enough to ensure negligible numbers of these near-simultaneous photon arrivals.

The efficiency of the detector to detect annihilation events in the gas region was measured in the following way. A ^{22}Na source of known activity was placed at varying positions along the path of the positrons through the gas-filled region. The source is encased in thin plastic which converts all positron emission by the source into 511 keV gamma ray radiation. At each source position, the gamma-ray counts were measured for 10 seconds using the setup described above. By dividing by the time and the known activity of the source, the detection efficiency as a function of axial position, $D(z)$, is found. This measurement was performed for several radial detector positions to allow the signal to be reduced if necessary by moving the detector away from the interaction region. The results are shown in Fig. 3.6.

To reduce the frequency of counts unrelated to the interaction of the positron beam with the test gas, gamma photons are counted only during a 15 μs time period during the positron beam dump. For experiments allowing positrons a single pass through the test gas region, this window was set to include the time when the positrons are passing through the cell. When the reflector electrode is used to reflect the beam back through the cell, the time window is set to begin only after the entire pulse has passed through the cell at least one time. The average number of passes the positrons make through the gas cell in the 15 μs time window can then be calculated from the length of the beam line, the length of the interaction region and the positron kinetic energy in both regions.

3.7 Reducing background counts

As mentioned above, the cross section for direct annihilation is typically orders of magnitude smaller than the cross sections for other scattering processes. If the gas pressure is also low, great care must be taken to reduce background counts which would interfere with the measurement. For example, for the smallest energy-resolved Z_{eff} measured to date (argon, see Sec. 5.7), the measured annihilation signal in the setup described is just over one count per 10^7 positrons passing through the cell. The background counts must be reduced well below this level if the measurement is to be valid.

Background counts can come from either cosmic radiation or from the annihilation of positrons in other areas of the apparatus. During the trapping and cooling phases, there is substantial annihilation of the trapped positrons. During the dump phase, the positron beam must often be apertured to en-

sure a well-defined positron beam width. This creates annihilation radiation as positrons strike the aperture. Also, positrons can annihilate (or possibly form positronium) with other gases in the vacuum system. Finally, in previous experiments, the positrons were collected on a metal plate after passing through the cell. Annihilation from positrons striking the collector is a potentially serious source of background counts.

Counts due to dark noise of the detector and to cosmic radiation at energies much higher that 511 keV are eliminated by counting gamma rays using a single channel analyzer. Only photons with energy near 511 keV are counted as annihilation events. This is discussed in Sec. 3.6.

To reduce counts due to 511 keV gamma rays from annihilation events other than those involving the test gas, the radiation detector and the vacuum chamber surrounding the annihilation cell are encased in 5 cm of lead. Inside the vacuum chamber, copper is used to further isolate the detector as much as possible from gamma ray radiation originating outside the annihilation cell. Both of these features are labelled in Fig. 3.5.

Annihilation with gases which compose the base pressure in the vacuum system is also a concern. With the use of cryogenic vacuum pumps, regular baking and care in keeping surfaces clean, the base pressure of the vacuum system is typically less than 10^{-9} torr which is four orders of magnitude smaller than typical test gas pressures. It is also important that each of the pumps in the experiment be oil free, since the annihilation rates for hydrocarbons molecules are very large.

As discussed above, an electrode can be used to reflect the positrons without allowing them to strike the collector. This has two effects. First, the annihilation radiation from positrons annihilating on the collector is eliminated. Second, the positrons are guided back through the cell multiple times, increasing the signal from annihilation with the test gas.

Finally, the annihilation events are recorded only if they fall within a 15 μs time window during which the positrons are passing through the cell. Events occurring at other times can only be due to one of the noise sources discussed above and so are not counted.

Employing all of these techniques simultaneously has enabled us to reduce our background counts to 1 count per 10^9 positrons passing through the cell. This is measured by performing the experiment without a test gas.

3.8 Computation of Z_{eff}

For each data point, radiation events are recorded using between 3,000 and 15,000 positron pulses. The ratio, f, of the detected counts to the total number of positrons passing through the cell is related to the cross section, σ, by

$$f = \sigma n \int D(z)dz, \tag{3.3}$$

where the integration is over the path of the positrons in the gas-filled region, $D(z)$ is the detection efficiency and n is the target density. In the calculation of f, the number of positron passing through the cell must be adjusted if the positrons make several passes through the cell due to reflection by the reflector electrode. This average number of passes is calculated as described in Sec. 3.5.

The cross section, σ is related to Z_{eff} by

$$\sigma = \frac{\pi r_0^2 c Z_{eff}}{v} \tag{3.4}$$

with symbols defined as in Eq. 2.1 and v as the velocity of the positrons in the interaction region. From this, Z_{eff} is easily computed.

3.9 Verifications

Two important checks were made on the results of the described experiment. The first is to establish that the annihilation measured is due exclusively to the interaction of positrons with single target molecules. The second ensures that other scattering processes (e.g. elastic and inelastic scattering) have a negligible effect.

To confirm the dominance of two-body interactions, the measurements are performed at several pressures. Annihilation rates for processes involving just one target atom or molecule depend linearly on the target density (pressure). By contrast, processes involving two or more targets should have a super-linear dependence. These three(or more)-body interactions can be either a single process involving two or more targets such as positron attachment to molecular clusters, or in consecutive processes such as inelastic collision followed by annihilation on a second target. The linear dependence of the annihilation rates on test gas pressure for the results presented here confirm that only interactions with single target atoms or molecules are involved. A specific example with accompanying data is shown in Fig. 4.2 below.

Since elastic and inelastic scattering can change the energy of positrons in the beam and also change the total path length through the gas cell, it is important

to establish that the effect of these processes can be neglected. In the "multiple pass" setup (described in Sec. 3.5) positrons transit the cell several times. If other scattering channels significantly affect the energy distribution of the positron beam, such effects would be more pronounced after the positrons have made several passes through the cell. To investigate this, annihilation counts are recorded for the first 15 μs after the positrons enter the cell (time enough for positrons to transit the cell ~ 5 times) and again for the 15 μs immediately following this time period. Appreciable effects due to elastic or inelastic scattering would be manifest in significant differences between the annihilation rate measured in the two time periods. Direct annihilation during this time period has little effect on the positron beam as less than 0.1% of positrons are annihilated in 15 μs. If a significant, systematic difference was found between rates measured in the two time periods, the gas pressure was reduced until such effects were eliminated.

3.10 Error analysis

For the data shown in this thesis, the error bars indicate the random error. This is dominated by the statistical error due to low count rates and is given by $Z_{eff}/\sqrt{N}$ where N is the total number of annihilation events detected.

3.10.1 Error in the magnitude of Z_{eff}

Systematic errors are not expected to affect the *shape* of the Z_{eff} spectra for a given molecule significantly, but may change the overall magnitude of the measurement. Some potential sources of systematic error are discussed and their effect estimated below:

1. *Pressure measurement.* The test gas pressure was monitored and maintained by feedback from a PID controller to a piezo-electric needle valve. The pressure was measured using a capacitance manometer at higher pressures (> 20 μtorr) or an ion gauge at lower pressures. For the capacitance manometer, there is substantial drift in a random direction over time on the order of 1-2 μtorr. For pressures near the lower end of its range, this drift can contribute 5% to the systematic error.

   For lower pressures that were measured with the ion gauge there is an uncertainty in the gas-dependent ion gauge sensitivity. The sensitivity was calibrated at higher pressures to measurements using the capacitance manometer which has no gas dependent sensitivity and extrapolating linearly toward lower pressures. Since the calibration is done over a short

period of time, the drift in the capacitance manometer can be neglected. The error due to an observed non-linearity in the sensitivity is estimated to be 5-10%.

2. *Positron number* . As mentioned, the number of positrons is measured by observing the charge deposited on a collector plate. The charge-sensitive amplifier used is calibrated to within 1%. When averaged over several hundred positron dumps, this number can be known to within 1%. There can, however, be subtle changes in either the moderator strength or the efficiency of the buffer gas trap over the course of a data run. The number of positrons is typically measured before and after a run and these measurements are found to agree within 5%.

3. *Number of passes.* The number of passes that the positrons make through the interaction region during the counting window is computed from the energy of the positrons in both the interaction region and the remainder of the beam line. The energy of the positrons in the interaction region is known, as discussed below, to within a few percent. The energy in the remainder of the cell is taken to be e times V_c, the retarding potential cutoff. This cutoff potential, though, can differ from the bias on the trap potential barrier by as much as 200 mV. This is a 5% error for a typical 4 V transport energy. However, since the number of passes depends on the velocity and since the time delay through the non-interaction region is about half of the total delay, uncertainty in the number of passes contributes maximally an error of a few percent.

Taking these effects into account, the total systematic error can be as large as 12%. The error will be largest for gases with very large Z_{eff} that must be measured at very low pressures and slightly larger at higher energies where the error in the number of passes is largest.

3.10.2 Error in positron energy

A couple of factors contribute to the uncertainty in the given positron energy. As mentioned, the uniformity of the potential in the gas region was verified by comparing the retarding potential cutoff to a time-of-flight energy measurement (Sec. 3.5). These are found to agree to about 5 meV. Other potential sources of error in positron energy include calibration of the biasing amplifiers, drift in the transport energy over the course of a data run and inadequate thermalization of the positron motion perpendicular to the magnetic field. All of these effects

are substantially smaller than the inherent thermal width of the positron beam (25 meV).

Chapter 4

Vibrational Feshbach Resonances in the Z_{eff} Spectra for Alkane Molecules

The energy-resolved annihilation rate for certain molecules exhibits large resonances due to trapping of positrons into temporary bound states with target molecules. These temporary bound states are similar in many ways to the negative ion (Feshbach) resonances observed in electron scattering. The data shown are the first experimental evidence of positron binding to gas phase molecules. Measurements of the positron affinities for molecules can be extracted from these data.

This chapter focuses on the annihilation rates for alkanes and some closely related molecules including alkenes, ring hydrocarbons and fluoro-alkanes. The alkanes were chosen as a model species for the study of large Z_{eff} because they are conveniently available in a wide range of sizes. As described in previous chapters, the value of Z_{eff} for thermal positrons increases exponentially with molecular size in the alkanes. Here, we explore the dependence of the Z_{eff} resonance features on minor changes to the shape and chemical composition of target molecules.

4.1 Energy-resolved Z_{eff} for butane: an example of resonant enhancement of annihilation

Figure 4.1 shows the normalized annihilation rate, Z_{eff} (see Sec. 2.2 for an explanation of Z_{eff}), as a function of the incident positron energy for butane

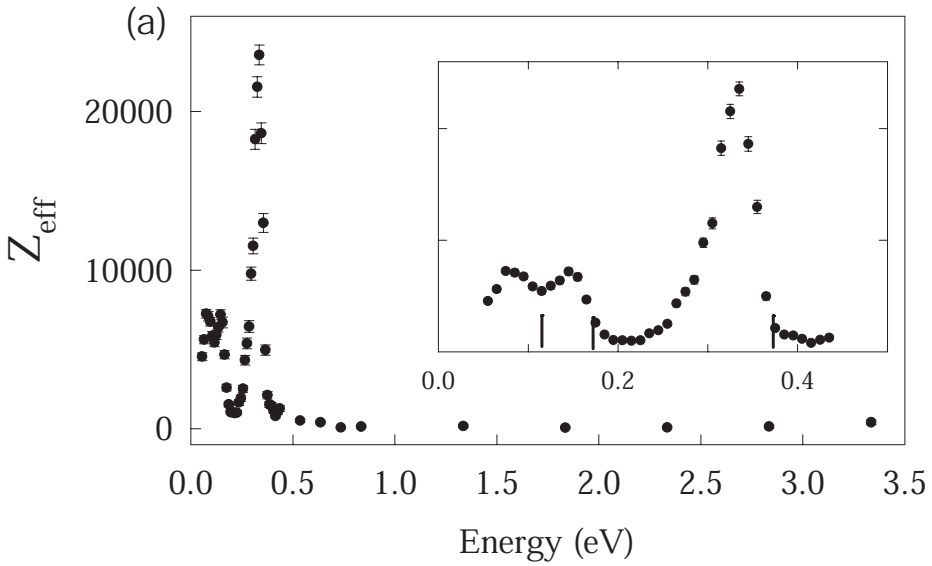

(b)

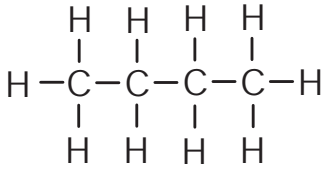

Figure 4.1: (a) The annihilation parameter, Z_{eff}, as a function of incident positron energy for butane. Vertical bars on the inset curve represent the energies of the vibrational modes of the molecule. Data from ref. [23]
(b) Kekulè structure for butane.

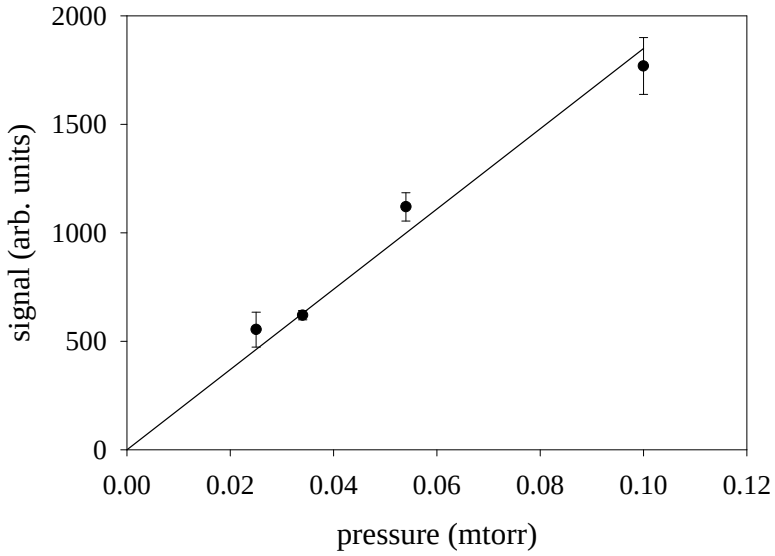

Figure 4.2: The positron annihilation signal as a function of butane pressure. The positron energy for these measurements was 0.32 eV. The solid curve is a linear fit to the data constrained to pass through (0,0).

(C_4H_{10}). For positrons with kinetic energy greater than $\sim$ .5 V, the spectrum is flat and Z_{eff} is only modestly larger than the actual number of electrons (in this case, 34). For lower incident energies, however, several enhancements of width about 40 meV can be seen centered at $\sim$ 320 meV, 150 meV and 90 meV. These resonance structures are each positioned at energies about 30 meV less than the energy of the vibrational modes of the molecule (marked as vertical lines on the abscissa). It should be noted that butane is only one example of these types of resonances. I will examine butane in some detail before presenting the spectra for a number of other molecules which exhibit similar resonance features. The analysis which follows could be applied to any of these spectra.

The experiments were performed at several pressures. The measured annihilation signal is shown in Fig. 4.2 for several pressures of butane. For these experiments, the positron energy was 320 meV. The linearity of the data leads to the conclusion that the measured annihilation rate is due almost exclusively to interactions between a single positron and a single target molecule. Since the signal due to positron interaction with, say, two molecules, either simultaneously or in two separate scattering events, would have a density-squared dependence.

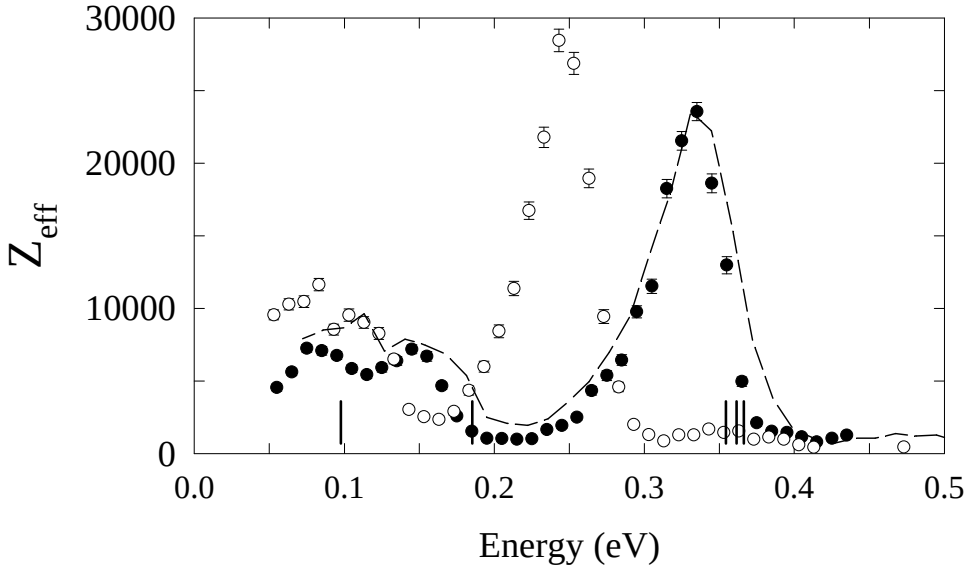

Figure 4.3: The annihilation parameter, Z_{eff}, for butane-d_{10} (C_4D_{10}) (○) and butane (C_4H_{10}) (●). The dashed curve is Z_{eff} for butane-d_{10} with the positron energy scaled to account for the reduction in the vibrational frequencies due to replacement of the hydrogen atoms with the more massive deuterium (see text). Data from [23].

As discussed in Sec. 2.2, Z_{eff} is the effective number of electrons per molecule participating in the collision as if electron-positron correlations were negligible. Since the observed values of Z_{eff} near the resonances are orders of magnitude larger than the actual number of electrons per molecule it is clear that an explanation of this spectrum requires a model which goes beyond simple weakly-correlated collisions. For positron energies greater than ~ 1 electron Volt, where Z_{eff} is on the order of 100, such a simple, weak-correlation model may be more appropriate.

Since the resonances occur only for positrons with energies in the range of the vibrational modes of the molecule, it is important to study the relationship between the Z_{eff} spectrum and molecular vibrations. The substitution of deuterium (D) atoms for hydrogen atoms in butane changes the vibration spectrum with minimal changes to the electronic structure. In Fig. 4.3, I present the energy-resolved Z_{eff} spectra for butane-d_{10} (C_4D_{10}). For comparison, the dashed line in Fig. 4.3 shows the measured spectrum for butane-d_{10} with the energy scaled by $(\mu_D/\mu_H)^{1/2}$, where μ_D and μ_H are the reduced masses respec-

tively of the deuterium and hydrogen atom calculated for a free carbon-hydrogen (carbon-deuterium) pair. The dashed curve is also scaled in magnitude for comparison with the butane data. The excellent agreement between the two data sets is evidence that the resonances are caused by an interaction of the positron with molecular vibrations.

4.2 Comparison with capture resonances in electron scattering

Similar resonant cross sections are often seen in electron scattering experiments. These are referred to as negative ion resonances or Feshbach resonances and can be understood following the analysis by Feshbach [18, 19]. If the combined energy of the incoming projectile and target molecule together is nearly degenerate with the energy of a combined state of the projectile and target (possibly in an excited vibrational or electronic state), then coupling to this combined state is enhanced. Often this increased coupling enhances the cross section for another escape channel (for example, elastic or inelastic scattering or dissociative attachment). To illustrate, Feshbach resonance enhancement of dissociative attachment can be represented in the following way [74]:

$$\begin{aligned} e^-(E) + \mathrm{XY}(\nu, J) \longrightarrow (\mathrm{XY}^-)^* \quad &\longrightarrow \quad e^-(E' = E) + \mathrm{XY}(\nu, J) \ \ \text{(elastic)} \quad (4.1) \\ &\longrightarrow \quad e^-(E' \neq E) + \mathrm{XY}(\nu', J') \ \ \text{(inelastic)} \\ &\longrightarrow \quad \mathrm{X} + \mathrm{Y}^- \ \ \text{(dissociative attachment).} \end{aligned}$$

(4.2)

Each of these processes can occur without the intermediate state,$(\mathrm{XY}^-)^*$, but increased population of this resonance state enhances the cross section for the decay channels on the right if the coupling between the intermediate state and the decay channels (final states) is strong. The condition for resonance is that the energy of the initial state be very close to the energy of the intermediate state.

This is seen in many types of electron scattering measurements for many different targets. Figure 4.4 shows an example of a Feshbach resonance in dissociative attachment of methyl iodide (CH_3I) by electron impact [74]. Here the cross section is enhanced by the CI stretch excited state of the CH_3I^- ion. The ion is weakly bound with respect to reemission of the electron but readily dissociates into CH_3 and I^-. When the electron energy is appropriate to form the excited CH_3I^- complex, the dissociative attachment cross section is enhanced.

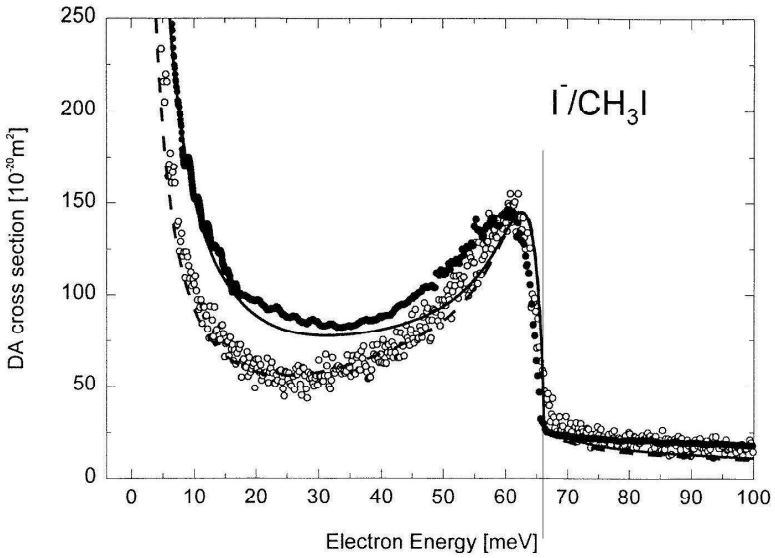

Figure 4.4: Dissociative attachment cross-section for electron incident on methyl iodide (CH_3I). The resonance is caused by interaction with the CI stretch excited state of the CH_3I^- ion. The energy of this mode (66 meV) is marked by a vertical line. This figure was previously published by Schramm, Fabrikant, Weber, Leber, Ruf and Hotop in reference [74].

4.3 The Feshbach resonance picture for positron annihilation

The Feshbach resonance picture can describe positron scattering and incorporate the possibility of annihilation. To describe this new channel, we adjust Eq. 4.2 to incorporate the annihilation channels:

$$\begin{aligned} \mathrm{e}^+(E) + \mathrm{A}(\nu, J) \longrightarrow (\mathrm{e}^+\mathrm{A})^* &\longrightarrow \mathrm{e}^+(E' = E) + \mathrm{A}(\nu, J) \quad \text{(elastic)} \\ &\longrightarrow \mathrm{e}^+(E' \neq E) + \mathrm{A}(\nu', J') \quad \text{(inelastic)} \\ &\longrightarrow \mathrm{A}^+(\nu', J') + 2\gamma \quad \text{(resonant annihilation)} \end{aligned} \tag{4.3}$$

$$\mathrm{e}^+(E) + \mathrm{A}^+(\nu, J) \longrightarrow \mathrm{A}^+(\nu', J') + 2\gamma \quad \text{(direct annihilation).} \tag{4.4}$$

Here, $(\mathrm{e}^+\mathrm{A})^*$ represents a positron attached to the excited target. If, in the intermediate state, the overlap of the wave functions of the positron and the target electrons is enhanced over the case of the positron in a free state, then the annihilation rate will be enhanced when the temporary state is populated.

The enhancement should occur when the energy of the incident free positron and initial state target, $\mathrm{e}^+(E) + \mathrm{A}(\nu, J)$, is very close to the energy of the intermediate positron-target state, $(\mathrm{e}^+\mathrm{A})^*$. If we make the assumptions that the positron has very little effect on the energies of the vibrations and that the binding of the positron to the molecule is independent of the vibrational state of the molecule, this condition can be written as

$$E + E_0 = E_{ex} - E_{bind} \tag{4.5}$$

where E is the incident positron energy, E_0 is the energy of the initial state target, E_{ex} is the energy of the target in an excited state and E_{bind} is the binding energy of the positron-target complex. Rearranging Eq. 4.5, we find that the positron energy, E, must be very close to

$$E \simeq E_{ex} - E_0 - E_{bind}. \tag{4.6}$$

That is, the resonant enhancement of Z_{eff} should occur when the incident positron energy is lower than the energy of the excitation by E_{bind}, the binding energy of the positron-target complex.

For the specific case of a vibrationally excited resonance state, the population of the state can be represented in another way. Figure 4.5 shows hypothetical potential energy curves for the bare target and the target with a positron attached. The curves represent the energy of the two systems as a function of the

normal coordinate, Q_ν, of a specific vibrational mode of the molecule. We have drawn the curve for the positron-target complex lower than that of the bare molecule to indicate that the presence of the positron lowers the ground state energy. The magnitude of this decrease is the binding energy of the complex and is indicated by $E_{binding}$. For the system to transition from the ground state of the bare molecule to the first excited state of the positron-molecule complex, the incident positron must provide the energy, E_{res}. It can be seen from the diagram that the resonant energy of the incident positron is given by Eq. 4.6.

There is, of course, another possible path to annihilation represented by the last line in Eq. 4.4 wherein the positron annihilates directly from the free state. This channel is expected to have a smooth energy dependence for positron energies much lower than the threshold for positronium (Ps) formation. Absent any resonant enhancement, the contribution of this channel to Z_{eff} is on the order of Z, the total number of electrons in the target. This channel is responsible for Z_{eff} for butane at energies between 0.5 eV and the Ps threshold where the initial state energy is well separated from that of resonant states.

4.4 Feshbach resonance analysis of the butane spectrum

Considered in this Feshbach resonance picture, we can draw some conclusions about the interaction of positrons with butane. For butane (Fig. 4.1), the intermediate resonant state is a positron attached to a vibrationally excited butane molecule. Thus (eq. 4.6), the energy difference between the center of the resonance and the energy of the excited vibrational mode of the molecule is a measurement of the binding energy of the positron-molecule complex. This analysis assumes that the presence of the positron has only a small effect on the vibrational frequencies of the molecule. Within the limits of this assumption, the binding energy of a positron with a butane molecule, or positron affinity for butane, is concluded to be 30 meV. It should also be noted that there exist several vibrational modes within a 10 meV range of 360 meV. It is not clear which of these nearly degenerate modes is excited in the intermediate state and this contributes to the uncertainty in the measurement of the binding energy.

As will be discussed in more detail below, these experiments are the best evidence to date of the existence of bound states of positrons with neutral atoms or molecules. Bound states were conjectured to explain large annihilation rates [24, 28, 77, 81], but experimental evidence has been lacking.

The varying heights of the peaks in Fig. 4.1 can be analyzed to draw con-

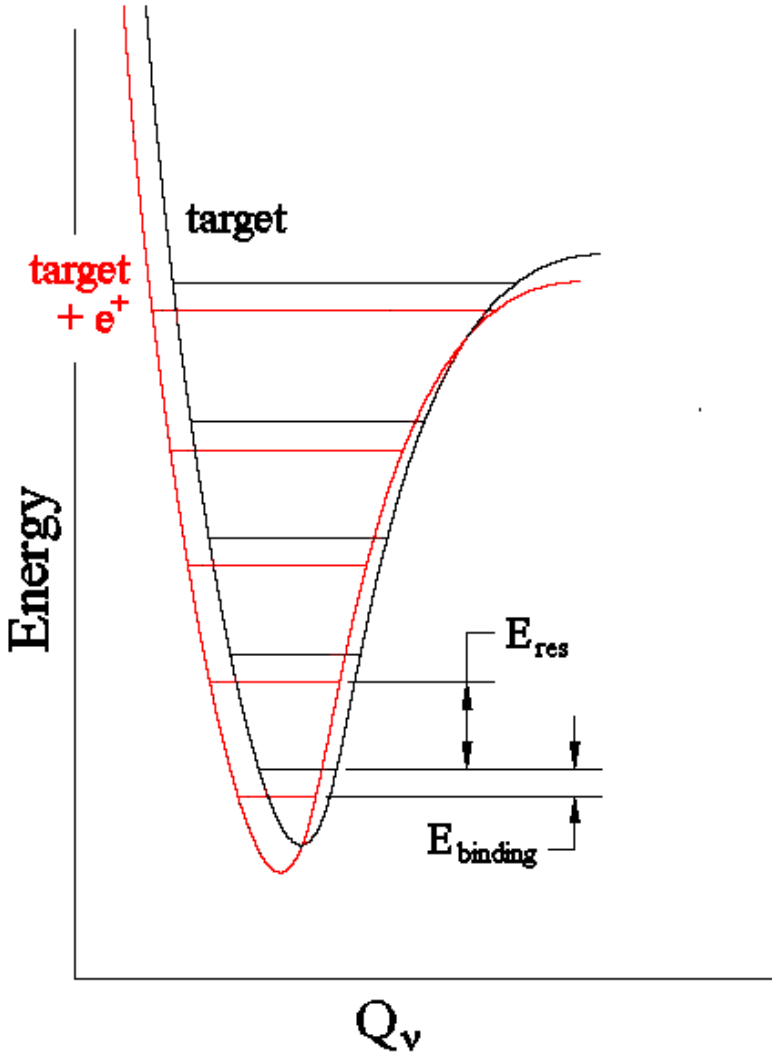

Figure 4.5: Hypothetical dependence of potential energy on the normal coordinate Q_ν of a normal vibrational mode for a bare target and for a positron-target complex. A downshifting due to the presence of the positron is labelled as $E_{binding}$. The energy E_{res} is the center of the predicted Feshbach resonance.

Table 4.1: The symmetry, energy and infrared activity of all of the vibrational modes for butane (C_4H_{10}).

No.	Sym. Species	Type of mode	Energy (meV)	IR active?
1	a_g	CH3 d-str	368	N
2	a_g	CH3 s-str	356	N
3	a_g	CH2 s-str	354	N
4	a_g	CH3 d-deform	181	N
5	a_g	CH2 scis	179	N
6	a_g	CH3 s-deform	171	N
7	a_g	CH2 wag	169	N
8	a_g	CH3 rock	143	N
9	a_g	CC str	131	N
10	a_g	CC str	104	N
11	a_g	CCC deform	53	N
12	a_u	CH3 d-str	368	Y
13	a_u	CH2 a-str	363	Y
14	a_u	CH3 d-deform	181	Y
15	a_u	CH2 twist	156	Y
16	a_u	CH3 rock	118	Y
17	a_u	CH2 rock	91	Y
18	a_u	CH3-CH2 torsion	24	N
19	a_u	CH2-CH2 torsion	13	N
20	b_g	CH3 d-str	368	N
21	b_g	CH2 a-str	361	N
22	b_g	CH3 d-deform	181	N
23	b_g	CH2 twist	161	N
24	b_g	CH3 rock	146	N
25	b_g	CH2 rock	100	N
26	b_g	CH3-CH2 torsion	28	N
27	b_u	CH3 d-str	368	Y
28	b_u	CH3 s-str	356	Y
29	b_u	CH2 s-str	354	N
30	b_u	CH3 d-deform	181	Y
31	b_u	CH2 scis	181	Y
32	b_u	CH3 s-deform	171	Y
33	b_u	CH2 wag	160	Y
34	b_u	CC str	125	Y
35	b_u	CH3 rock	120	Y
36	b_u	CCC deform	34	Y

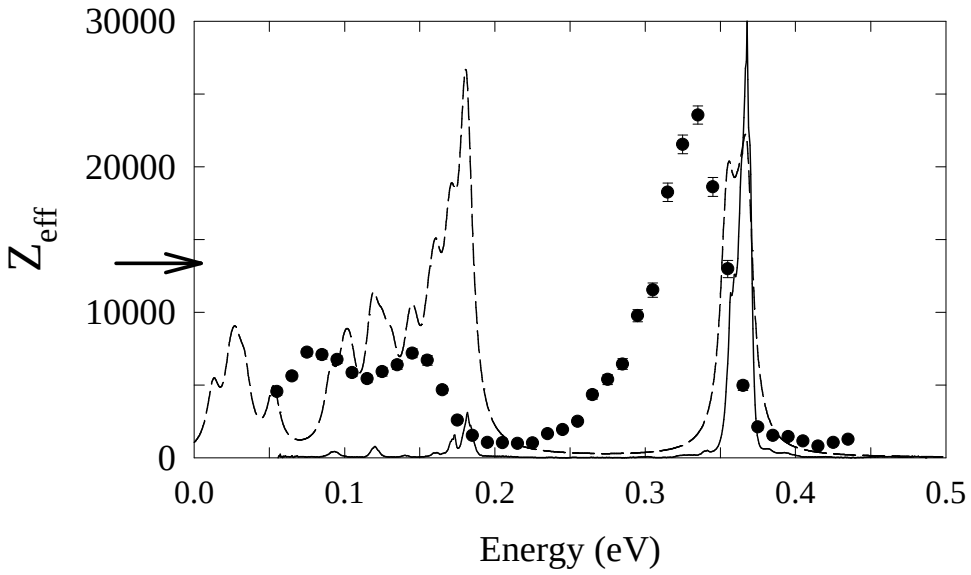

Figure 4.6: The annihilation parameter, Z_{eff}, for butane (C_4H_{10}) compared with the infrared absorption spectrum (solid line) and the vibrational modes with equal weight broadened by 10 meV (dashed line).

clusions about the effectiveness of the capture of the positron by the excitation of individual vibrational modes. Figure 4.6 shows the Z_{eff} spectrum for butane together with the smoothed linear vibrational mode density of butane. Each of the fundamental vibrational modes of butane contributes a Lorentzian line shape of equal height and width 10 meV to the dashed curve in Fig. 4.6. The vibrational modes for butane are also displayed in table 4.1 [76]. Note in particular that, in Fig. 4.6, the Z_{eff} spectrum and the vibrational mode spectrum are qualitatively similar albeit with different peak heights. Also, the entire spectrum is down shifted by 30 meV. In much of the following we will focus on the peak associated with the CH stretch mode of the alkane molecules (E$\simeq$ 360 meV) because we can easily distinguish this large, isolated resonance. However, it is important to keep in mind that there are similar resonant enhancements near the other vibrational modes as well.

Butane was among the first molecules shown to exhibit vibrational Feshbach resonances (VFRs). Resonance features have been observed in the Z_{eff} spectra for many other molecules. We continue now with a comparison of the Z_{eff} spectra for the alkane molecules before examining fluoroalkanes, double- and triple-bonded hydrocarbons and non-linear hydrocarbons.

4.5 Increasing binding energy for large alkanes

Butane is just one example of a single-bonded (saturated) hydrocarbon, an alkane molecule or paraffin. The chemical formulae for alkane molecules are given by C_nH_{2n+2} (n=1,2,3...). Resonance structures similar to those discussed above have been observed in the Z_{eff} spectrum for all of the alkane molecules studied thus far with the exception of methane (CH_4). The Z_{eff} spectra for these molecules are shown in Fig. 4.7. The spectrum for methane is not included in Fig. 4.7, but will be presented and discussed in Sec. 5.1.

In each of these spectra, similar resonance structures are observed. As the size of the molecules increases, the Z_{eff} spectrum changes in two major ways. First, the resonant enhancements of Z_{eff} appear at decreasing positron energies. This is particularly apparent in the largest resonance associated with the CH stretch vibrational mode. In ethane (C_2H_6), this resonance is centered at $\sim$ 370 meV. As the size of the alkane molecule increases, the center of the resonance moves steadily downward in energy. In the framework of the vibrational Feshbach model, the energy of the intermediate (resonance or Feshbach) state is decreasing because the binding energy of the positron to the molecule is increasing with molecular size. Thus, vibrational Feshbach resonances enable us to measure the "positron affinity" of the various targets. We note, of course,

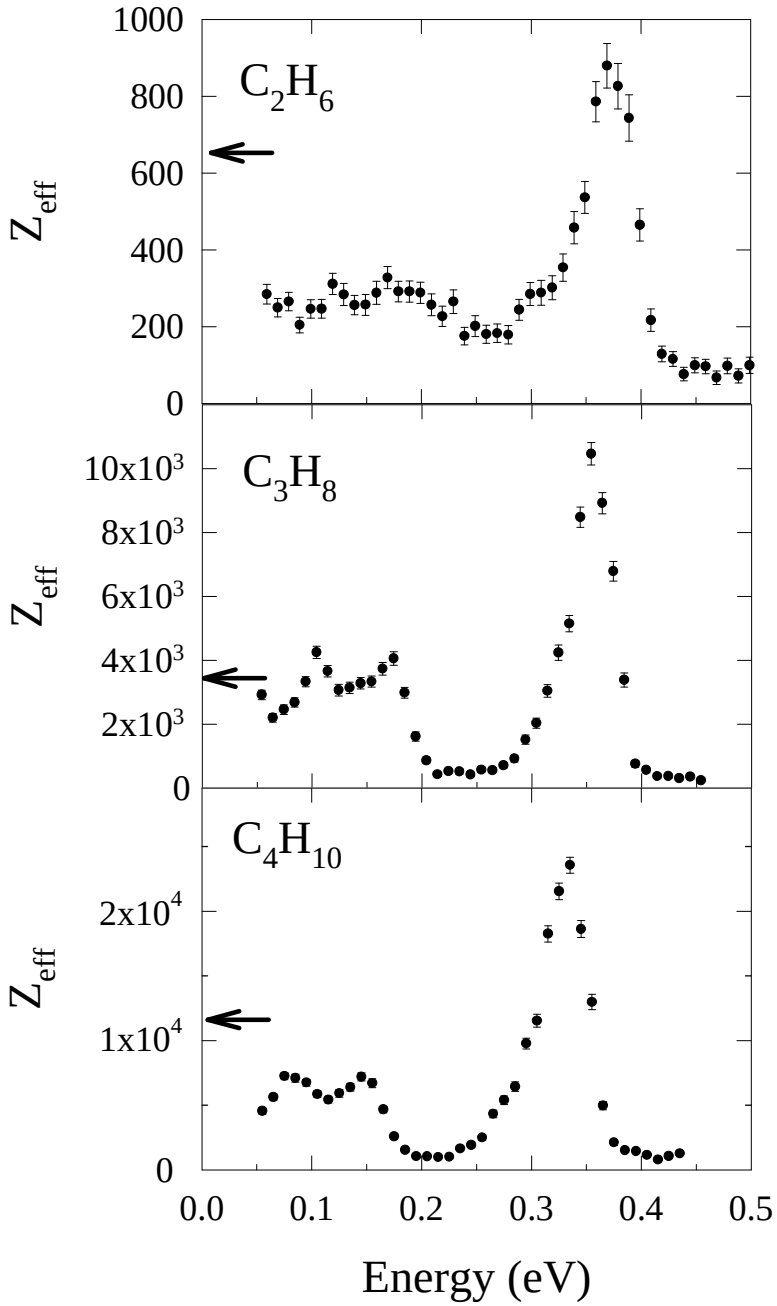

Figure 4.7: Z_{eff} as a function of incident positron energy for the alkanes (C_nH_{2n+2}). Arrows on the vertical axis indicate Z_{eff} for a room temperature thermal distribution of positrons. Data from reference [4].

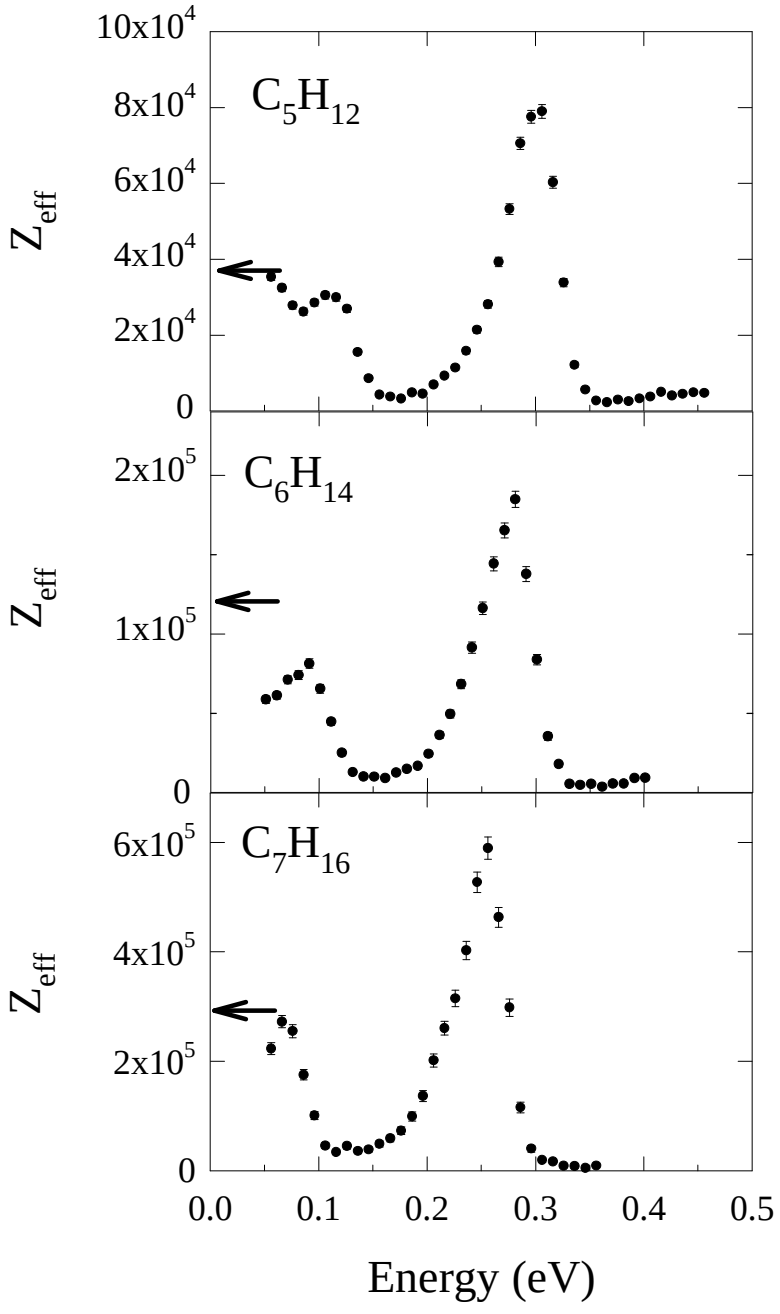

Figure 4.7: Z_{eff} as a function of incident positron energy for the alkanes (C_nH_{2n+2}). Arrows on the vertical axis indicate Z_{eff} for a room temperature thermal distribution of positrons. Data from reference [4].

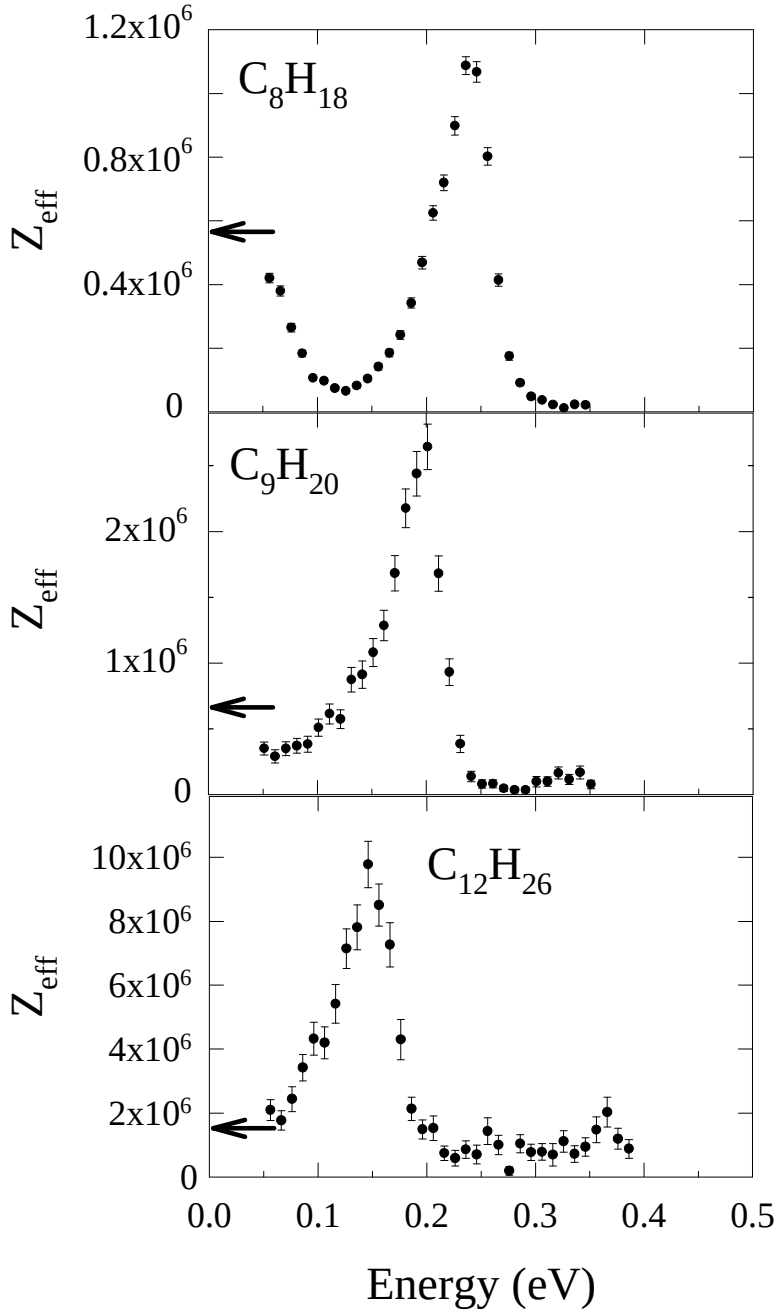

Figure 4.7: Z_{eff} as a function of incident positron energy for the alkanes (C_nH_{2n+2}). Arrows on the vertical axis indicate Z_{eff} for a room temperature thermal distribution of positrons. Data from reference [4].

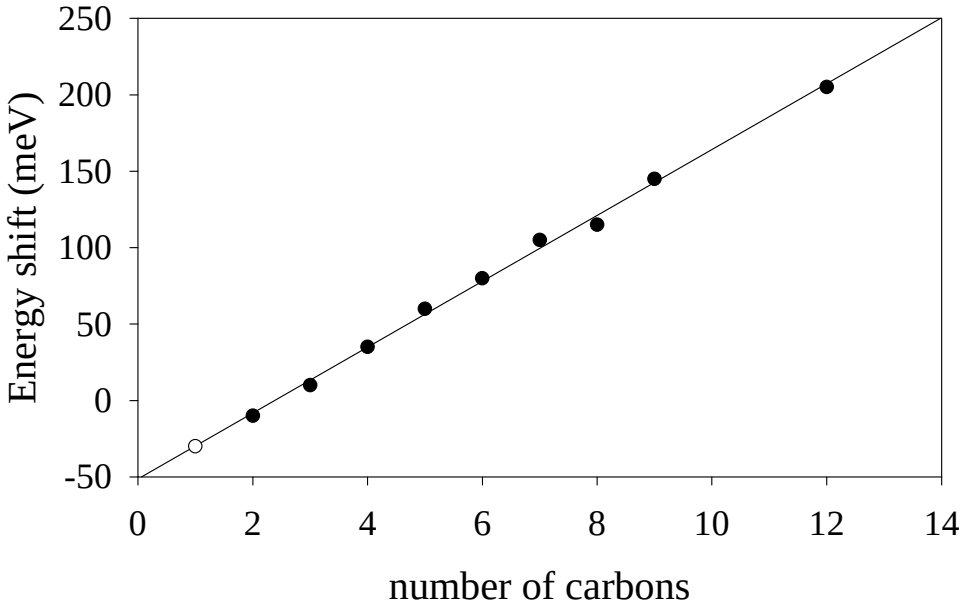

Figure 4.8: Energy shift as a function of the number of carbon atoms for the alkanes. Here, the energy of the CH stretch vibrational resonance is subtracted from the energy of the CH stretch vibrational modes. The solid curve is a linear fit to the data. The open circle is an extrapolation of the linear fit for methane. This extrapolation indicates an unbound state for methane of energy +30 meV.

that the entire Z_{eff} spectrum is shifted including those features associated with lower energy vibrational modes. We focus on the peak associated with the CH stretch mode because it is pronounced and well separated from other resonances.

The second change in the Z_{eff} spectra with increasing molecule size is the rapid increase in the magnitude of Z_{eff}. This will be discussed in section 4.8.

Figure 4.8 shows the difference between the center position of the CH stretch resonance and the energy of the CH stretch modes for the alkanes as a function of the number of carbons in the alkane molecule. It shows a nearly linear relationship between binding energy and number of carbons. In each of the alkane molecules, there are a number of CH stretch vibrations. For the purpose of this analysis, the energy of the CH stretch mode in all molecules is taken to be 360 meV. However, it should be noted that several vibrational modes are found within a 20 meV range of 360 meV for all of the alkane molecules. Also, the energy spread in the positron beam and the asymmetric shape of the resonance make it difficult to locate the center of the resonance more accurately than about 10 meV. With these qualifications in mind, Fig. 4.8 can be taken as a measurement of "positron affinity" for the molecules. This linear relationship between molecular size and positron affinity was proposed early by Surko, Passner, Leventhal and Wysocki [81] from examination of annihilation rates for thermal positrons and using estimates based on the theory of unimolecular reactions which ignores some aspects considered later by Gribakin [28].

4.6 Additional deuterated alkanes

In addition to the butane-d_{10} measurements discussed earlier, measurements have also been made nonane-d_{20} (C_9D_{20}). The Z_{eff} spectrum for this molecule is shown in Fig. 4.9. We can examine the isotope effect due to deuteration more closely. A careful examination of the energy scaling factor, ξ, due to deuterium substitution provides more information about the specific vibrational mode excited. The scaling of the spectrum is complicated by the energy shift due to positron binding. If we attribute the shift to the positron-electron correlations which are not expected to be affected by small motions of the nuclei, deuteration is not expected to change the magnitude of the shift. Scaling only the mode energy, deuteration should cause the peak to appear at an energy $\Delta\epsilon = (E_{ex} - E_0)(1 - \sqrt{\xi})$ lower than for the hydrogenated molecule, irrespective of the magnitude of the energy shift. This energy shift with deuteration is observed to be $\Delta\epsilon = 80 \pm 5$ meV for both butane (C_4H_{10}) (Fig. 4.3) and nonane (C_9H_{20}) (Fig. 4.9). These are the only two molecule whose deuterated isotope were studied. Since there is little change in the energy of the C-H stretch modes

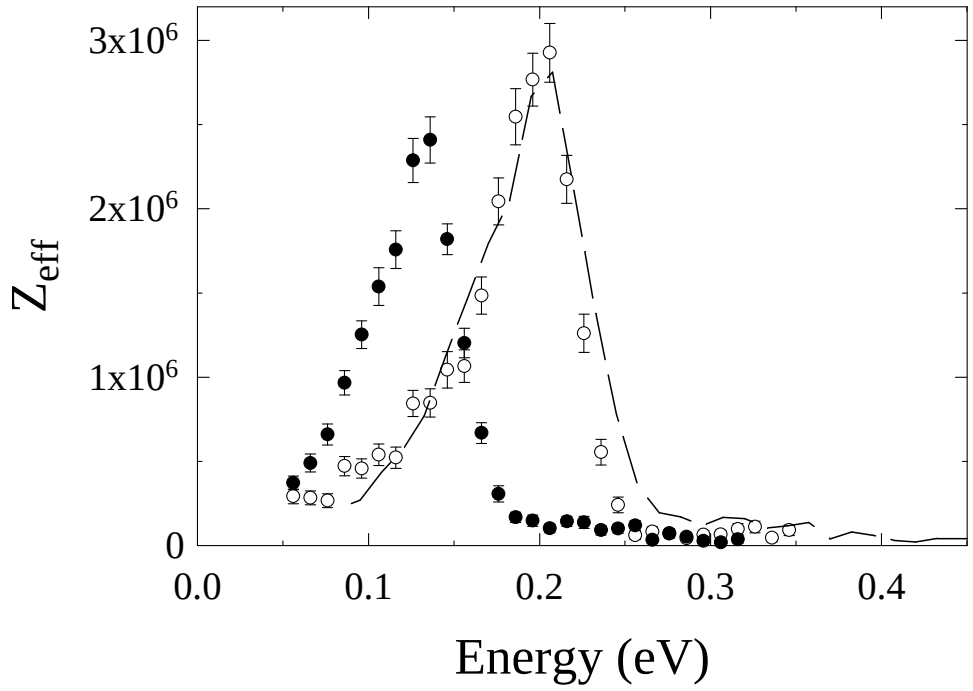

Figure 4.9: Positron annihilation rate, Z_{eff}, as a function of incident positron energy for nonane (○) and nonane-d_{20} (●) in the range of energies $50 \leq E \leq 450$ meV. Dashed line indicates Z_{eff} for nonane-d_{20} scaled for a reduced mass ratio, $\xi = 0.64$ and scaled in amplitude (by 1.167) to match the C-H peak for nonane.

for the two molecules [76], this agreement is encouraging. The magnitude of the shift may be used to identify the particular vibrational mode or modes associated with the resonance. As stated earlier, the ξ factor can be calculated from the motion of the atoms in the mode. In highly symmetric modes in alkanes, the carbon atom moves very little so the reduced hydrogen (deuterium) mass is equal to its actual mass. This would make ξ exactly 0.5 and predict a shift of 105 meV. On the other hand, in a mode in which all of the hydrogen (deuterium) atoms move together, the momentum of each carbon atom must cancel the momentum of approximately two hydrogen (deuterium) atoms. Taking the atomic weight of carbon as 12 amu, this makes ξ equal to $[2/(12+2)]/[4/(12+4)] = 0.57$. For this type of mode, the predicted shift is 90 meV, which is much closer to the observed value of 80 meV. This suggests that the mode excited is not the symmetric CH stretch, but rather one in which hydrogen atoms move out of phase.

4.7 Shape of the CH stretch resonance peak

Since the CH stretch vibrational resonance is well separated from the other features in the spectrum, we can analyze it in more detail. In spite of the differences in the magnitude and mean energy of the resonance peaks in these molecules, the *shape* of the CH stretch peak remains largely the same. Figure 4.10 shows the Z_{eff} spectra for two of the alkanes, propane (C_3H_8) and heptane (C_7H_{16}). Because of the effects described above, the spectrum for propane must be both scaled up in magnitude and shifted downward in energy. When this is done, the peak shapes match very well.

Also in Fig. 4.10, the peak shape is compared to a typical beam energy profile. The solid curve in that figure is the distribution of energies in a typical beam as measured by using the annihilation electrode as a retarding potential analyzer (see Sec. 3.3). The units are arbitrarily scaled for comparison with the Z_{eff} spectra. From this figure, it seems clear that, while the width on the high energy side of the peak can be attributed to the beam width, the low energy side shows broadening beyond the width of the beam. We are unable to determine whether this is the shape of a single resonance or whether it is due to the contribution of another of the several CH stretch modes with slightly lower energy.

This shape is reminiscent of the symmetric Feshbach resonance in dissociative attachment from CH_3I (see Fig. 4.4). There, the sharp edge on the high energy side was attributed to the opening of the inelastic channel, in which the electron vibrationally excites the molecule and still has enough energy to escape to the continuum [74]. However, in the case of resonances in the positron annihilation

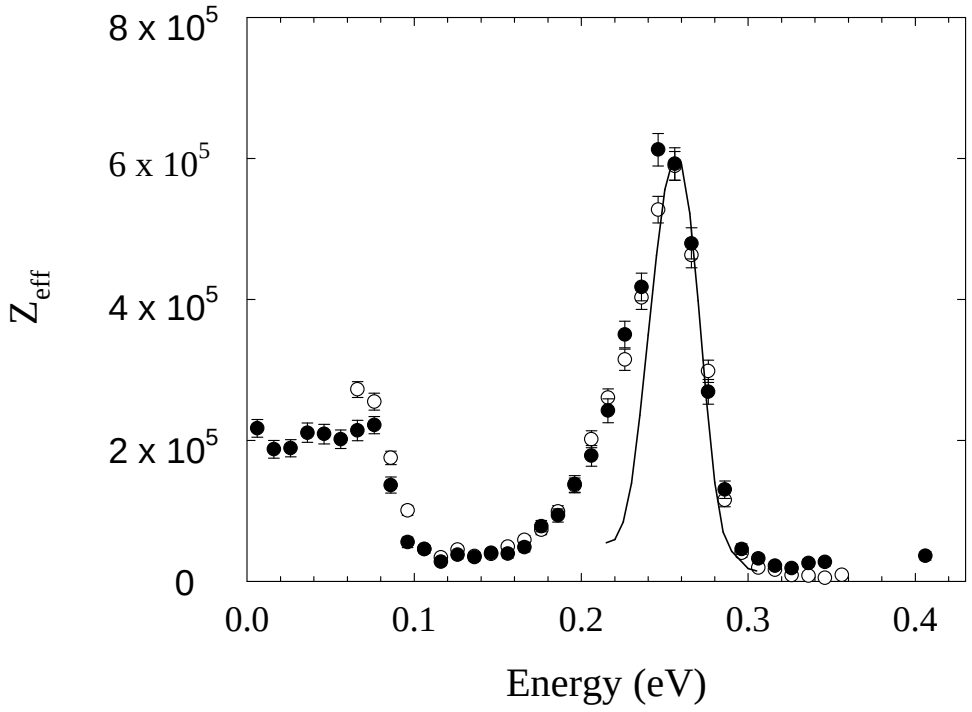

Figure 4.10: Z_{eff} for (•) propane (C_3H_8) and (○) heptane (C_7H_{16}). The spectrum for propane is scaled by a factor of 60 and shifted downward in energy by 100 meV (see text). The solid line is the energy distribution of positrons in the incident beam. It is arbitrarily scaled for comparison.

rate for large molecules, the peak can be downshifted by many tens of meV from the vibrational mode energy. The sharp edge is, therefore, well separated from the threshold for inelastic excitation. It seems clear that a different mechanism is at work in the positron case.

4.8 Factors affecting the magnitude of resonance features in Z_{eff}

The second change in the Z_{eff} spectrum as we move to larger molecules is a rapid increase in the magnitude of Z_{eff}. This strong dependence on molecular size was seen in earlier measurements using thermal distributions of positrons [44, 81].

To better understand the magnitude of Z_{eff}, we again follow an analysis similar to that used for resonances in electron scattering. Enhancement of the annihilation cross section via a Feshbach resonance state is given by the Breit-Wigner formula [87]

$$\sigma_{ann}(E) = \frac{\pi}{k^2} \frac{\Gamma_{ann}\Gamma_{cap}}{(E - E_r)^2 + (\frac{\Gamma_{tot}}{2})^2}, \tag{4.7}$$

where E_r is the energy of the resonant state, Γ_{ann} is the width of the Feshbach state due to positron-electron annihilation, Γ_{cap} is the width of the state due to escape through the same channel through which the positron entered and Γ_{tot} is the total width of the resonance state including contributions from all decay channels. By substitution into Eq. 3.4, Z_{eff} as a function of positron energy is

$$Z_{eff}(E) = \frac{v}{r_0^2 ck^2} \frac{\Gamma_{ann}\Gamma_{cap}}{(E - E_r)^2 + (\frac{\Gamma_{tot}}{2})^2}. \tag{4.8}$$

The Z_{eff} measured by the experiments in this thesis is actually a convolution of the energy distribution of the positron beam with Eq. 4.8. If the energy distribution is much broader than the width of the resonance, this convolution can be approximated by [27]

$$Z_{eff}(\text{measured}) = f(E_r) \frac{2\pi v}{r_0^2 ck^2} \frac{\Gamma_{ann}\Gamma_{cap}}{\Gamma_{tot}}, \tag{4.9}$$

where $f(E)$ is the energy distribution of the positron beam normalized according to $\int f(E)dE = 1$. For a beam with a gaussian energy distribution as in the experiments in this thesis, this expression reaches a maximum value when the mean positron energy is E_r.

The total width of the resonance state, Γ_{tot}, is the sum of the widths due to each of the possible decay channels of the state. This includes the decay to

annihilation as well as escape to the free positron state by deexcitation of the vibration:

$$\Gamma_{tot} = \Gamma_{ann} + \Gamma_{esc}. \tag{4.10}$$

Here Γ_{ann} is the width due to annihilation of the positron and Γ_{esc} is the total width due to all allowed channels involving escape of the positron to the contiuum. When this expression is substituted into Eq. 4.9, we find

$$Z_{eff}(\text{measured}) = f(E_r)\frac{2\pi v}{r_0^2 ck^2}\frac{\Gamma_{ann}\Gamma_{cap}}{\Gamma_{ann} + \Gamma_{cap} + \sum\Gamma_i}. \tag{4.11}$$

Here we have used that fact that Γ_{esc} is equal to $\Gamma_{cap} + \sum\Gamma_i$. The first term, Γ_{cap} is the width due to escape from the state by de-excitation of the same vibrational mode that was excited in trapping. Since this process is the inverse of the capture process, its rate (and hence its width) is the same. The result of escape to this channel is elastic scattering.

The second term, $\sum\Gamma_i$ represents escape by de-excitation of other vibrational modes. This process can be represented, for example, as follows

$$e^+(E) + A(\nu_1 = 0, \nu_2 = n) \longrightarrow (Ae^+)^* \longrightarrow e^+(E' < E) + A(\nu_1 = 1, \nu_2 = n-1). \tag{4.12}$$

It requires a target molecule with more than one vibrational mode and an experimental setup in which at least some target molecules are vibrationally excited prior to interaction with the positron. The situation in which this term is large will be considered in Sec. 7.2.

Of course, the actual *number* of resonances is also very important for comparison with the observed Z_{eff} spectrum. The experimental resolution of the experiment discussed here is often insufficient to distinguish between the various vibrational modes of the molecule. In butane, for example, the large peak associated with the CH stretch modes of the molecule could be due to the positron interacting with any of the ten CH stretch modes of the molecule, all of which fall within 20 meV of one another.

4.8.1 Estimating Γ_{cap}

In a simple perturbative estimate of the capture width, it is assumed that there exists a resonance state consisting of a positron bound to a vibrationally excited target molecule. This is represented as

$$|\Psi(\nu = n+1)\phi_{bound}\rangle, \tag{4.13}$$

where Ψ depends only on the position of the nuclei with ν refering to the vibrational level of a specific normal mode of the molecule and ϕ incorporates the

motion of the electrons and positron with the nuclei effectively fixed. With this notation, we intentionally imply the use of the Born-Oppenheimer approximation to separate the motion of the nuclei from that of the positron and electrons.

This state and the state consisting of the electronic ground state target and a free positron,

$$|\Psi(\nu = n)\phi_{free}(\mathbf{k})\rangle, \tag{4.14}$$

are both eigenstates of the elastic scattering Hamiltonian which neglects the dependence of the potential seen by the positron on the deviations of the nuclear positions. This dependence can then be restored perturbatively. For small vibrational amplitudes, the potential seen by the positron can be expanded as a Taylor series in the nuclear coordinates about the equilibrium position,

$$H(\mathbf{Q}) = H(\mathbf{Q_0}) + \frac{\partial H}{\partial Q_i}\delta Q_i + \frac{\partial^2 H}{\partial Q_i \partial Q_j}\delta Q_i \delta Q_j + ..., \tag{4.15}$$

where Q_i are the normal vibrational coordinates and sums over i and j are implied. For low amplitude vibrations, the largest perturbative term which couples $|\Psi(\nu = n+1)\phi_{bound}\rangle$ and $|\Psi(\nu = n)\phi_{free}(\mathbf{k})\rangle$ is

$$\langle\Psi(\nu = n+1)\phi_{bound}|\frac{\partial H}{\partial Q_\nu}\delta Q_\nu|\Psi(\nu = n)\phi_{free}(\mathbf{k})\rangle = \tag{4.16}$$

$$\langle\Psi(\nu = n+1)|\delta Q_\nu|\Psi(\nu = n)\rangle\langle\phi_{bound}|\frac{\partial H}{\partial Q_\nu}|\phi_{free}(\mathbf{k})\rangle. \tag{4.17}$$

The expression can be thus separated since H operates on the wave function in positron and electron position space and δQ_ν refers to the nuclear positions. The two parts of the wave function (ϕ and Ψ) can be separated in the Born-Oppenheimer approximation.

The first factor above can be evaluated by the standard quantum mechanical treatment of the harmonic oscillator (see section 2.3 in ref. [32]):

$$\langle\Psi(\nu = n+1)|\delta Q_\nu|\Psi(\nu = n)\rangle = \tag{4.18}$$

$$\langle\Psi(\nu = n+1)|i\frac{a_+ - a_-}{\omega\sqrt{2m}}|\Psi(\nu = n)\rangle = \tag{4.19}$$

$$\sqrt{\frac{(n+1)\hbar}{2m\omega}} \tag{4.20}$$

In the above expressions $a_\pm$ are the raising and lowering operators of the harmonic oscillator and m is the effective mass of the normal mode.

From Fermi's Golden Rule, the complete expression for Γ_{cap} in this approximation is

$$\Gamma_{cap} = \frac{2(n+1)\hbar\pi}{2m\omega}\left|\langle\phi_{bound}|\frac{\partial H}{\partial Q_\nu}|\phi_{free}(\mathbf{k})\rangle\right|^2 \rho(E) \tag{4.21}$$

Here, $\rho(E)$ is the density of free states in energy space. It depends on the normalization of ϕ_{free}. The careful evaluation of this expression would give an idea of the relative probabilities of (temporary) positron capture by the excitation of various vibrational modes (referred to by the index ν). However, this requires knowledge of the wave function of the positron-molecule complex and of the dependence of H on the nuclear positions.

As has been pointed out by Nishimura and Gianturco [67], one specific contribution to the potential seen by the positron can be examined further. At large distances, the potential is dominated by the effect of a permanent or vibrationally induced dipole when one exists. The contribution to Γ_{cap} from the coupling term with the longest range is given by

$$\Gamma_{cap}^{(dipole)} = \frac{2(n+1)e^2\pi\hbar}{2m\omega}\left(\frac{\partial p}{\partial Q_\nu}\right)^2 \left|\langle\phi_{bound}|\frac{cos(\theta)}{r^2}|\phi_{free}(\mathbf{k})\rangle\right|^2 \rho(E), \quad (4.22)$$

where p is the electric dipole moment of the molecule, θ gives the orientation of the moment with respect to the incoming positron and r refers to the positron position relative to the molecule. For vibrational modes with energy much greater than k_BT, the n can be dropped and, to compare with experiment, the expression should be averaged over all angles:

$$\Gamma_{cap}^{(dipole)} = \frac{2e^2\hbar}{2m\omega}\left(\frac{\partial p}{\partial Q_\nu}\right)^2 \int_0^\pi \left|\langle\phi_{bound}|\frac{\cos(\theta)}{r^2}|\phi_{free}(\mathbf{k})\rangle\right|^2 \rho(E) r\sin(\theta) d\theta. \quad (4.23)$$

This term is very similar to the rate of vibrational excitation by photon absorption. The cross section for photon absorption is given by [85]

$$\Gamma = \frac{8\pi^3}{3\hbar\omega}\left(\frac{\partial p}{\partial Q_\nu}\right)^2 \rho(E). \quad (4.24)$$

It also depends on the oscillator strength, $(\partial p/\partial Q_\nu)^2$, but is missing the multiplicative factor involving the matrix element. Figure 4.11 compares the Z_{eff} spectrum of propane to the measured photon absorption cross section multiplied by the square root of energy. The reason for the extra factor is that Z_{eff} relates to cross section as

$$\sigma \propto \frac{Z_{eff}}{\sqrt{E}}. \quad (4.25)$$

In the figure, the absorption rate is scaled for comparison to Z_{eff} and is also shown smoothed by convolution with a gaussian line shape of width 25 meV. Two points can be made about the discrepancy between the solid curve and the Z_{eff} data. First, Z_{eff} is directly proportional to Γ_{cap} only in the case where Γ_{cap} makes a negligible contribution to the denominator of equation 4.11. Where

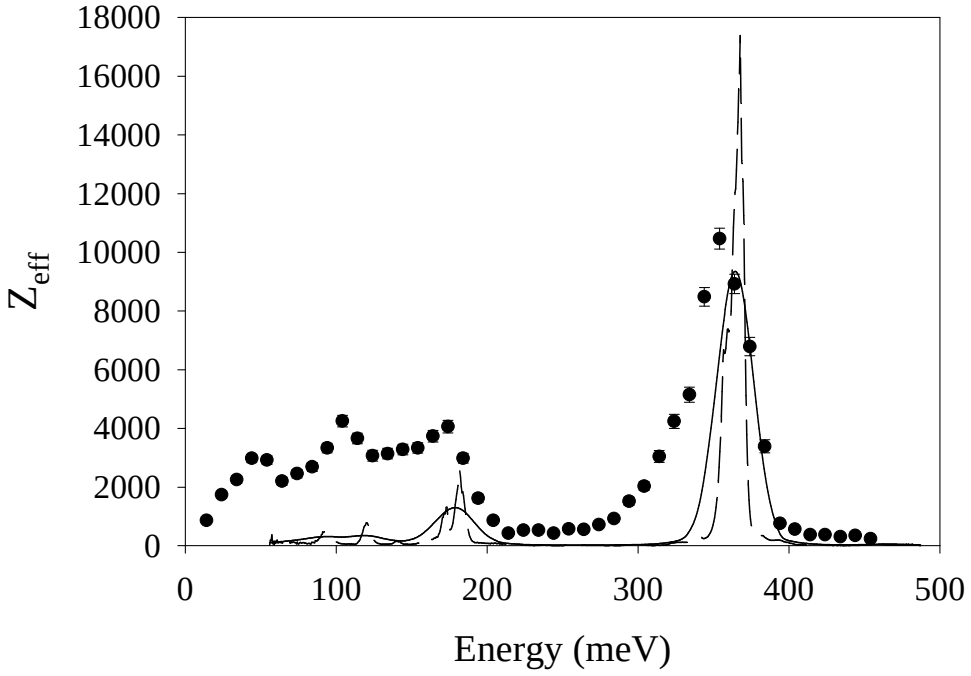

Figure 4.11: The Z_{eff} spectrum for propane (•) compared with the photon absorption rate for the same molecule multiplied by the square root of energy (dashed line, see text). The solid curve is the dashed curve convolved with a gaussian line shape with 25 meV width.

Γ_{cap} contributes in the denominator, the dependence of Z_{eff} on Γ_{cap} is weaker. Second, the energy dependence of the matrix element term (not present in the photon computation) may serve to enhance the magnitude of the resonances at lower energies. This term is difficult to investigate without an accurate computation incorporating the positron-electron interactions fully.

This type of analysis also explains the absence of resonances associated with vibrational overtones or combination modes. If we consider as our resonant state the state with bound positron bound to a doubly (vibrationally) excited target, then expression 4.18 is zero. Overtones or combination modes can be excited only in higher order approximation involving the

$$\frac{\partial^2 H}{\partial Q_i \partial Q_j} \delta Q_i \delta Q_j \tag{4.26}$$

term. If the expansion (Eq. 4.15) is perturbative, these terms are second order and the capture rates, Γ_{cap}, for these higher order modes are much smaller than for the fundamental modes.

We can also use Eq. 4.23 to predict the differences between the Z_{eff} spectra for alkanes and for their deuterium-substituted counterparts. Consider the CH stretch resonance in the spectra for butane and d-butane. Since the mode is the same and the molecules are electronically identical, the term

$$\left(\frac{\partial p}{\partial Q_\nu} \right)^2 \tag{4.27}$$

should be unchanged by deuteration. However, there is still an energy dependence in two places. The dependence is explicit in the factor

$$\frac{2e^2\pi}{2m\omega}, \tag{4.28}$$

and implicit in the factor

$$\left| \langle \phi_{bound} | \frac{\cos(\theta)}{r^2} | \phi_{free}(\mathbf{k}) \rangle \right|^2 d\theta. \tag{4.29}$$

The explicit term can be easily accounted for. Taking into account only this $1/\omega$ dependence, we expect the peak height in d-butane to be larger than that in butane by a factor of ~ 1.33. The measured ratio is 1.2. The comparison of nonane and deuterated nonane (C_9D_{20}) does not fit this analysis well. As can be seen in Fig. 4.9, the peak height for deuterated nonane is *smaller* than for nonane which is the opposite of the effect for butane. As in the comparison to the infrared spectrum, we have not considered either the energy dependence of the matrix element factor or the contribution of Γ_{cap} to the denominator in Eq. 4.11. These factors may account for the disagreement.

4.9 Z_{eff} below 50 meV

As previously discussed, due to other scattering processes, energy-resolved measurements with the trap-based beam at energies less than 50 meV are unreliable. We can, however, draw some conclusions about the behavior of Z_{eff} at very low energies from the comparison of previous results to these more recent measurements.

Figure 4.12 compares the maximum value of Z_{eff} in the energy-resolved spectrum to the measured value of Z_{eff} for a Maxwellian distribution of positrons at 300 K. For each of the alkanes molecules measured, this maximum occurs at the top of the resonance corresponding to the excitation of the CH stretch vibrational modes of the molecule. The values of Z_{eff} for thermal positrons are consistently a factor of about two lower than the height of the peak even as the values of Z_{eff} change by three orders of magnitude. This consistency between the two measurements suggests that, for the alkane molecules with at least two carbon atoms, vibrational Feshbach resonances are responsible for the large values of Z_{eff} at energies below 50 meV as observed in the earlier measurements using thermal positrons. This cannot be said of all of the molecules studied. I will present cases (Secs. 5.2 and **??**) for which Z_{eff} for low positron energies seems to be due to some other mechanism.

For alkanes with more than 8 carbons, the value of Z_{eff} for thermal positrons fails to rise as quickly as the height of the CH stretch peak (see Fig. 4.12). The ratio of the height of the CH stretch peak to the thermal Z_{eff} rises to ~ 5 for nonane (C_9H_{20}) and dodecane ($C_{12}H_{26}$) as compared with $\sim$2 for the smaller alkanes. We believe the reason for this is the depression in the linear mode spectrum between the CH stretch modes (360 meV) and the CH scissors modes (180 meV). This can be seen for butane (C_4H_{10}) in Fig. 4.1. The absence of vibrational modes in this range of energies causes the dip in Z_{eff} at about 200 meV in butane. As the molecules increase in size and the positron binding energy increases, this dip moves downward in energy. For nine carbons, the binding of the positron has moved this depression into the range of the thermal distribution at 300 K. The thermal Z_{eff} is therefore reduced compared with the height of the CH stretch peak. Note that, in Fig. 4.7, the thermal Z_{eff} (shown as an arrow on the ordinate axis) is within a factor of two of the value of Z_{eff} at the lower end of the energy-resolved spectrum for nearly all of the alkanes measured.

A maximum Z_{eff} for methane (CH_4) is not shown in Fig. 4.12. The spectrum for methane is very different from that of the other alkanes. It will be presented and discussed in Chap. 5.

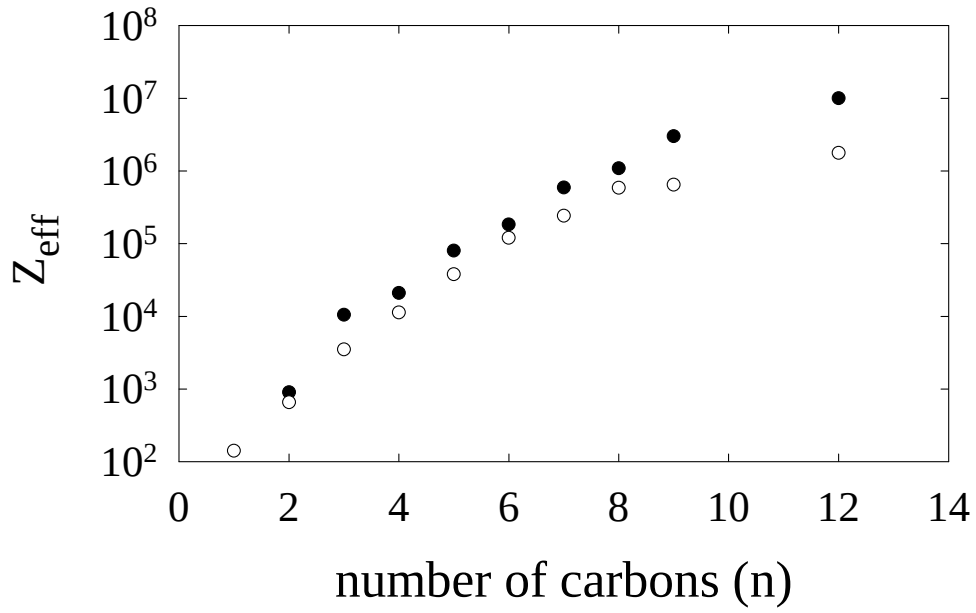

Figure 4.12: A comparison of the maximum value of Z_{eff} in the energy-resolved annihilation spectra (•) with Z_{eff} as measured for a Maxwellian distribution of positrons at 300 K (○). The full energy-resolved spectra are presented in Fig. 4.7. The data for thermal positrons are taken from a number of sources [35,38,41,52,70,86] and compiled together in Ref. [40].

Table 4.2: Values of Z_{eff} for various fluoro-alkanes, fluoro-alkenes and fluorobenzenes for thermal distributions of positrons at 300 K. Where multiple values appear, they indicate Z_{eff} for different structural isomers. Data taken from Ref. [40].

Group	No F	1 F	2 F's	3 F's	4 F's	5 F's	Perfluoro-
Methane	142	1,390	799	247	54.4		54.4
Ethane	660	3,030		1,600 1,510	1,110	467	149
Propane	3,500		8,130	3,350			
Hexane	120,000	269,000					535
Benzene	15,000	45,100	32,800 13,100	10,100	2,760	1,930	1,200

4.10 Effects of fluorine substitution on Z_{eff}

The changes in Z_{eff} with halogen substitution are summarized in table 4.2. These effects have remained largely unexplained although a few models have been put forward [28]. As explained in Sec. 2.7, previous data using thermal distributions of positrons established that, for the alkanes, the replacement of a single hydrogen atom with a fluorine atom ($C_nH_{2n+1}F$) increases Z_{eff} for positrons with energy below 50 meV. The effect can be as large as a factor of ten in smaller alkanes and tends to be less dramatic for larger molecules. The substitution of two fluorine atoms ($C_nH_{2n}F_2$) tends to decrease Z_{eff} from the value for the singly fluorinated compound, but not to the level of the fully hydrogenated compound. The value of Z_{eff} continues to decrease as more fluorine atoms are substituted. In most cases, the fully fluorinated (perfluoro-) alkane exhibits a Z_{eff} significantly smaller than that of the fully hydrogenated equivalent. Refer to Table 4.2 for a more complete list of these Z_{eff} values.

We make one small observation. Table 4.2 lists two Z_{eff} values for difluorobenzene. For these isomers, Z_{eff} for thermal positrons changes greatly depending on the relative positions of the two fluorine atoms. When the fluorine atoms are attached to adjacent carbons, Z_{eff} is 32,800. When the fluorines are separated by one or more methyl groups, Z_{eff} drops to less than 14,000 [39]. This phenomenon has not been explained.

4.10.1 Energy-resolved Z_{eff} spectra for fluoro-alkanes

Fig. 4.13 shows the Z_{eff} spectra for 1-fluorohexane and 1-fluorononane. These molecules differ from the alkanes, hexane and nonane, only by the substitution of one hydrogen atom (attached to the first carbon) with a fluorine atom. The substitution is specifically for a hydrogen atom which is part of the methyl (CH_3) groups at either of the two ends of the molecule. The effect on Z_{eff}, however, is quite dramatic. In both cases, we see a dramatic reduction in the magnitude of the peak associated with the CH stretch vibrational mode. For each, some of the CH stretch resonance remains. In 1-fluorohexane, the peak is reduced by a factor of more than twenty. In 1-fluorononane, the effect is less pronounced, reducing the height of the resonance peak by a factor of two or three.

A remarkable observation in the spectrum for nonane, where the CH stretch resonance is still clearly visible, is that the energy position of the resonances seems not to have changed significantly. Since it is from the position of the resonance that we extract our measurement of the binding energy of the positron-molecule complex, we interpret this to mean that the positron is bound to the molecule just as strongly as in the case of the fully hydrogenated molecule.

We can compare the infrared absorption of these molecules to investigate how much of this reduction in Z_{eff} can be attributed to changes in the dipole oscillator strength of the vibrational mode. Figure 4.14 shows the infrared absorption spectra for 1-fluorohexane and for hexane. These measurements were taken using a simple Fourier transform infrared spectrometer. The samples were diluted to 0.2 molar concentration in a carbon disulfide solvent. Unfortunately, the exact path length of the sample holder is not known and therefore absolute molar absorptivities cannot be determined. However, since the setup was the same for all four molecules, the *relative* magnitudes are reliable. The background due to the solvent was measured and subtracted to obtain the data in the figure.

We can see, as expected, that the infrared absorption is largely unchanged with a single fluorine substitution. The slight reduction in the spectra for the fluorinated molecules is likely due to a reduction in the *number* of CH stretch modes by one.

As can be seen from Eq. 4.11, the height of the resonance peaks in the Z_{eff} spectrum can be reduced by decreasing positron-electron overlap (represented by Γ_{ann}), reducing coupling from the free state to the the positron bound state (Γ_{cap}) or increasing escape to one or several alternate channels (Γ_i). The analysis in Sec. 4.8.1 breaks Γ_{cap} down further into several factors (Eq. 4.23). The first is constant if the peaks compared are at the same energy. Changes in the second term should be reflected in the photon absorption spectrum. In Fig. 4.14 we

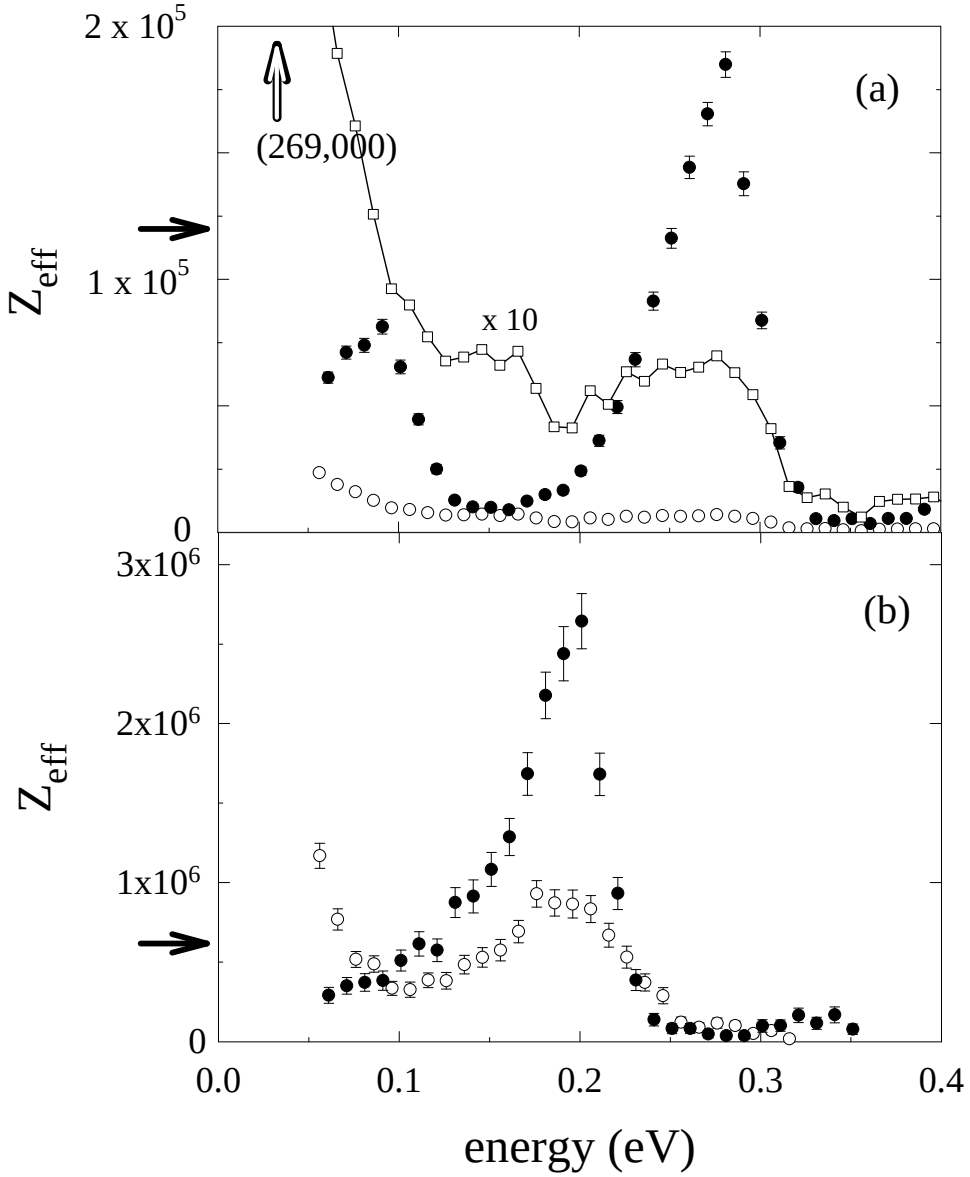

Figure 4.13: The energy-resolved Z_{eff} spectra for (a, ○) 1-fluorohexane ($C_6H_{13}F$), and (b, ○) 1-fluorononane ($C_9H_{19}F$), compared with their fully-hydrogenated equivalents, (a, •) hexane (C_6H_{14}) and (b, •) nonane (C_9H_{20}). In plot (a), the squares indicate the data for 1-fluorohexane multiplied by 10. The arrows on the ordinate indicate the value of Z_{eff} for a room temperature thermal distribution of positrons. The annihilation rate for 1-fluorononane has not been measured using thermal positrons.

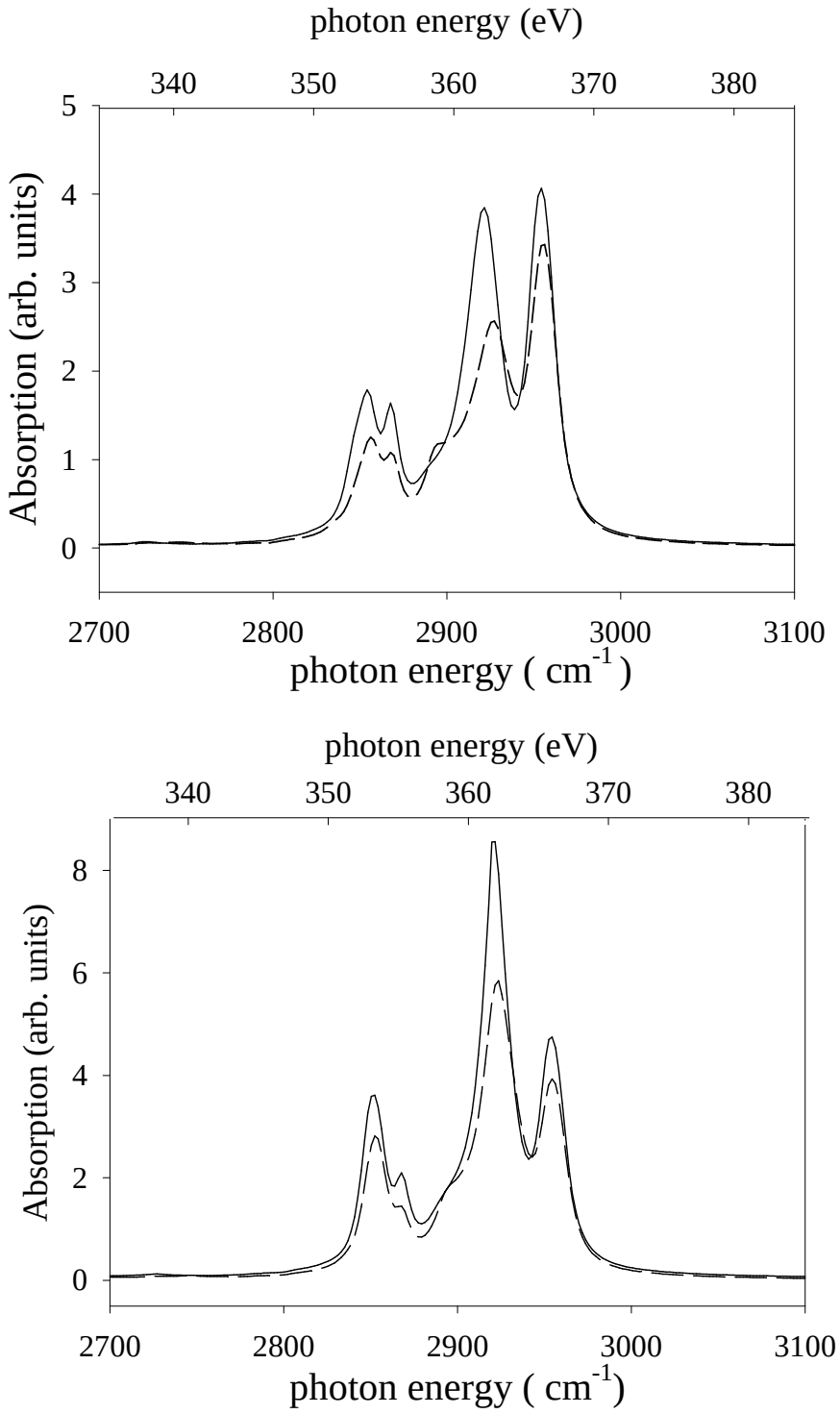

Figure 4.14: (above) Infrared absorption for hexane (—) and 1-fluorohexane (- -) over the range of the CH stretch vibrational energies. (below) IR absorption for nonane (—) and 1-fluorononane (- -). The units of absorptivity are arbitrary, but are the same for all four molecules (see text).

showed that the photon absorption is slightly weakened by fluorine substitution, but by no means to the degree that Z_{eff} is reduced. The third term has a complicated dependence on the shape of both the bound state and the scattering wavefunction for positrons incident on the target with fixed nuclei.

The other major effect from single fluorination of large molecules is an increase in Z_{eff} for positrons with very low energy. In the spectra for 1-fluorononane [Fig. 4.13 (b)], Z_{eff} rises as the energy of the positron decreases at the lower end of the experimental range. Although it is not visible in the energy-resolved spectrum, the same effect seems to be at work in 1-fluorohexane. The evidence for this is seen in the Z_{eff} value for thermal distributions of positrons. The thermal Z_{eff} of 269,000 is significantly larger than any of the energy-resolved structure. This phenomenon is not well understood. If this large signal is to be attributed to low-lying Feshbach resonances, it must be explained why the resonances at low energy are enhanced while the high energy resonances are suppressed. On the other hand, the magnitude of the low energy enhancement seems too large to be due to interaction with a near zero energy state as discussed by Goldanskii and Sayasov [24], and Gribakin [28].

4.10.2 Doppler-broadening of annihilation radiation for fluoroalkanes

An analysis of the doppler-broadened widths of the annihilation radiation from fluoroalkanes suggests that the positron annihilates electrons in the C-H bonds and those in the C-F bonds with equal probability. In reference [43], Iwata and collaborators have studied the width of annihilation radiation for fluorine-substituted alkanes. They fit the shape of the annihilation spectrum using as a fit parameter the fraction of annihilation with electrons attached to the fluorine atoms (as opposed to the hydrogen atoms). This analysis indicates that positron annihilate with approximately equal probability on all valence electrons. This seems to rule out models which involve localization of the positron wave function near either the fluorine or hydrogen atoms.

4.11 Effects of double and triple bonds on Z_{eff}

To this point, we have considered only hydrocarbons with single bonds. In Fig. 4.15 we compare the spectrum of ethane (H_3C-CH_3) with that of ethylene (H_2C=CH_2) and acetylene(HC≡CH). The familiar CH stretch resonance is present in ethane, is reduced in ethylene, and is absent or beneath the resolution of the experiment in acetylene. We note that this reduction in the height of the

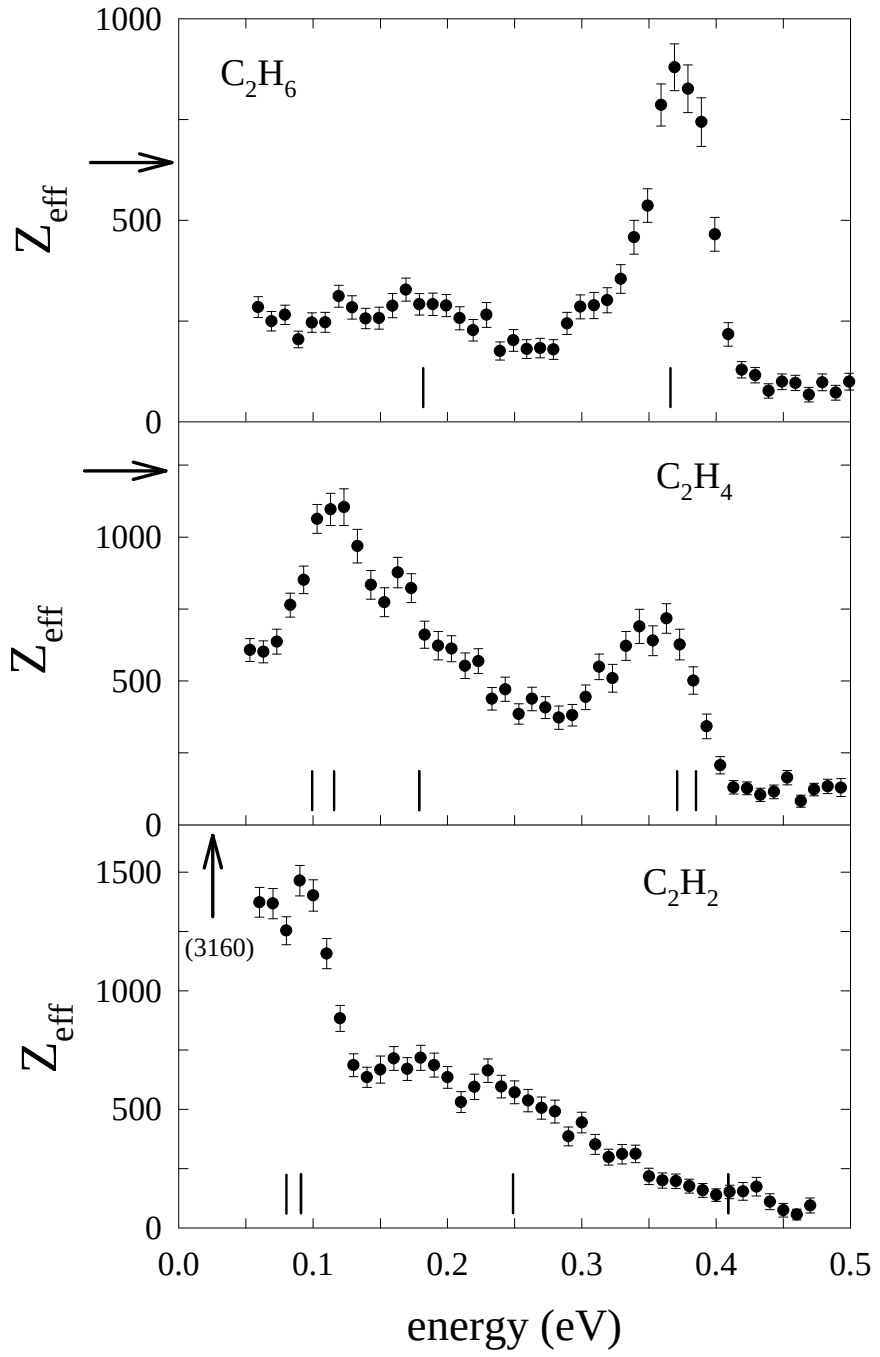

Figure 4.15: The energy-resolved Z_{eff} spectrum for (a) ethane (H_3C-CH_3), (b) ethylene ($H_2C{=}CH_2$) and (c) acetylene($HC{\equiv}CH$). Vertical lines on the abscissa indicate some of the vibrational modes of the molecules. Data from reference [23].

peak is nearly commensurate with the reduction in the number of CH stretch modes of the molecule. The CH stretch peak of height ∼900 in ethane should be reduced to 600 in ethylene and to 150 in acetylene just to compensate for the reduced number of modes.

It is not as easy to explain the appearance of the resonance near 100 meV in ethylene or the dramatic enhancement at low energies in acetylene. As indicated by the arrows on the ordinate in Fig. 4.15, Z_{eff} for low energy positrons increases as the number of hydrogen atoms is reduced and the CC bond is strengthened.

4.12 Molecular isomers

Changing the shape of the molecule, without significantly changing the chemical composition, seems to have little effect on the Z_{eff} spectrum. One example of this can be seen in the comparison of pentane($CH_3(CH_2)_3CH_3$) and 2-methylbutane ($CH_3(CH_2)_2(CH_3)_2$). The Z_{eff} spectrum for each molecule as well as the Kekulé structures for these molecules are shown in Fig. 4.16. The spectra near the CH stretch resonance are identical to within the experimental resolution. The two spectra begin to deviate at lower positron energies and it is clear from the measurements with thermal positrons that such deviation continues below 50 meV. By changing the shape of the carbon "backbone" of the molecule, we have changed the positions and character of the vibrational modes. The differences are most notable at low energies where modes often involve motion of the carbon atoms themselves. We therefore might expect some deviation in the Z_{eff} spectra at these energies.

The fact that no change was seen in the resonance associated with the CH stretch modes points to the fact that the positron bound state wave function is largely the same for the two molecules. This is further evidence that the positron interacts with the molecule as a whole and has a diffuse wave function primarily outside the electron cloud.

4.13 Z_{eff} for ring hydrocarbons

Annihilation studies of ring hydrocarbons can potentially give us some insight into the importance of the terminal CH_3 groups and of the motion of the carbon backbone of molecules. To this end, we made measurements of Z_{eff} for benzene (C_6H_6) and cyclohexane (C_6H_{12}). The nuclear positions of these molecules are presented in figure **??**. Cyclohexane contains only single bonds with two hydrogens bonded to each carbons atom, whereas benzene has some double bonding

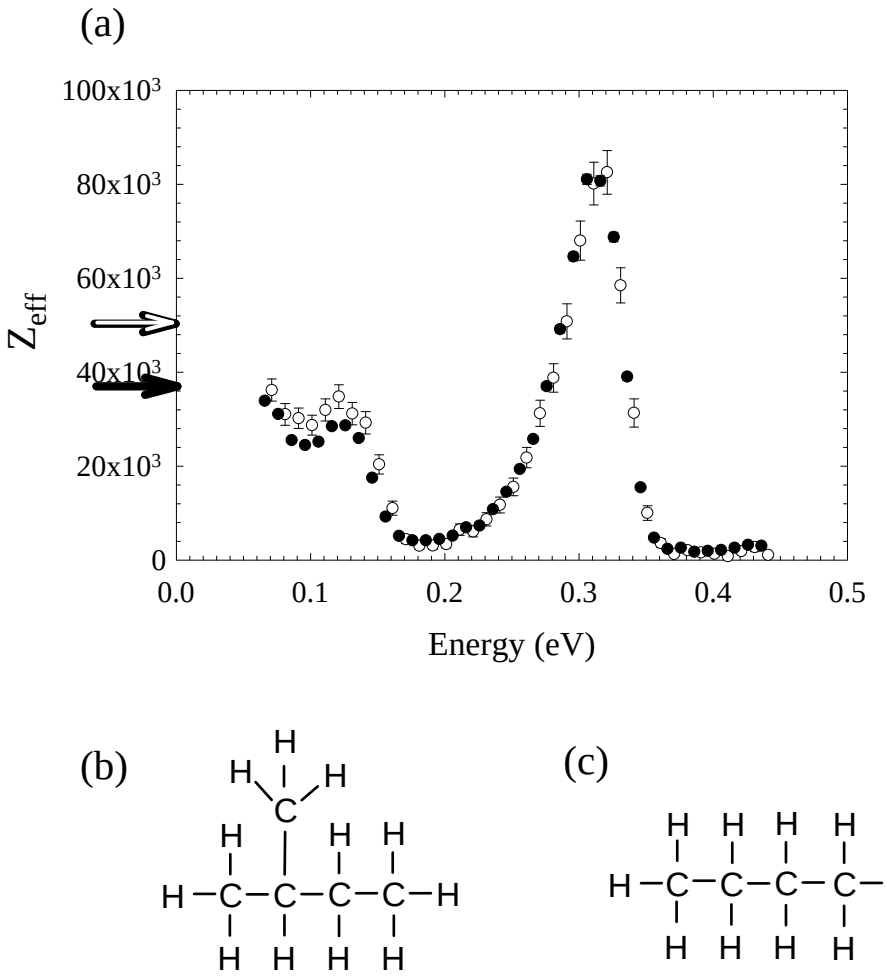

Figure 4.16: (a) The energy-resolved Z_{eff} spectrum for (○) 2-methylbutane (isopentane) and (●) pentane. Both molecules have the chemical formula C_5H_{12}. Arrows on the ordinate axis indicate Z_{eff} for thermal distributions of positrons.
(b) The Kekulé structure for 2-methylbutane, also known as isopentane.
(c) The Kekulé structure for pentane.

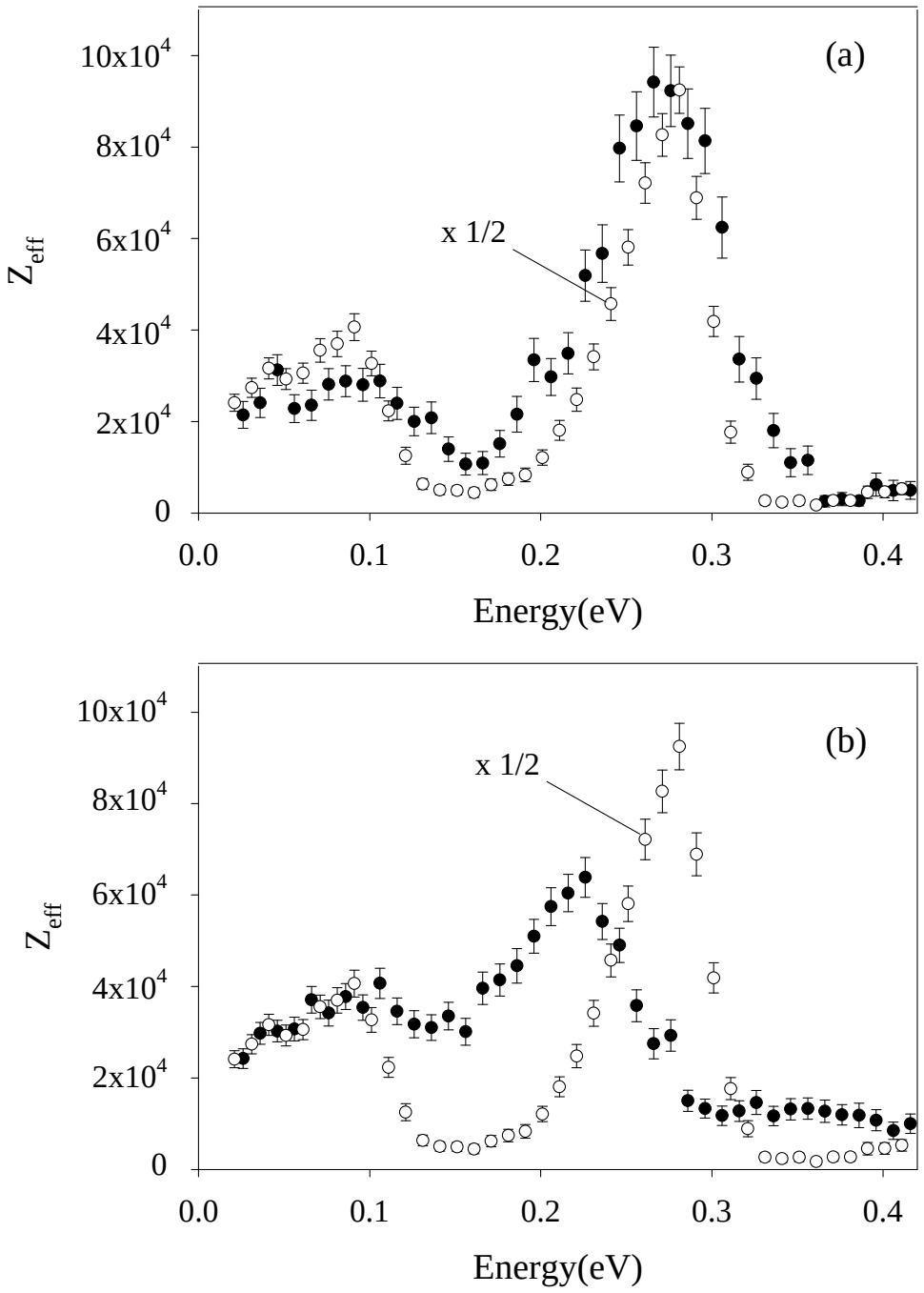

Figure 4.17: The energy-resolved Z_{eff} spectra for (a, •) cyclohexane (C_6H_{12}); and (b, •) benzene (C_6H_6). In both figures, the open circles are the data for hexane (C_6H_{14}) scaled by 0.5 for ease of comparison.

between carbons and only one hydrogen per carbon atom. These data are shown in Fig. 4.17.

For both of these examples, the overall magnitude of Z_{eff} is significantly smaller than for the linear hexane (C_6H_{14}). Examining the oscillator strengths of the various modes for the molecules (Fig. 4.18) gives some explanation. Benzene, of course, has half as many CH stretch modes as the other two molecules. This is evident in the predicted IR spectrum. This seems to adequately explain the reduction in the magnitude of the CH stretch resonance in the Z_{eff} spectrum for benzene.

Cyclohexane, on the other hand, has nearly the same number of CH stretch modes as hexane and, as can be seen in Fig. 4.18 the modes are predicted to be just as infrared active. It is strange, then, that the CH stretch peak in the Z_{eff} spectrum for cyclohexane is so much smaller than for the linear n-hexane. This perhaps indicates that the terminal methyl (CH_3) groups are important to VFR enhancement of Z_{eff}.

Another important result in the comparison of the three six-carbon molecules is the energy position of the largest resonant enhancement. While the largest peak in the spectra for hexane and cyclohexane are at approximately the same mean energy, the peak for benzene appears at a much lower energy. In light of our vibrational Feshbach resonance model, we interpret this to mean that the positrons are more strongly bound to the benzene molecule than to the other two molecules.

One possible reason for this is the planar shape of the benzene molecule. Three-dimensional renderings of cyclohexane and benzene are shown in Fig. 4.19. The planar shape of the benzene molecule gives an approaching positron access to large, diffuse electron clouds above and below the plane of the molecule. Hexane and cyclohexane are much closer to an effective sphere. We conjecture that the presence of these accessible electron clouds enables large positrons binding.

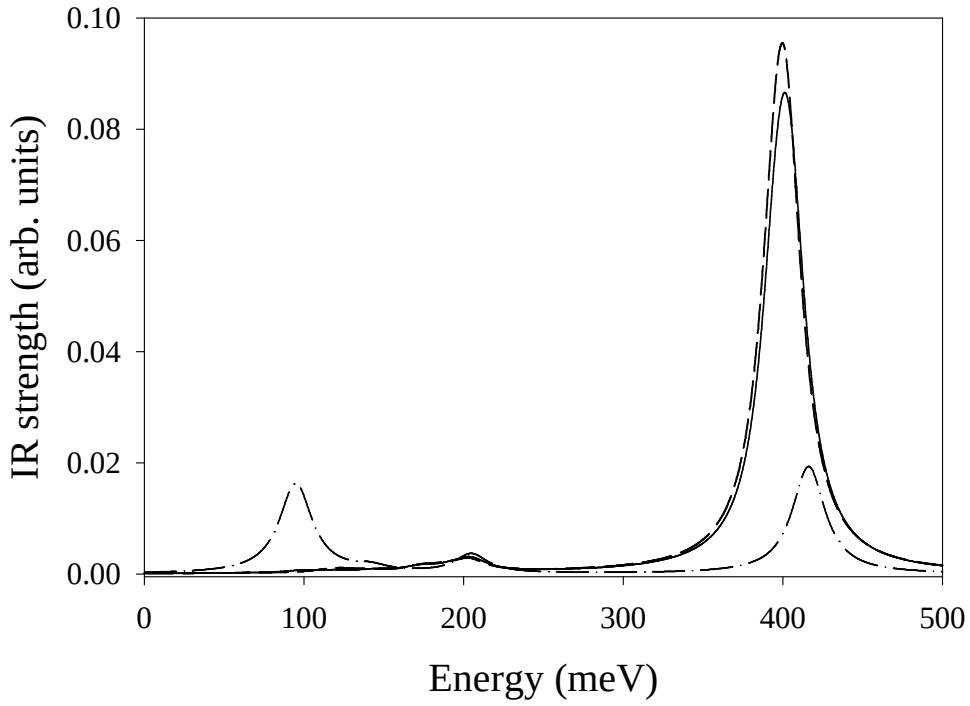

Figure 4.18: The infrared absorption spectrum for hexane (—), cyclohexane (– –) and benzene (– · –) as computed using the GAMESS quantum computational package [73].

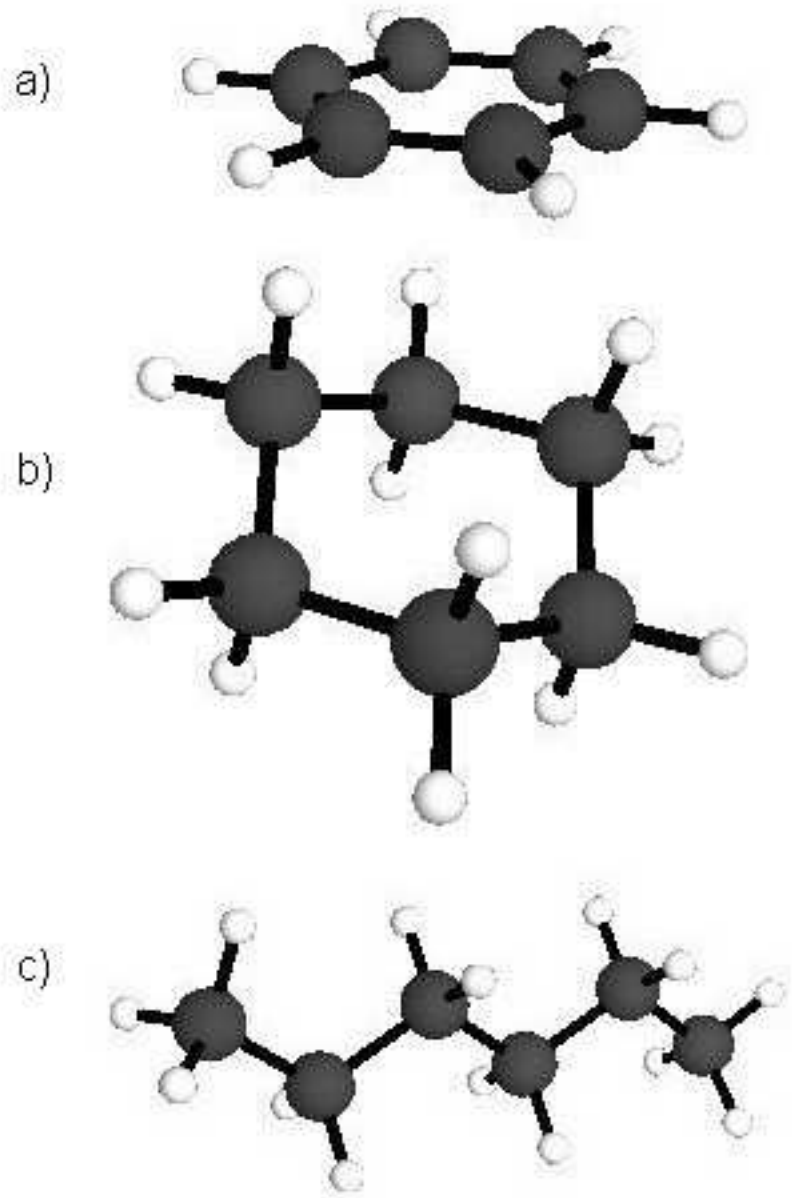

Figure 4.19: Three dimensional renderings of a) benzene; b) cyclohexane; and c) hexane as generated by MacMolPlot [5].

Chapter 5

Annihilation for Smaller Molecules

Large numbers of particles, combined with the difficulty of incorporating the positronium channel, make accurate calculations for the large alkanes very challenging. To better connect with computational models of positron annihilation, we have measured energy-resolved Z_{eff} for some smaller molecules including methane, the fluoromethanes, noble gases and ammonia. In this chapter, I also discuss Z_{eff} for positrons in the energy range between the vibrational modes and the threshold for positronium formation.

5.1 Z_{eff} for methane

As mentioned previously, methane (CH_4), the smallest of the alkanes, has a Z_{eff} spectrum very different from the spectra of the other alkanes. The energy-resolved Z_{eff} spectrum for methane is shown in Fig. 5.1. In contrast to the other alkanes, the spectrum has no visible resonance features. Also, Z_{eff} is much smaller than for the other alkanes, which is consistent with the trend seen for the larger alkanes. In light of the trend in positron binding energies for the alkanes, it is not surprising that the spectrum for methane shows no vibrational Feshbach resonances. Extrapolation of the data in Fig. 4.8, would predict the binding energy for methane to be -30 meV (i.e. an unbound state).

Since methane does not exhibit vibrational Feshbach resonances, it is a good case in which to consider other possible contributions to Z_{eff}.

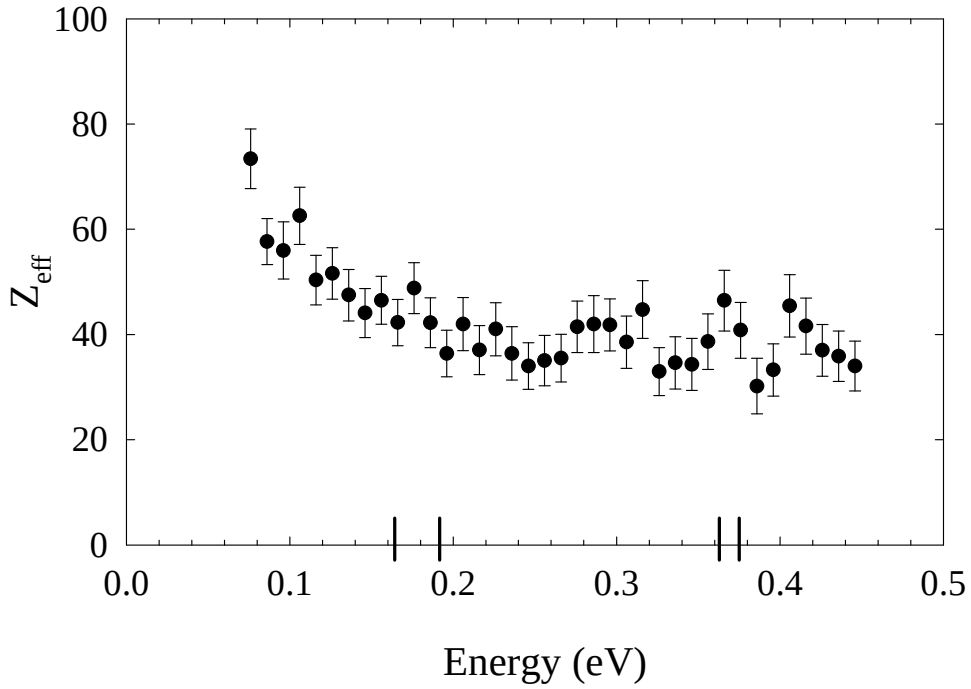

Figure 5.1: The energy-resolved Z_{eff} spectrum for methane (CH_4). The lines on the abscissa indicate the energies of all of the fundamental vibrational modes of methane. The value of Z_{eff} for methane measured using thermal distributions of positrons is 142.

5.2 Z_{eff} at very low positron energy

A recent treatment of positron annihilation on molecules by Gribakin suggests that Z_{eff} may be enhanced at very low energies due to a low-lying positron virtual state or a weakly bound state [28]. He proposes to estimate Z_{eff} by assuming that annihilation occurs only in a thin shell at the outer edge of the electron wave function. By using the asymptotic form of the scattered positron wave function to compute the overlap of the positron and electron wave functions (see Ref. [28]), he concludes that, for low energy positrons, there is a contribution to Z_{eff} proportional to the elastic scattering cross section. If there exists a state of the positron-target system with energy either slightly above or slightly below zero, this cross section may become very large for low energy positrons. Specifically,

$$Z_{eff} \propto \frac{1}{E + |\varepsilon_0|} \tag{5.1}$$

where E is the energy of the incoming positron and ε_0 is the energy of the positron-target state. As ε_0 moves closer to zero, the scattering length diverges and Z_{eff} becomes very large.

This mechanism is independent of the enhancement due to vibrational Feshbach resonances and so, in principle, both mechanisms can be operative for a single target.

For comparison, it is simplest to study a target with absent or very small resonant enhancements. Methane (CH_4) and carbon tetrafluoride (CF_4) are two examples of molecules for which no resonances have been observed. Figure 5.2 shows the Z_{eff} spectra for methane and carbon tetrafluoride (CF_4). For both molecules, the Z_{eff} spectra has been fit to a function consistent with equation 5.2

$$Z_{eff}(E) = \frac{A}{E + B} + Z_{eff}^{(dir)} \tag{5.2}$$

where A and B are fit parameters and $Z_{eff}^{(dir)}$ is the non-resonant contribution to Z_{eff} which we take to be equal to the Z_{eff} measured for positron energy larger than 1 eV. This non-resonant contribution is 20 for methane and 10 for CF_4 and is independent of positron energy. (This Z_{eff} for higher positron energies is interesting in itself and is the subject of Sec. 5.6.)

The fit (Eq. 5.2) is subject to the additional constraint that it be appropriate to produce the measured value of Z_{eff} for a room temperature thermal distribution of positrons. That is

$$Z_{eff}(T = 300\text{K}) = \frac{2}{\sqrt{\pi}}(k_b T)^{-3/2} \int \left(\frac{A}{E + B} + Z_{eff}^{(dir)} \right) \exp(-E/k_b T) \sqrt{E} dE. \tag{5.3}$$

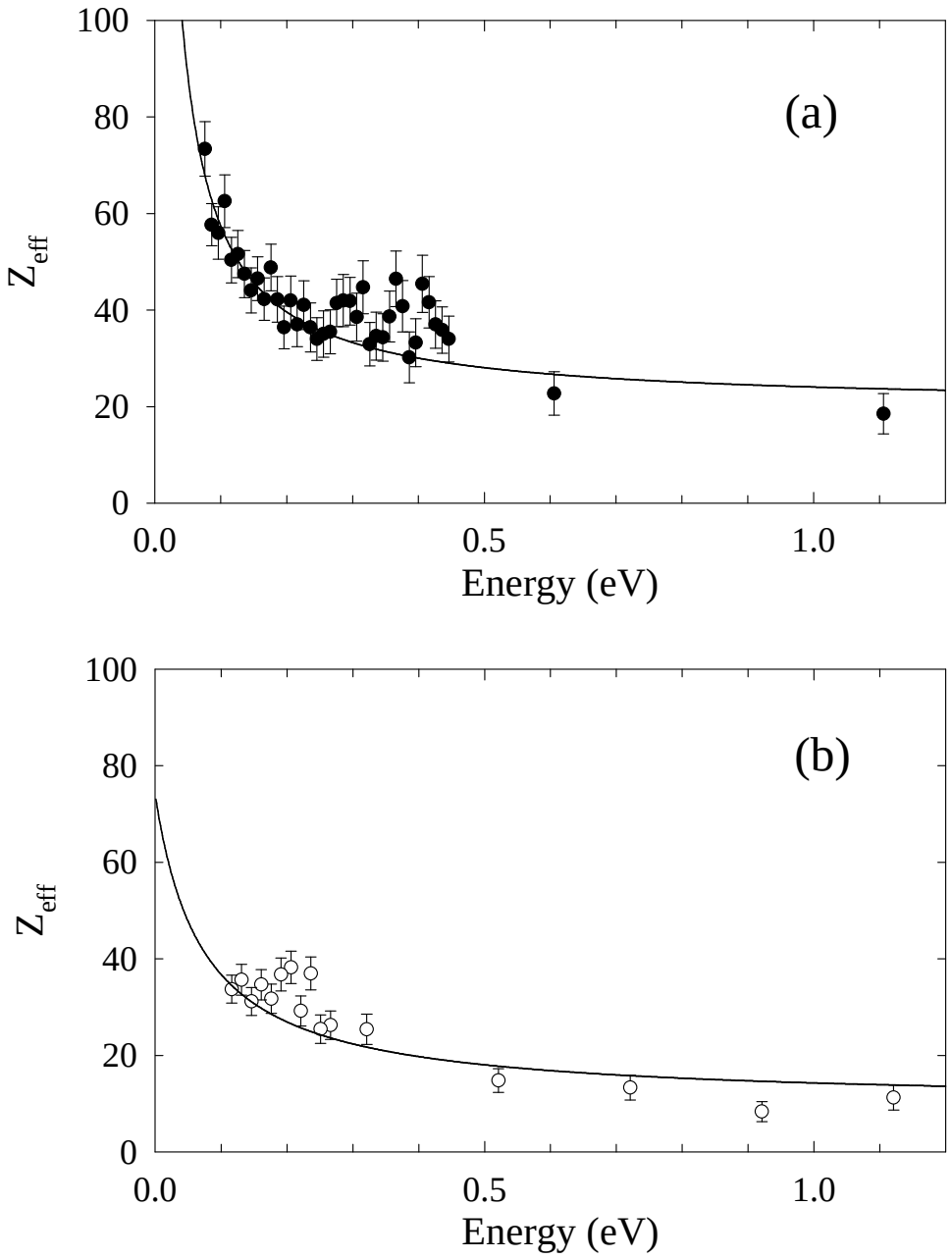

Figure 5.2: Z_{eff} for methane and carbon tetrafluoride (CF_4). The solid lines indicate fits to the functional form in Eq. 5.2. The parameters, A and B, for the curves shown are $A = 4.1$ and 4.6 and $B = 10$ meV and 80 meV for methane and carbon tetrafluoride, respectively (see text). This figure was previously published in reference [57].

With only one remaining degree of freedom, the best fit occurs when $A = 4.1$ and 4.3 and $B = 10$ meV and 80 meV for methane and CF_4, respectively. This indicates a positron-molecule state with energy $\pm$ 10 meV for methane and $\pm$ 80 meV for CF_4. Because a virtual state and a bound state give the same contribution to Z_{eff} it is impossible to determine the sign of the energy [57].

These values can be compared to an analysis by Gribakin [28]. By fitting the trend in Z_{eff} for the fluoromethanes, Iwata *et al.*, based on the Gribakin model, predicted a bound state for methane with energy -28 meV and an unbound or virtual state for carbon tetrafluoride with energy 170 meV. According to this model, fluorine substitution makes the molecular potential less attractive to a positron. The reason Gribakin advances for the increase in Z_{eff} from the first fluorine substitution is that a deeply bound positron state is moved closer to zero energy as the potential becomes less attractive. Further fluorination then moves the state beyond and above zero reducing Z_{eff} for low positron energies.

While the spectrum shown in Fig. 5.2 is consistent with this picture (i. e. a bound state with energy -10 meV), the trend of binding energies for the alkanes as shown in Fig. 4.8 would indicate not a bound state, but a *virtual state* of energy $\sim$ 30 meV. In this line of reasoning, further fluorination would lead to a higher energy virtual state and therefore predict that Z_{eff} would decrease monotonically with the number of fluorine atoms. Thus, the Iwata analysis and the extrapolated binding energy from energy-resolved data lead to different conclusions with regard to positron binding to methane. Related to this discussion, in the next section, we present energy resolved annihilation rates for the fluorine-substituted methanes.

5.3 Fluoromethanes

Figure 5.3 shows the energy resolved annihilation rate for all of the fluorinated methanes. As is seen for fluorination of other molecules, the first fluorine substitution increases Z_{eff} dramatically. Subsequent fluorination reduces Z_{eff} until it is smaller in overall magnitude than for methane, the fully hydrogenated molecule.

As mentioned earlier, methane is the only one of the alkane molecules not found to exhibit resonant enhancements of Z_{eff} in the range of the molecular vibrations. However, with the substitution of one hydrogen with a fluorine to make CH_3F, a resonance appears centered at 155 meV. This resonance persists for the fluoromethanes with more fluorine atoms, although its magnitude is reduced.

It is difficult to assign this resonance to a particular vibrational mode since

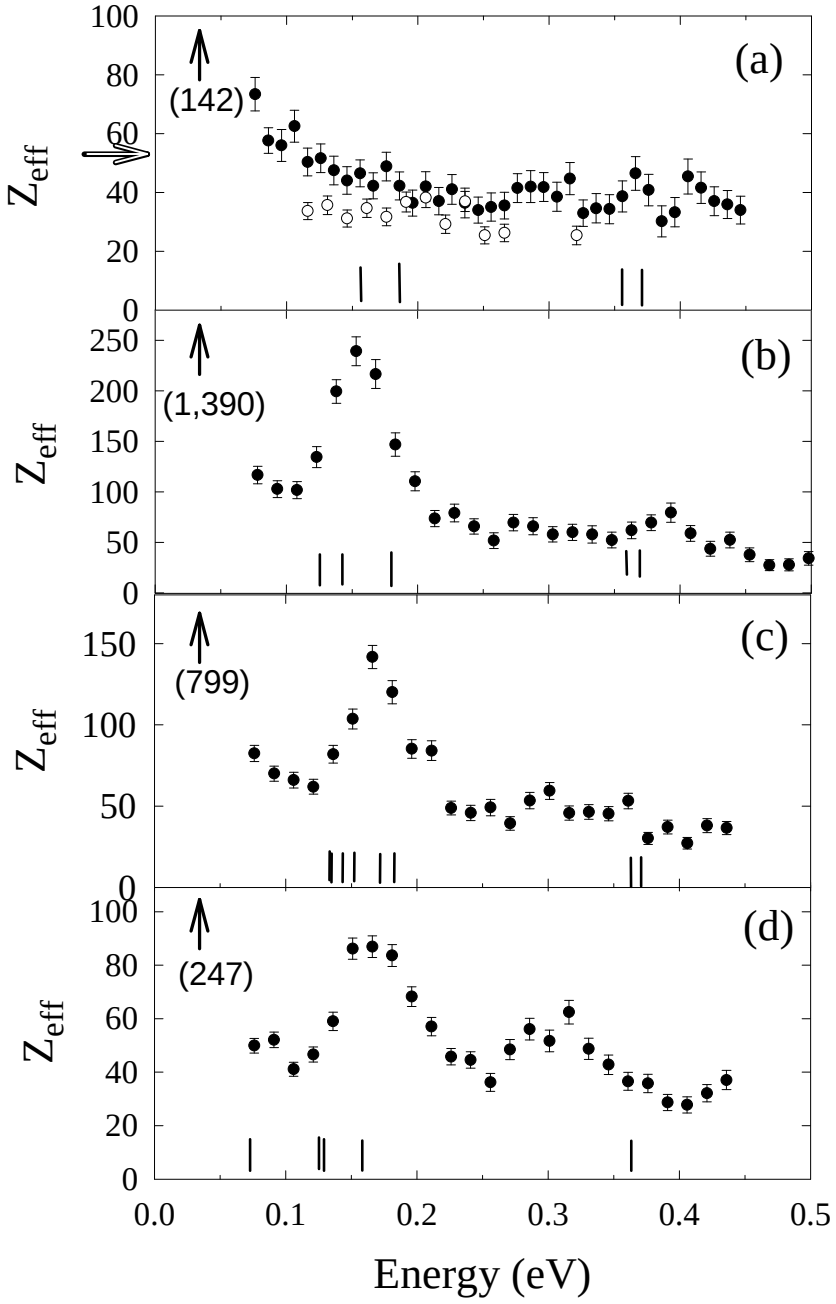

Figure 5.3: Z_{eff} for (a) CH_4 (•) and CF_4 (○), (b) CH_3F, (c) CH_2F_2 and (d) CHF_3. Vertical lines indicate the vibrational modes of the molecules. In (a), only the modes for methane (CH_4) are shown. The values of Z_{eff} for Maxwellian distributions of positrons (300 K) are shown on the ordinate axes.

it lies between the CF stretch mode at ∼130 meV and the CH deformation modes at ∼180 meV. The CF stretch mode is at lower energy than the center of the resonance which seems to conflict with some aspects of the vibrational Feshbach model (see Sec. 5.5 for a more thorough discussion of the position of the resonance in methyl fluoride). This would indicate that the CH deformation modes near 180 meV are mediating positron trapping in this case. However, we note that the infrared absorption signal indicates that these modes have weaker oscillator strengths.

The fluoromethanes raise another interesting question in view of the vibrational Feshbach model. The partially fluorinated molecules are all examples of molecules for which it is clear that some vibrational modes can mediate positron trapping while others cannot. Each of the partially fluorinated molecules has at least two modes, well separated in energy, with significant infrared activity so the reason for the significant difference in the interaction of the positrons with these two modes is unclear. Several other examples of this phenomenon will be discussed below.

For the fluoromethanes, Z_{eff} at energies below 50 meV is clearly much larger than that observed in the energy-resolved spectra. This is evident in the comparison of these recent energy-resolved experiments to the results of previous experiments using positrons in thermal equilibrium with the target gas. In Fig. 5.3 the value of Z_{eff} from these previous experiments is marked on the ordinate. In each case, Z_{eff} for the thermal positrons is several times larger than Z_{eff} for the energy-resolved spectrum. Section 5.2 discussed a model of positron scattering at very low energies. A similar mechanism may be operative in other partially fluorinated methanes.

5.4 Ammonia

In previous work, nitric compounds have shown higher annihilation rates than similar compounds without nitrogen. For example, the Z_{eff} for benzene using thermal positrons at 300 K is 15,000. If one of the hydrogens is replaced by an amine group (NH_2) to form aniline, Z_{eff} increases to 400,000. For comparison, replacement of a hydrogen atom in benzene with a methyl group (toluene) gives Z_{eff}=190,000.

Motivated by this result as well as a desire to make measurements of computationally tractable targets, we examined the energy-resolved Z_{eff} spectrum for ammonia (NH_3). As shown in Fig. 5.4, hints of resonant features can be seen, but no narrow feature dominates the spectrum. Instead, Z_{eff} rises rapidly as the positron energy is decreased. This is especially clear if we consider the measured

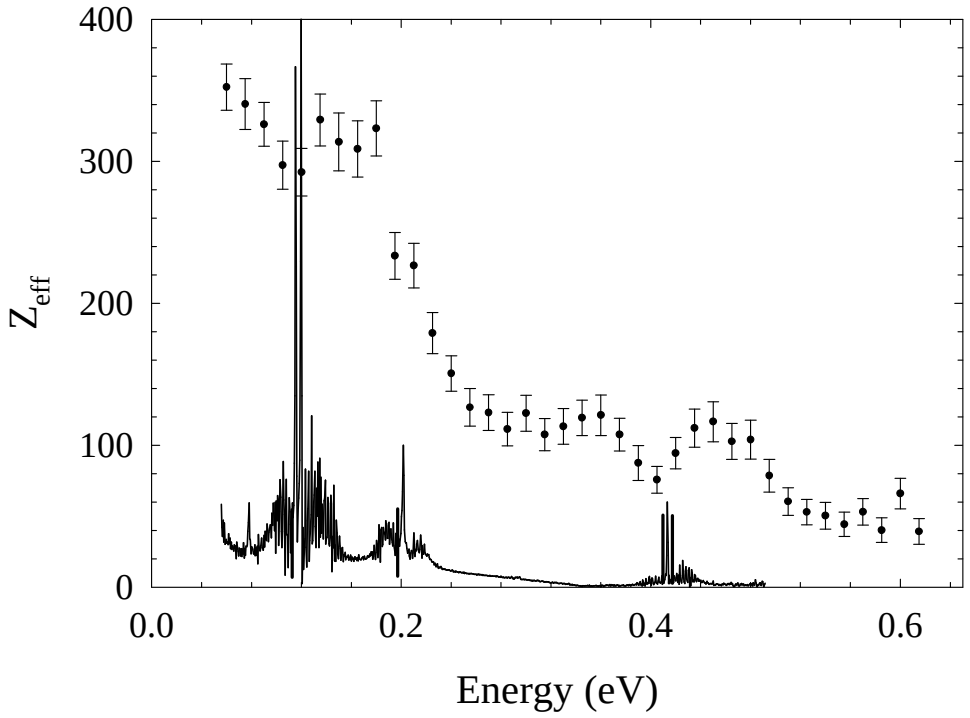

Figure 5.4: Energy-resolved Z_{eff} for ammonia(NH_3) molecules. The Z_{eff} for thermal positrons at 300 K interacting with ammonia is 1600. The solid line is the infrared absorption spectrum for ammonia with arbitrary units.

value of Z_{eff} for thermal distributions of positrons. For ammonia, this value is 1600–significantly larger than the values in the energy-resolved spectrum. It is noteworthy that the vibrational mode with energy near 200 meV is only weakly active in the infrared spectrum.

A similar fit to that used in section 5.2 was attempted for ammonia. However, the constraint that the curve reproduce the measured value of Z_{eff} for thermal positrons forces the curve significantly higher that the values of Z_{eff} is the energy-resolved spectrum. We conclude that a near zero energy state cannot alone be responsible for the value of Z_{eff} for thermal positrons.

5.5 Vibrational modes of the positron-molecule complex

To this point, we have assumed that the presence of the positron has no effect on the vibrations of the molecule. This allowed us to compute the positron-molecule binding energies taking the energy of the vibrational excitation to be the known vibrational mode energies of the bare molecule. A more rigorous computation would require using the mode energies of the molecule with the attached positron, which are unknown.

Some findings, however, suggest that this assumption may not be precisely justified. Figure 5.5 shows the spectrum for ethane. The resonance associated with the C-H stretch mode of the molecule seems to be centered at 370 meV which is exactly the energy of the highest of the C-H stretch modes. In the context of the vibrational Feshbach model and assuming the vibrational energies of the positron-molecule complex are the same as those of the bare molecule, this would mean that, in order that the positron be bound to the molecule, the complex has a higher ground state energy than the bare molecule; that is, the interaction is repulsive overall. In such a case, the complex would quickly dissociate into the bare molecule and a free positron and very little enhancement of Z_{eff} would be expected. So, if the vibrational Feshbach model is to apply to explain the resonances in ethane, the vibrational energies of the positron-molecule complex must be several meV higher than the energies of the bare molecule.

Another example is methyl fluoride (CH_3F). The Z_{eff} spectrum and infrared absorption spectrum for this molecule are shown in Fig. 5.6. In this case, there are resonances in the Z_{eff} spectrum at energies 30 to 40 meV higher than the two most prominent features in the infrared spectrum.

In electron scattering, the vibrational modes of a molecular ion can some-

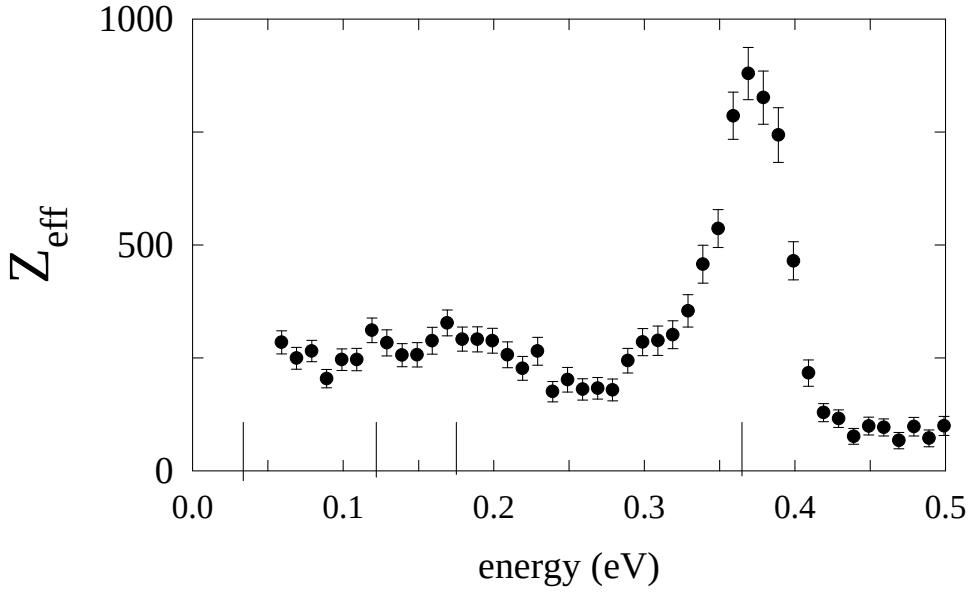

Figure 5.5: The energy-resolved Z_{eff} spectrum for ethane (C_2H_6). A few representative vibrational modes of the molecule are marked on the abscissa.

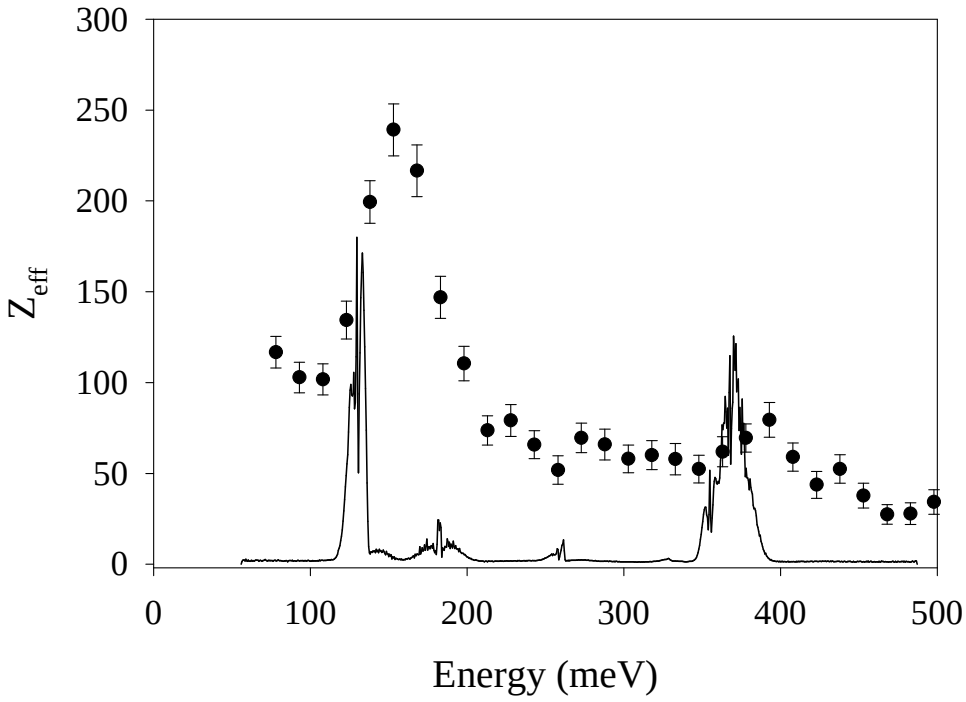

Figure 5.6: The energy-resolved Z_{eff} spectrum for methyl fluoride (CH_3F). The solid line is the infrared absorption spectrum with arbitrary units.

Table 5.1: Z_{eff} for positrons with energy greater than 0.5 eV, but less than the threshold for positronium formation. This is labelled as $Z_{eff}{}^{(dir)}$. The value of Z_{eff} for thermal positrons, $Z_{eff}{}^{(therm)}$, divided by the atomic number, Z, is given where available in the last column.

target	$Z_{eff}{}^{(dir)}$	atomic number (Z)	$Z_{eff}{}^{(dir)}$/Z	$Z_{eff}{}^{(therm)}$/Z
methane (CH_4)	20±3	10	2.0	14.2
CF_4	10±3	42	0.23	1.30
CH_3F	21±3	18	1.2	77.2
CHF_3	31±4	34	0.91	7.26
ethane	32±4	18	1.8	36.7
propane	55±42	26	2.1	134.6
butane (C_4H_{10})	100±38	34	2.9	332.4
d-butane (C_4D_{10})	137±32	34	4.0	
pentane (C_5H_{12})	246±56	42	5.9	900
argon	13.2 ± 0.5	18	0.73	1.88
xenon	53 ± 6	54	0.98	7.43
ammonia	47 ± 9	10	4.7	160

times differ from the modes of the neutral molecule. For example, the vibrational mode in $NO^-(^3\Sigma)$ is weaker than the same mode in the NO neutral by 60 meV [1]. Because of the anti-symmetrization requirement on the electron wave functions, the added electron in this case must occupy an anti-bonding orbital which weakens the mode. It is not clear whether the addition of a positron should increase or decrease the vibrational energy.

5.6 Z_{eff} at higher positron energies

There is a substantial range of energies between the vibrational modes of the molecule (where vibrational Feshbach resonances are observed) and the threshold for positronium formation. In this range of energies, we find that the annihilation rate depends less strongly on positron energy. We expect the interaction to be with the target as a whole rather than with individual vibrational modes or composite particles. As such, it is computationally less intimidating than the problem at lower energies and may be handled by a much simpler model.

Although a more detailed study of Z_{eff} in this range is certainly in order, I present here only a single value for each target. These values, hereafter referred

to as $Z_{eff}{}^{(dir)}$, given in Table 5.1, represent an average of several measurements for positron energies greater than 0.5 eV, but below the threshold for positronium. The errors given in the table represent the standard deviations in the several measurements made in the reported energy range. Often these errors are large since other scattering processes demand that test gas pressure be kept very low and this, in turn, reduces the count rates.

We note a trend, evident in Table 5.1, that molecules with large values of $Z_{eff}{}^{(dir)}$ at energies higher than the vibrational modes are those molecules which also have large Z_{eff} values for thermal positrons, $Z_{eff}{}^{(therm)}$. The exceptions to this trend are ammonia and methane which have unusually high $Z_{eff}{}^{(dir)}$ values compared with molecules with similar $Z_{eff}{}^{(therm)}$ values.

5.7 Z_{eff} for noble gases

The noble gases have no vibrational modes to facilitate resonant annihilation. Data for argon and xenon are shown in Fig. 5.7. As can be seen in the figure, these data do not exhibit resonant features such as those observed in molecules. There is, however, an increase in Z_{eff} for very low positron energies due to positron-atom virtual states, predicted by all of the theoretical treatments to date [55, 58, 65]. Comparisons with three different theories are shown in the figure for both targets. The agreement with experiment is very good in argom, although in the case of xenon the experimental results tend to give a larger Z_{eff} by about a factor of two for positrons with several volts of energy. The measurement of argon represents the smallest energy-resolved Z_{eff} measured to date.

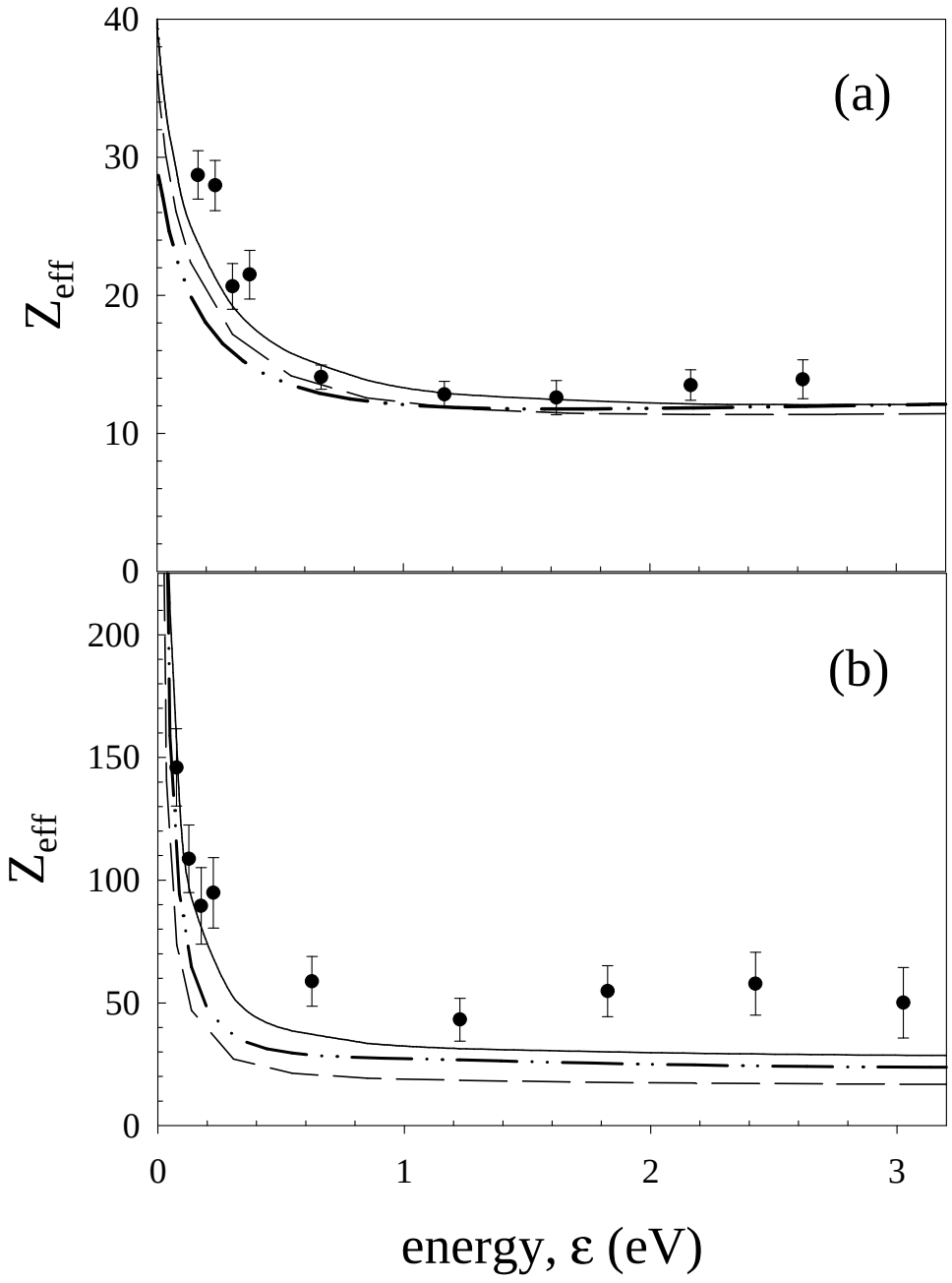

Figure 5.7: Z_{eff} for argon (a) and xenon (b) together with theoretical predictions from a model-potential (—) [65], from polarized orbital theory (– –) [58] and from many-body theory (– · · –) [55]. Data from Ref. [57].

Chapter 6

Progress in the Theory of Positron Annihilation on Molecules

The work in this thesis and earlier work by Iwata *et al.* [38,41,46] sparked considerable interest in the theoretical problem of positrons interacting with molecules. Calculations of Z_{eff} using various methods have recently been performed. This chapter briefly reviews this work and its relationship to the experimental results in this thesis.

6.1 Basic vibrational Feshbach resonance theory

Many of the details of the vibrational Feshbach resonance (VFR) picture remain unclear at the point of this writing. For example, it is still difficult to explain the rapid increase in $Z_{eff}{}^{(therm)}$ for increasing molecule size (see Fig. 2.1). Gribakin [27,28] and later Gribakin and Gill [30] proposed that this increase can be attributed to the rapid increase in the density of vibrational Feshbach resonances with molecule size. This idea was also discussed earlier by Surko *et al.* [81].

Since the earliest measurements in this thesis, it has become clear that vibrational Feshbach resonances are associated only with the fundamental vibrational modes. The number of fundamental modes is *linear* with the size of the molecule making it difficult to account for the rapid increase in Z_{eff} with molecular size without incorporating combination and overtone modes. To reconcile the mode density explanation with these recent observations, Gribakin and Gill [30] proposed that the fundamental modes act as "doorways." The positron is initially trapped by exciting a fundamental mode of the molecule. This vibrational

energy is then spread among the other isoenergetic modes including overtones and combination modes. The number of these modes has a steep dependence on the size of the molecule. The assumption that the vibrational energy is spread among all isoenergetic modes of the molecule leads to a dependence on molecular size which is actually *too* steep as shown in Fig. 6.1. In this figure, the density of vibrational levels (including overtones and combination modes) was deduced from the measured values of Z_{eff} to arrive at the open circles on the plot. The solid lines are the actual level density from a quantum mechanical calculation. The solid circles match the positron binding energy of the molecules with the computed level density to show what the curve should look like if all modes participated. This analysis seems to indicate that, if the doorway picture is correct, that only a subset of the molecular modes participate.

In Sec. 7.2, I will discuss another proposed explanation for the strong dependence of Z_{eff} on molecular size.

6.2 Static calculations

The exact mechanism of the positron-molecule binding and structure of the bound positron wave function are also unknown. However, several recent calculations have moved us closer to some understanding. Several attempts have been made to calculate the interaction of the positron with molecules in the fixed nuclei approximation.

6.2.1 Configuration interaction ground state calculations

Tachikawa, Buenker and Kimura [82] added a positron to configuration interaction (CI) calculations of urea ($(NH_2)_2CO$) and acetone ($(CH_3)_2CO$). These calculations compute the full Hamiltonian of the systems by expanding the wave function in terms of Gaussian-type functions (GTFs) then diagonalizing to find eigenfunctions and eigenenergies. Tachikawa *et al.* used GTFs which are more diffuse to describe the positron wave function. Their results predict bound states for both molecules with binding energies of 450 meV for urea and 150 meV for acetone. We note that both of these molecules have large permanent dipole moments (3.99 debye and 3.26 debye for urea and acetone, respectively) and that molecules with a dipole moment greater than 1.624 debye are shown to be capable of binding an extra *electron* in a diffuse dipole bound state. These diffuse states are far outside the electron cloud where a positron and an electron should interact very similarly with the target molecule. Since both of these molecules have dipole bound states for electrons, it is not surprising that to find a posi-

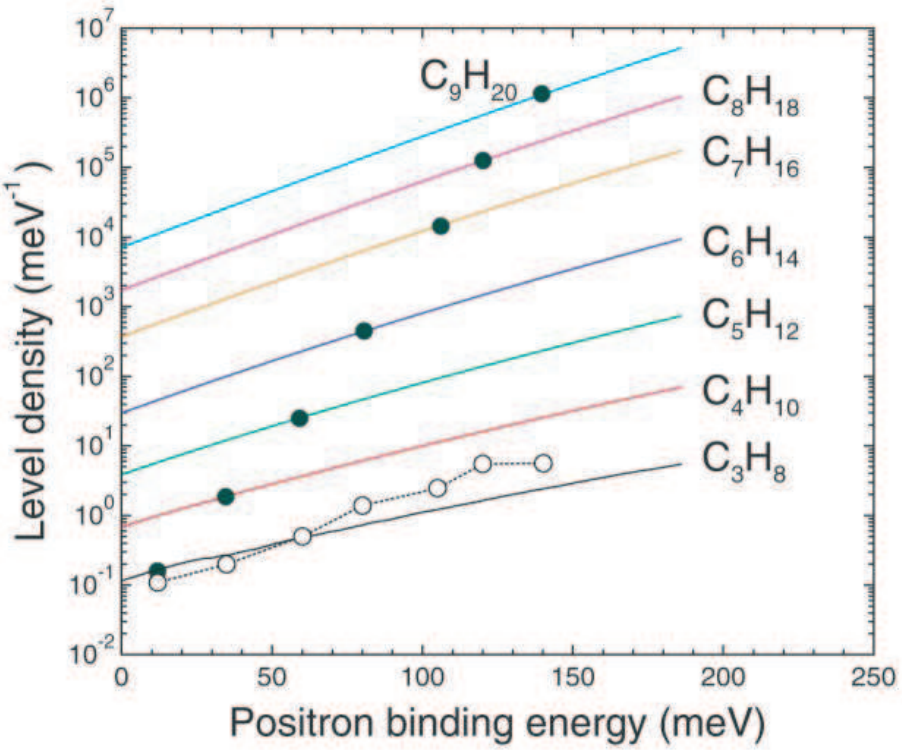

Figure 6.1: The solid curves give the density of all vibrations, including overtones and combination modes, as a function of energy. The open circles are the predicted density as derived from the measurements of Z_{eff} for thermal distributions of positrons for the alkanes as a function of the binding energy. The solid circles are the intersection of the measured binding energy and the solid curves. This would be the predicted vibrational level density if all modes participated in the vibrational Feshbach resonance. This figure was previously published by Gribakin and Gill in Ref. [30].

tron bound state as well. However, these calculations confirm the importance of positron-electron correlations in positron-molecular systems and give an idea of the shape of positron bound states.

6.2.2 Density functional models

Occhigrossi and Gianturco have computed both scattering and annihilation rates for a number of hydrocarbons including acetylene (C_2H_2), ethylene (C_2H_4), ethane (C_2H_6) and benzene (C_6H_6) [69]. They compute a potential for the positrons by using the simple polarization potential at large positron-molecule distances and by incorporating electron-positron correlations in the local density approximation (LDA) at smaller distances. The short range correlations are derived from a calculation of the correlation energy of a single positron in an electron gas as a function of the electron density. The correlation potential at every point in space is then taken to be a function only of the electron density in the undistorted target molecule. The wave function for positron scattering from this potential gives the elastic scattering in the fixed nuclear approximation. To compute Z_{eff}, they integrate the positron-electron overlap (Eq. 2.2) from the positron scattering wave function and the electron wave functions in the undistorted target.

For the equilibrium nuclear geometry, the Z_{eff} as computed above is much smaller than the observed values. For example, the predicted value of Z_{eff} for acetylene by this method is less than 50 compared with the observed value of 3,160 [43]. Also, since the calculation does not include the interaction of the positron with the vibrations of the molecule, it naturally does not produce resonances of the type observed in these molecules at positron impact energies far above room temperature thermal energy.

Occhigrossi and Gianturco did point out that the computed Z_{eff} for acetylene rises very rapidly as the length of the CH bond is reduced as shown in Fig. 6.2 [69]. A normal coordinate of -1 in this figure corresponds to a potential energy of 4.35 eV and so is not consistent with experiments at room temperature. However, the model does demonstrate the importance of the nuclear positions and nuclear motion in annihilation rate calculations.

6.2.3 Schwinger multichannel method

The last fixed nuclei calculation I will discuss employs the Schwinger multichannel method and has been used by several groups of authors from Universidade Estadual de Campinas in São Paulo [7–9, 21, 53, 54]. It involves expansion in terms of Gaussian type functions and variation to minimize the energy subject to

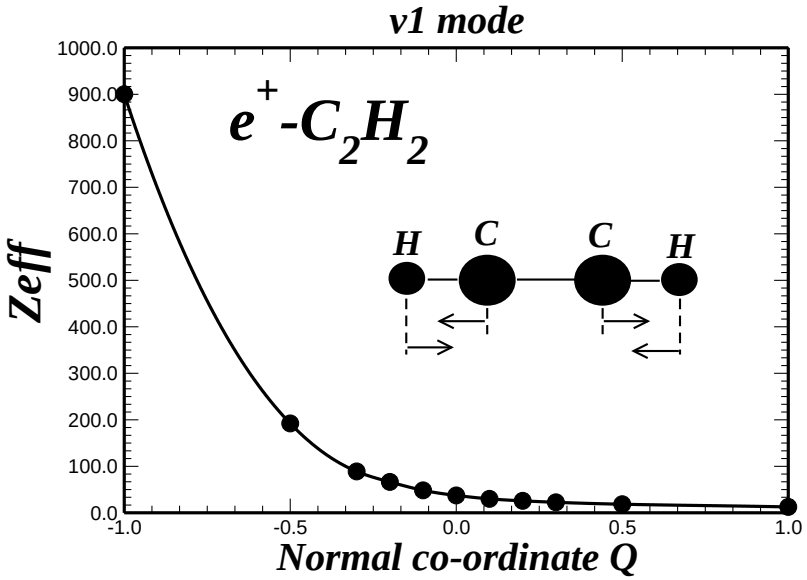

Figure 6.2: Z_{eff} for acetylene as a function of the length of the CH bond as computed by Occhigrossi and Gianturco. This figure was previously published by Occhigrossi and Gianturco in Ref. [69].

scattering boundary conditions. Additionally, the computation is simplified by dealing separately with the target channels that are open (energetically-allowed) and those that are closed (disallowed). In particular, the target states of channels involving ionization are not well known and so must be approximated.

This technique treats the full scattering system including contributions due to virtual excitations of the target which account for long- and short-range polarization effects. It predicts both elastic scattering cross sections and Z_{eff}. As with other methods involving expansion of the wave function in terms of basis functions, the ability to represent the important virtual Ps contribution depends on the size and composition of the basis set.

The results of one such calculation for ethylene are shown in Fig. 6.3. The calculation underestimates Z_{eff} compared with experiment (see Fig. 4.15). This demonstrates the need for very large basis sets to account for strong electron-positron correlations and of the importance of incorporating nuclear motion in annihilation rate calculations.

6.3 Incorporating nuclear motion

Nishimura and Gianturco incorporated nuclear motion into the calculation of the type described in Sec. 6.2.2 [67, 68]. By constructing interaction potentials from the undistorted electron density of the target, they computed the positron scattering wave functions for a range of nuclear geometries and internuclear separations. They then computed the total multichannel scattering wave function by integrating the interaction potential over the vibrational states of the molecule. The interaction potential used was not the full interaction potential, but a multipole expansion of just the static potential (i.e. ignoring all distortion of the electron density and short range electron-positron correlations).

The results of this work was that the incorporation of the CH stretch vibrations strengthens the positron-molecule interaction and creates virtual states of energy less than 2 meV which enhance the elastic and inelastic cross sections. Nishimura and Gianturco suggest that these virtual states, when interacting with a large density of multimode vibrational states could give rise to very large values of Z_{eff}.

Gribakin performed a calculation of positron annihilation on the Kr_2 dimer [29], the results of which is shown in Fig. 6.4. By choosing a molecule with large interatomic separations, he was able to replace the complicated positron atom interactions with a "zero-range potential" chosen to match the polarized-orbital calculations for positron scattering from atomic krypton. Using measured parameters of the dimer, Gribakin was able to calculate the energy of the e^+-Kr_2

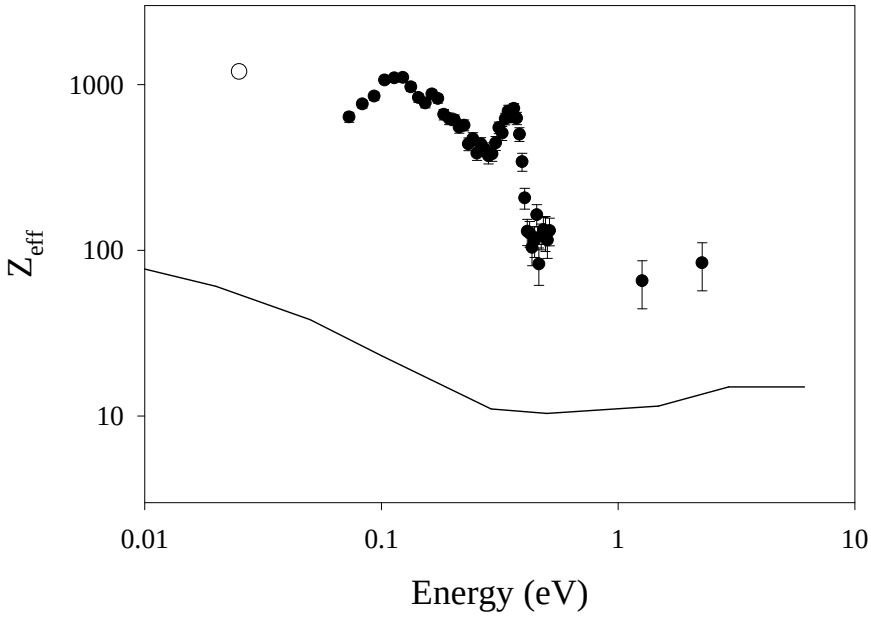

Figure 6.3: The solid curve gives Z_{eff} for ethylene as a function of positron energy as computed by da Silva, Germano and Lima using the Schwinger multi-channel method. This computation was previously published by da Silva, Germano and Lima in Ref. [8] and revised in reference [15]. The filled circles are the energy-resolved data for ethylene measured using the trap-based beam. The single open circle is the data for thermal distributions of positrons due to Iwata, Greaves and Surko [38].

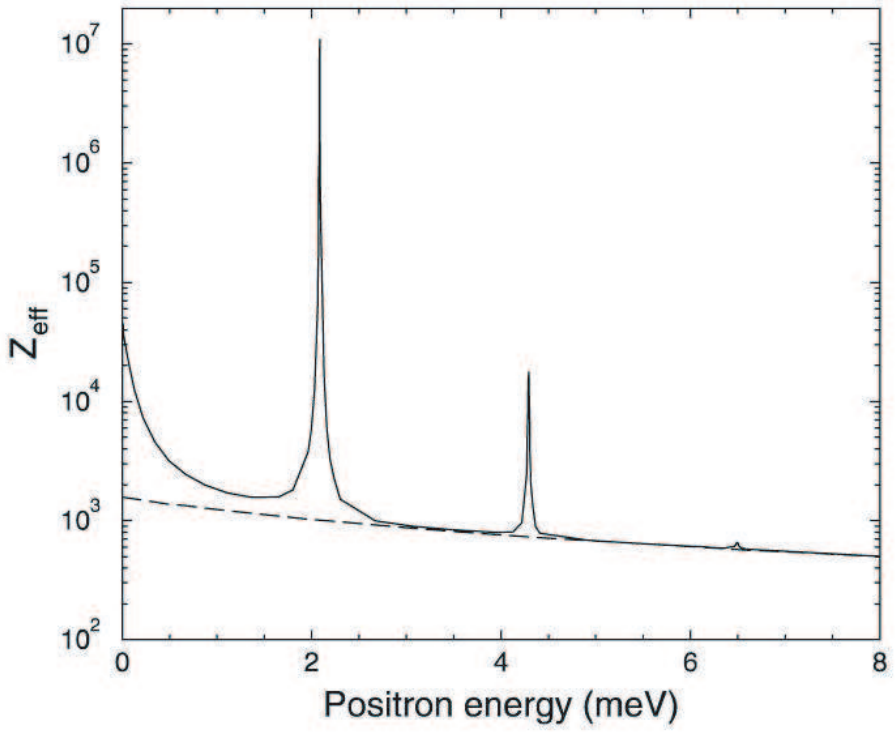

Figure 6.4: Z_{eff} for Kr_2 as calculated by Gribakin. The dashed curve is the calculation in the fixed nuclear approximation. The solid curve is the calculation incorporating the nuclear motion. This figure was previously published by Gribakin in Ref. [29].

complex as a function of the interatomic spacing and predict a bound state of the positron with the dimer incorporating the nuclear motion. The binding of the ground state is predicted to be 4.51 meV.

This model can also be used to predict the position and shape of vibrational Feshbach resonances for Kr_2. The resonant states are vibrationally excited states of the e^+-Kr_2 complex. Gribakin predicts two very strong resonances for positrons with energy 2.1 meV and 4.3 meV. According to the calculation, these resonances are very narrow ($\Gamma \sim 3.5\mu$eV) and the lowest of these has a fairly large maximum value of $Z_{eff}(> 10^7)$ When convoluted with the experimental resolution of the experiments in this thesis, the height of this resonance would be about 1500. The predicted resonance is shown in Fig. 6.4.

On an experimental note, measurement of Z_{eff} at such low positron energies (i. e. < 50 meV) cannot be performed with the current setup.

6.4 Direct annihilation near the positronium threshold

A paper by Laricchia and Wilkin [50, 51] sparked considerable recent discussion of the behavior of Z_{eff} close to the threshold for positronium formation. Following the first measurements of Z_{eff} using thermalized positrons in a buffer gas trap (see Sec. 2.6), Laricchia and Wilkin postulated that the large values of Z_{eff} observed for thermal positrons are due to the formation of "virtual positronium" atoms with the molecular electrons. Since the positron energies in these experiments are far below the threshold for positronium formation, Laricchia and Wilkin postulated that these virtual states were limited in lifetime by the uncertainty principle

$$\delta t \approx \frac{\hbar}{|E - E_i + 6.8\text{eV}|}, \tag{6.1}$$

where E is the energy of the incident positron, E_i is the ionization energy of the molecule and 6.8 eV is the binding energy of the positronium atom. These virtual states are expected to enhance the overlap of the wave function of the positron with that of the molecular electrons which enhances annihilation. Virtual Ps formation has played a role in modelling of positron scattering processes where its inclusion has significantly improved agreement between theory and experiment [17, 36].

Laricchia and Wilkin also made attempts to estimate the magnitude of the enhancement and concluded that the majority of annihilation of these virtual positronium states happens not with the electron-positron pair themselves but by "pick-off" annihilation of the positron with the electrons not involved in the virtual state positronium atom.

This virtual Ps model was motivated largely by a scaling relationship proposed by Murphy and Surko [66] and described by

$$\ln(Z_{eff}) \approx \frac{A}{E_i - 6.8 \text{ eV}} + B. \tag{6.2}$$

In this expression, E_i is the ionization energy of the target and A and B are constants independent of the target. This scaling rule shows remarkable agreement with the values of Z_{eff} for a number of molecules over a wide range of

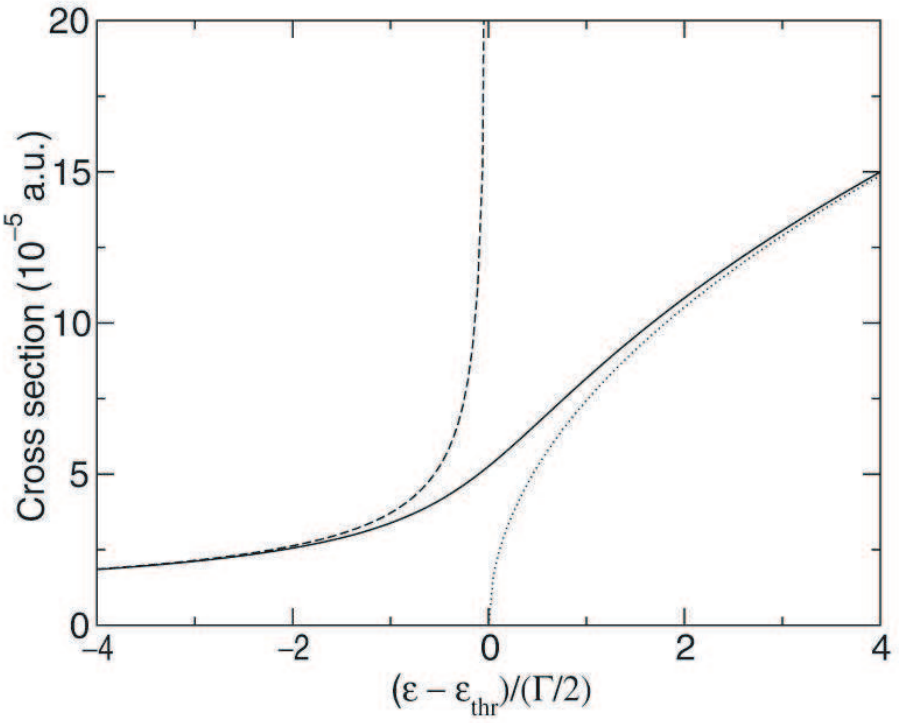

Figure 6.5: Annihilation cross section near the positronium threshold as a function of the dimensionless ratio of energy above positronium threshold divided by the positronium lifetime, Γ, as computed by Gribakin and Ludlow [31]. The solid curve incorporates the lifetime of the virtual positronium to self-annihilation. The dashed and dotted curves represent direct annihilation and real Ps formation respectively when the lifetime is ignored. This figure was previously published by Gribakin and Ludlow in Ref. [31].

parameters. It should be noted that there are classes of molecules which do not follow this scaling (see Sec. 2.6).

The virtual positronium model as it relates to positron annihilation rates has been criticized by two groups of authors. Mitroy and Ryzhikh [63] pointed out that Laricchia and Wilkin's estimates of the overlap between the positron and the molecular electrons was much higher than is typical of similar systems such as positrons in metals or calculated bound states of positrons with atoms. Mitroy and Ryzhikh claimed that these estimates were invalid and that the large values of Z_{eff} require other explanations.

Gribakin and Ludlow criticized the energy dependence predicted by Laricchia and Wilkin, claiming that the latter failed to consider the kinetic energy of the virtual positronium atom [31]. They showed that the annihilation cross-section has a much slower $(E-E_i-6.8\text{eV})^{-1/2}$ dependence on E. Gribakin and Ludlow's predicted enhancement is also much smaller than that of Laricchia and Wilkin. Further, Gribakin and Ludlow argued that the finite lifetime of the virtual positronium due to self-annihilation eliminates the divergence at the positronium threshold. Their predictions of annihilation cross section (incorporating both direct annihilation and Ps formation) are shown in Fig. 6.5.

Igarashi, Kimura and Shimamura attempted a unified treatment of annihilation, positronium formation and ionization for atomic hydrogen [37]. For their computation, they treat the positron and electron in hyper-spherical coordinates and add a purely imaginary decay term which describes positron-electron annihilation. They diagonalize the Hamiltonian by expanding in terms to Slater-type orbitals (STOs) some centered around the proton and some around the positron. Their findings indicate a contribution from partial waves of varying angular momentum, l, which depends on energy like

$$Z_{eff} \propto \frac{1}{(E - E_{Ps})^{l+1/2}}. \tag{6.3}$$

The dominant contribution is by the s-wave, the dependence of which is as predicted by Gribakin and Ludlow [31].

From the experimental side, we have made measurements of Z_{eff} for a number of atoms and molecules within less than one electron Volt of the threshold for positronium formation and find no enhancements of the type predicted by Laricchia and Wilkin (e. g. see Figs. 4.1 and 5.7). Measurements closer to the Ps threshold are currently impossible because the positrons in the high energy tail of the positron energy distribution begin to form real positronium. Although the number of positrons in the tail is small, the cross section for positronium formation is comparatively extremely large and so this signal swamps the direct annihilation signal. The measurements made to date, however, establish that virtual Ps formation is not responsible for the large Z_{eff} for thermal positrons. However, testing the scaling predicted by Gribakin and Ludlow, and Igarashi *et al.* is beyond current experimental capabilities.

Chapter 7

Additional Observations

Many aspects of low energy positron annihilation warrant further exploration. Careful examination of the Z_{eff} spectrum for dodecane ($C_{12}H_{26}$) suggests the presence of both a ground state positron bound state and a "positronically" excited state. Also, we modify the vibrational Feshbach model to incorporate positron escape from its bound state by de-excitation of thermally excited vibrations of the molecule and compare this with the data for the alkanes.

7.1 Annihilation for very large alkanes–second positron bound state?

We expect that as the attraction between the positron and target molecule increases with increasing molecular size, the attractive well should become deep enough to support a second bound state. As we move to larger and larger alkanes, a second set of resonances should appear just a few meV below the vibrational modes of the complex. These resonances are due to population of the first (positronic) excited state of the positron-molecule complex by vibrational excitation. With increasing size (and corresponding increase in binding), this resonance should also move downward in energy.

Figure 7.1 shows the Z_{eff} spectrum for dodecane ($C_{12}H_{26}$). It shows the usual large peak associated with the CH stretch mode at a position consistent with the trend among the alkanes (see Fig. 4.8). In addition, a small second peak is observed at 360 meV. It is much smaller than the peak associated with the ground positronic state. To rule out interactions with multiple target particles, Z_{eff} in these energy ranges was measured for several pressures. These measurements confirm that the peak is indeed due to interactions with just one target molecule.

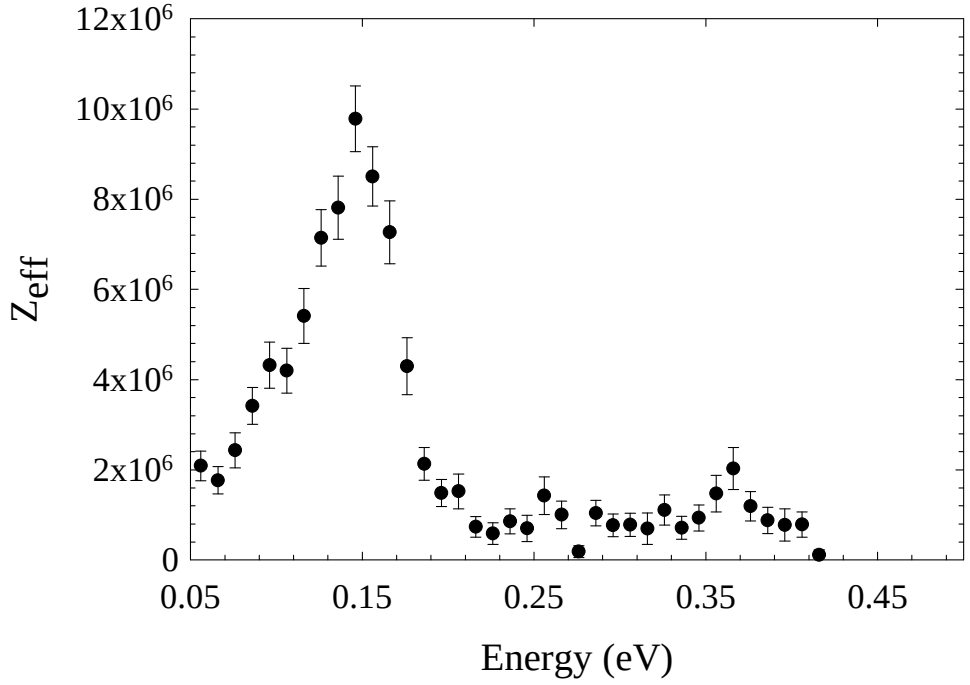

Figure 7.1: The energy-resolved Z_{eff} spectrum for dodecane ($C_{12}H_{26}$)

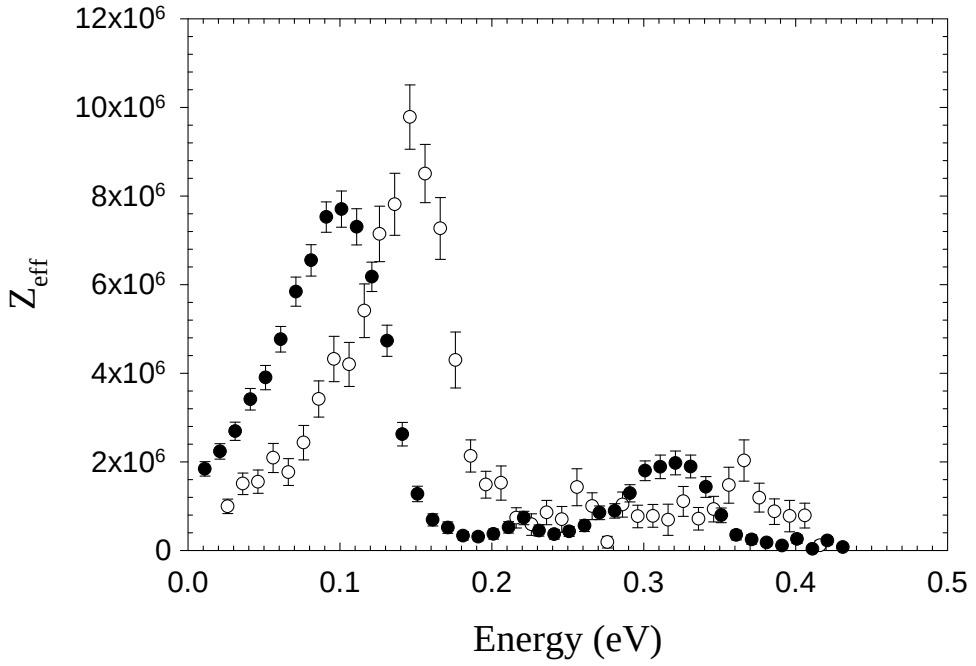

Figure 7.2: The energy-resolved Z_{eff} spectrum for tetradecane ($C_{14}H_{30}$) arbitrarily scaled (•) and for dodecane(∘) with absolute scaling.

A similar result is seen in the spectrum for tetradecane ($C_{14}H_{30}$) in Fig. 7.2. In this case, the pressure in the experimental setup is uncertain due to the extremely low pressures required. The data for tetradecane has been scaled for easy comparison with dodecane. In the tetradecane spectrum, we can clearly see both the higher and lower energy resonances. The binding for tetradecane appears to match the trend noted in reference [4] of a linear relationship between binding and molecular size for the alkanes.

It is an important question to ask why the resonance associated with the more strongly bound positron state is so much larger, and this may give insight into the dependence of Z_{eff} on molecule size. It has been proposed [28] that the increase in the overall magnitude of Z_{eff} with molecular size is due to redistribution of vibrational energy among the vibrational modes of the molecule. If only some of the vibrational modes can mediate positron trapping (or de-trapping), this redistribution reduces the escape width, Γ_{esc}. Phrased another way, the vibrational energy is "lost" to nuclear motion which is unusable by the posi-

tron to escape the bound state. This is the doorway state model forwarded by Gribakin and Gill [30] and discussed in Sec. 6.1.

In this model and considering the relative magnitudes of these two resonances, each associated with the same vibrational mode, one possibility is to conclude that the vibrational redistribution is stronger when the positron is in the lower energy bound state. It seems logical under this assumption that the non-linear effects responsible for the vibrational redistribution are strongly related to the details of the positron bound state.

Alternatively or additionally, we might conjecture that the positron in the less strongly bound state has a greater possibility of escape by de-excitation of another vibrational mode. In terms of Eq. 4.11,

$$Z_{eff}(\text{measured}) = f(E_r)\frac{2\pi v}{r_0^2 ck^2}\frac{\Gamma_{ann}\Gamma_{cap}}{\Gamma_{ann}+\Gamma_{cap}+\sum\Gamma_i}, \tag{7.1}$$

the total width in the denominator is dramatically larger for the excited state. This is discussed further in the next section.

7.2 Incorporating positron escape by de-excitation of thermally excited vibrations

In equation 7.1, we see that three quantities control the magnitude of each resonance in the Z_{eff} spectrum.

1. The rate of capture, Γ_{cap}.
2. The rate of annihilation while in the captured state, Γ_{ann}.
3. The rate of escape from the captured state by de-excitation of other "pre-excited" vibrational modes, $\sum\Gamma_i$.

Of these, Γ_{cap} has been discussed in Sec. 4.8.1 and Γ_{ann} depends in a complicated way on the shape of the positron bound state. The width due to annihilation, Γ_{ann}, has sometimes been estimated as the annihilation rate for the positronium atom, but this may not be warranted. In this section, we turn our attention to the last parameter, $\sum\Gamma_i$. We find that a simple model in which this term is very large reproduces some of the experimental results.

Figure 7.3 investigates the relationship between Z_{eff} (as represented by the height of the CH stretch peak) and positron binding energy for alkane molecules. In the figure, the dashed curve is a simple exponential function of binding energy

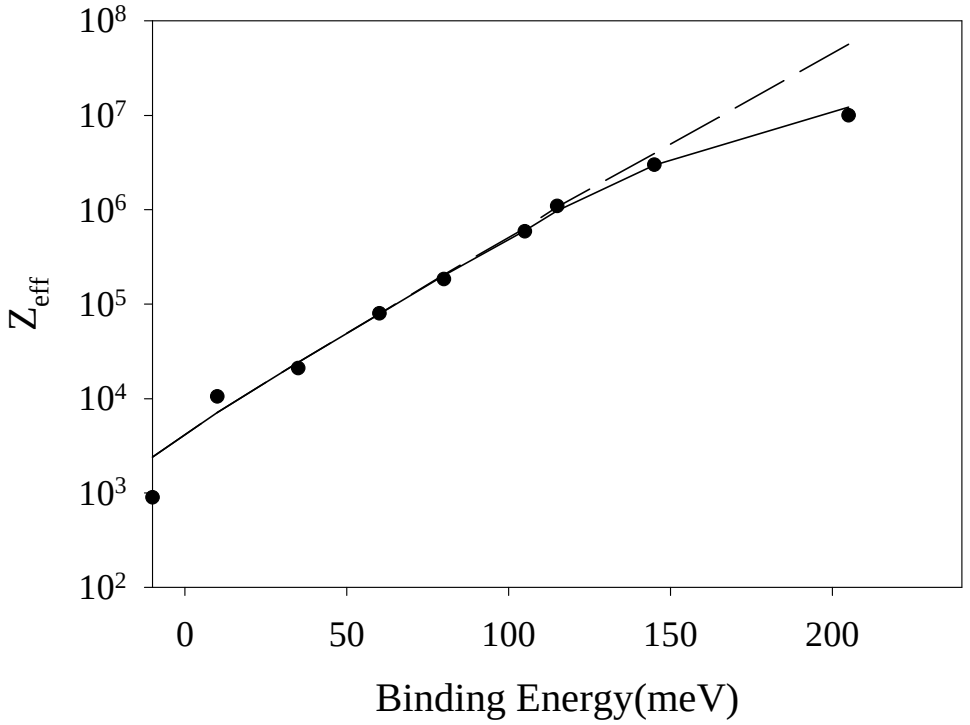

Figure 7.3: The height of the annihilation resonance associated with the CH stretch peak as a function of the positron binding energy. The binding energy is taken to be the center of the resonance in the energy-resolved Z_{eff} spectrum subtracted from 360 meV, the approximate energy of the CH stretch vibrational mode. The dashed curve is a simple exponential function multiplied by the total number of CH stretch modes of the molecule. The solid curve is a plot of equation 7.5 (see text).

multiplied by the total number of CH stretch modes of the molecule. The curve is given by

$$Z_{\mathit{eff}}(\text{peak}) = 600 \cdot (2n+2) \cdot \exp\left(\frac{E}{26\ \text{meV}}\right). \tag{7.2}$$

Here n is the number of carbon atoms in the molecule so that $2n+2$ is the number of CH stretch vibrational modes. The binding energy is ε_b and 26 meV is k_bT for a temperature of 300 K. The constant term, 600, is adjusted to fit the data.

This relationship between Z_{eff} and positron binding seems consistent with Eq. 4.11 if we make certain assumptions about the $\sum \Gamma_i$ term. Namely, this

term refers to the process in which the positron escapes from the resonant state by de-exciting a vibration which was excited *before the collision*. In the actual experiment at 300 K, the molecular vibrational modes are thermally excited. The summation can then be written

$$\sum_{E_i>\varepsilon_b} \Gamma_i \exp(-E_i/k_bT) \tag{7.3}$$

where E_i are the energies of the vibrational modes and the summation includes only those modes excited which have enough energy to push the positron out of its bound state. For a constant density of vibrational modes all with the same transition rate, this term can be approximated by

$$\Gamma_0 \rho \int_{\varepsilon_b}^{\infty} \exp(-E/k_bT) dE = \Gamma_0 \rho k_b T \exp(-\varepsilon_b/k_bT), \tag{7.4}$$

where Γ_0 is a representative transition rate and ρ is the density of vibrational modes in energy space. If this term is the dominant term in Γ_{tot}, the dependence of Z_{eff} on binding energy has the form of Eq. 7.2. As shown in Fig. 7.3, this fits the data reasonably up to a binding energy of about 120 meV.

The dashed curve seems to deviate significantly from the measured data for n greater than 8 ($\varepsilon_b > 120$). This might be explained by conjecturing that for molecules with a binding energy larger than $\sim$ 120 meV, the summation term no longer dominates the denominator of Eq. 4.11. The solid curve in Fig. 7.3 accounts for this. That curve is given by

$$Z_{\mathit{eff}}(\text{peak}) = (2n+2) \cdot \frac{600}{0.001 + \exp\left(-\varepsilon_b/26 \text{ meV}\right)}. \tag{7.5}$$

The constant in the denominator is a hypothetical contribution to the total width of the resonance due to both annihilation and escape to an elastic channel. While this term may not be exactly 0.001 or even exactly constant, the comparison of the predictions of Eq. 7.5 with the experiment demonstrates how a model involving escape by de-excitation of thermally excited modes can explain the dependence of Z_{eff} on molecular size.

This could be experimentally checked if the apparatus described here were modified to study gases which are cooled below room temperature. For gases at lower temperatures, the Boltzman term in the denominator of Eq. 7.5 is suppressed and Z_{eff} should increase dramatically. As discussed in the next section, these experimental modifications are underway.

Chapter 8

Summary and Concluding Remarks

8.1 Summary of results

The advent of the buffer-gas loaded positron trap has enabled previously impossible measurements of the annihilation parameter, Z_{eff} resolved as a function of positron energy. The spectra for many molecules, notably the alkanes, exhibit a number of large resonances at positron energies between zero and 0.5 eV. These resonances are due to molecular vibration-mediated trapping of positrons into bound states with the target molecules.

In this thesis, I have discussed the evidence in the Z_{eff} spectra for the presence of positron bound states with the alkane molecules. These resonances display the appropriate isotope effect and have energy positions similar to the infrared absorption of the same targets. The binding energy of the positron-molecule complexes can be deduced from the Z_{eff} spectrum. This binding tends to increase approximately linearly with the size of the alkane molecules.

Evidently, a similar process is responsible for the Z_{eff} values observed earlier using thermal distributions of positrons. The fact that the values of Z_{eff} for thermal positrons stays within a factor of 2-3 of the maximum Z_{eff} in the energy-resolved spectrum for the alkanes supports this claim. These large values of Z_{eff} have remained unexplained since they were first observed in 1963 [70]. Thus, the data and analysis described in this thesis resolves a mystery of nearly four decades in the field of positron annihilation.

In the same chapter, I discussed the effects on Z_{eff} of changing the shape of the molecule (while maintaining the same chemical formula) and of fluorine substitution. Changes in molecular shape do not appear to affect Z_{eff}, except

for the case of ring-shaped molecules for which Z_{eff} is notably smaller.

Fluorine substitution has two dramatic effects on the Z_{eff} spectra for the alkane molecules. First, the magnitudes of the high energy resonances ($\epsilon > 50$ meV) are greatly reduced, while Z_{eff} for positrons at lower energies ($\epsilon < 50$ meV) is enhanced. Also, both of these effects occur without significant changes to the position of the resonances and therefore the apparent binding of the positron to the molecule.

The picture for smaller molecules is much less clear. The fluoromethanes, including methyl fluoride, exhibit resonances near some modes, but not near others. Methane, which has no observable resonances, seems to be a good case for studying the energy dependence of Z_{eff} in the absence of Feshbach resonances. Both methane and carbon tetrafluoride can be fit with moderate success by a model incorporating the effect of a virtual or bound state near zero energy (see section 5.2). However, the predicted energies of these states seem to be in conflict with other approximations. Also, the spectra for partially fluorinated methane (e. g. CH_3F, CH_2F_2, etc.) are much less clear. More theoretical predictions for specific smaller molecules would be a welcome contribution to this discussion.

We have made measurements of Z_{eff} for two noble gases. In these cases, agreement with theory is good with the exception of the high energy (i. e., several eV) Z_{eff} for xenon. These measurements also demonstrate the capability of the current experiment to measure Z_{eff} values as low as 10.

Finally, Chap. 7 addressed two important aspects of energy-resolved annihilation rates which deserve further attention. The first is the possibility of a second positronic bound state of the positron-molecule complex. This is manifest in the appearance of a second resonance in the spectrum for dodecane. The second issue in Chap. 7 is the possible effect of molecule temperature on the magnitude of Z_{eff}. The dependence of Z_{eff} on the binding energy of the positron-molecule complex seems consistent with a model involving escape of the positron by de-excitation of thermally excited vibrational modes. Both of these ideas are unconfirmed, but seem to warrant further work.

8.2 Future Work

There are many open questions concerning vibrational Feshbach resonances in positron scattering. A number of these can be addressed with tools currently available or those under development. I list below a few of the areas which I expect will be most important in the near future.

1. *Halogen substituted methane derivatives.* Studies of the halogen substi-

tuted methanes will likely be important for connection with theoretical models of resonant positron annihilation and may address many unanswered questions. The fluorinated methanes are among the smallest molecules observed to exhibit vibrational Feshbach resonances. It is difficult to attribute these resonances to a particular vibrational mode and therefore to deduce the positron binding energy. As discussed, there is even some indication that VFR may appear at energies *above* the energy of the associated vibrational mode. It is not clear what this means for the Feshbach resonance picture. Studies of the isotope effect in these fluoromethanes or even studies of methane substituted with other alkanes (chlorine, bromine) may help to assign resonances in Z_{eff} to particular molecular modes. Also, methyl chloride and other chloromethanes have values of Z_{eff} for thermal distributions of positrons that are an order of magnitude larger than any of the fluoromethanes. This area deserves further investigation.

2. *Planar alkane molecules.* The apparent increased positron affinity for benzene (as compared with cyclohexane or hexane) may be either an isolated case or part of a general pattern of stronger binding to planar molecules. This thesis briefly discussed the possibility that the planar shape of the molecule allows the positrons access to the cloud of valence electrons without getting close to the repulsive carbon nuclei. Other examples of planar hydrocarbon molecules that could be investigated include 1,3,5-hexatriene, tris(methylene)cyclopropane, naphthalene and fulvene.

3. *Dependence of Z_{eff} on molecular temperature.* In light of the discussion in this thesis of the interaction of trapped positrons with pre-excited vibrational modes of target molecules, measurement of the Z_{eff} spectra for cooler molecules is warranted. If significant detrapping of the positron can arise from de-excitation of thermally excited vibrations, then cooling the target molecule should increase the lifetime of the positron in the bound state and thus increase the heights of the resonance features in Z_{eff}.

   In collaboration with J. A. Young and C. M. Surko, I am in the process of making modifications to the experimental setup to enable study of positrons incident on low temperature ($\sim$ 100 K) targets. If the dependence on molecule temperature predicted by Eq. 7.5 is observed, it would explain the exponential dependence of Z_{eff} on molecular size – a mystery for several decades. Also, it would concretely establish the utility of the Breit-Wigner formula in describing positron resonances and allow us to

draw conclusions about the relative rates of the various decay processes of the bound states. Thermal energy might also play a role in the observed asymmetric shape of the CH stretch peaks.

4. *Smaller molecules for connection with theory.* Many of the molecules studied in this work are computationally intimidating when one considers calculations which accurately treat electron-positron correlations. The search for molecules of modest size but with observable resonant features should continue.

   Also, for the smallest molecules studied here (ammonia, acetylene, methyl fluoride, etc.) the resonant signal is frequently indistinguishable from a non-resonant contribution to Z_{eff} with a much weaker energy dependence. Even modest improvements in experimental energy resolution and signal-to-noise ratio could yield valuable information and give guidance to theoretical investigations of this phenomenon. If, as described above, decreasing target gas temperatures yields larger Z_{eff} resonances, these smaller molecules may be excellent candidates for low temperature studies.

Our understanding of these resonances and the associated positron-molecule complexes would benefit greatly from further theoretical treatment. Although, of course, a full scattering treatment is desirable, a stationary potential curve calculation (of the type shown in Fig. 4.5) would be very insightful and may be more easily realized. First, it would establish, theoretically, the capability of the target molecule to bind a positron and predict the shape of the positron wave function. Second, there are a number of techniques used for electron scattering to estimate the shape of Feshbach resonances in energy space from the potential energy diagrams [33]. These techniques would appear to translate well into positron scattering and may give information at higher resolution than the available experimental data.

The formidable challenge here is the incorporation of the positronium formation channel which is very important even when closed. We note that the basis sets typical of quantum chemical computations are likely to be inappropriate to describe the highly correlated "virtual positronium" states. Some approaches to modelling positron scattering and annihilation have been discussed in Chap. 6.

Among my goals in this research has been measurement of annihilation rates for molecules which exhibit vibrational resonances but are computationally less daunting than, for example, the larger alkanes. I have measured a number of highly symmetric molecules (e. g. benzene, acetylene) and molecules with a modest number of particles (e. g. ammonia, methane) in hope of enabling more

rigorous computations. I also think an approach involving computation of positron binding to methylene chains ($(CH_2)_n$), which have attractive translational symmetry, would be fruitful.

These and other unexplored frontiers in the field of positron annihilation have made my work a pleasure and make it an exciting time to be involved.

References

[1] Dean T. Alle, Michael J. Brennan, and Stephen J. Buckman. Low energy total electron scattering cross section and electron affinity for no. *Journal of Physics B*, 29:L277–L282, 1996.

[2] C. D. Anderson. The apparent existence of easily deflectable positives. *Science*, 76:238–239, 1932.

[3] C. D. Anderson. The positive electron. *Physical Review*, 43:491–494, 1933.

[4] L. D. Barnes, S. J. Gilbert, and C. M. Surko. Energy-resolved positron annihilation for molecules. *Physical Review A*, 67:032706, 2003.

[5] B. M. Bode and M. S. Gordon. Macmolplot. *Journal of Molecular Graphics and Modelling*, 13:133–138, 1998.

[6] K. F. Canter. Slow positrons in rare gases. *Contemporary Physics*, 13:457–478, 1972.

[7] E. P. da Silva, J. S. E. Germano, , J. L. S. Lino, C. R. C. De Carvalho, A. P. P. Natalense, and M. A. P. Lima. Annihilation dynamics of positrons in molecular environments. *Nuclear Instrument and Methods in Physics Research B*, 143:140–148, 1998.

[8] E. P. da Silva, J. S. E. Germano, and M. A. P. Lima. Annihilation dynamics of positrons in molecular environments: theoretical study of low-energy positron-c_2h_4 scattering. *Physical Review Letters*, 77:1028–31, 1996.

[9] Euclimar P. da Silva, José S. E. Germano, and Marco A. P. Lima. Z_{eff} according to the schwinger multichannel method in positron scattering. *Physical Review A*, 49:R1527–R1530, 1994.

[10] S. A. Davies, M. Charlton, and T. C. Griffith. Free positron annihilation under the influence of a static electric field. *Journal of Physics B*, 22:327–40, 1989.

[11] M. Deutsch. Evidence for the formation of positronium in gases. *Physical Review*, 82:455–456, 1951.

[12] M. Deutsch. Three-quantum decay of positronium. *Physical Review*, 83:866–867, 1951.

[13] P. A. M. Dirac. On the annihilation of electrons and protons. *Proceedings of the Cambridge Philosophical Society*, 26:361–375, 1930.

[14] P. A. M. Dirac. A theory of electrons and protons. *Proceedings of the Royal Society of London*, 126:360–365, 1930.

[15] Màrcio T. do N. Varella, Claudia R. C. de Carvalho, and Marco A. P. Lima. The schwinger multichannel method (smc) calculations for z_{eff} were off by a factor of z. *Nuclear Instruments and Methods in Physics Research B*, 192:225–237, 2002.

[16] V. A. Dzuba, V. V. Flambaum, G. F. Gribakin, and W. A. King. Bound states of positrons and neutral atoms. *Physical Review A*, 52:4541–4546, 1995.

[17] V. A. Dzuba, V. V. Flambaum, G. F. Gribakin, and W. A. King. Many-body calculations of positron scattering and annihilation from noble gas atoms. *Journal of Physics B*, 29:3151–3175, 1996.

[18] H. Feshbach. Unified theory of nuclear reactions. *Annals of Physics*, 5:357–390, 1958.

[19] H. Feshbach. Unified theory of nuclear reactions ii. *Annals of Physics*, 19:287–313, 1962.

[20] P. A. Fraser. *Advances in Atomic and Molecular Physics*, 4:63, 1968.

[21] J. S. E. Germano and M. A. P. Lima. Schwinger mulktichannel method for positron-molecule scattering. *Physical Review A*, 47(5A):3976 – 82, 1993.

[22] D. W. Gidley, A. Rich, E. Sweetman, and D. West. New precision measurements of the decay rates of singlet and triplet positronium. *Physical Review Letters*, 49:525–528, 1982.

[23] S. J. Gilbert, L. D. Barnes, J. P. Sullivan, and C. M. Surko. Vibrational-resonance enhancement of positron annihilation in molecules. *Physical Review Letters*, 88:043201, 2002.

[24] V. I. Goldanskii and Y. S. Sayasov. On the resonance annihlation of positrons in collision with neutral atoms or molecules. *Physics Letters*, 13:300–301, 1964.

[25] R. G. Greaves and C. M. Surko. Solid neon moderator for positron trapping experiments. *Canadian Journal of Physics*, 51:445–8, 1996.

[26] R. G. Greaves and C. M. Surko. Inward transport and compression of a positron plasma by a rotating electric field. *Physical Review Letters*, 85:1883–1886, 2000.

[27] G. Gribakin. Theory of positron annihilation on molecules. In C. M. Surko and F. A. Gianturco, editors, *New Directions in Antimatter Physics and Chemeistry*, pages 413–435. Kluwer Academic Publishers, 2001.

[28] G. F. Gribakin. Mechanisms of positron annihilation on molecules. *Physical Review A*, A61:022720, 2000.

[29] G. F. Gribakin. Enhancement of positron annihilation on molecules due to vibrational feshbach resonances. *Nuclear Instruments and Methods in Physics Research B*, 192:26–39, 2002.

[30] G. F. Gribakin and P. M. W. Gill. The role of vibrational doorway states in positron annihilation with large molecules. *Nuclear Instruments and Methods in Physics Research B*, 221:30–35, 2004.

[31] G. F. Gribakin and J. Ludlow. Enhancement of positron-atom annihilation near the positronium threshold. *Physical Review Letters*, 88:163202/1–4, 2002.

[32] David J. Griffiths. *Introduction to Quantum Mechanics*. Prentice Hall, Upper Saddle River, New Jersey, 1994.

[33] J. B. Hasted and D. Mathur. Electron-molecule resonances. In L. G. Christophorou, editor, *Electron-Molecule interactions and their applications*, volume 1, pages 403–475. Academic, London, UK, 1983.

[34] G. R. Heyland, M. Charlton, T. C. Griffith, and G. Clark. The temperature dependence of free positron lifetimes and positronium fractions in gaseous co_2 and sf_6. *Chemical Physics*, 95:157–163, 1985.

[35] G. R. Heyland, M. Charlton, T. C. Griffith, and G. L. Wright. Positron lifetime spectra for gases. *Canadian Journal of Physics*, 60:503, 1982.

[36] J. W. Humberston. The scattering of low energy positrons by helium. *Journal of Physics B*, 6:L305–8, 1973.

[37] Akinori Igarashi, Mineo Kimura, and Isao Shimamura. Unified treatment of positron annihilation and positronium formation. *Physical Review Letters*, 89:123201, 2002.

[38] K. Iwata, R. G. Greaves, and C. M. Surko. Annihilation rates of positrons on aromatic molecules. *Hyperfine Interactions*, 89:271–8, 1994.

[39] Koji Iwata. *Positron Annihilation on Atoms and Molecules.* PhD thesis, University of California, San Diego, 1997.

[40] Koji Iwata. *Positron Annihilation on Atoms and Molecules.* PhD thesis, University of California, San Diego, 1997.

[41] Koji Iwata, R. G. Greaves, T. J. Murphy, M. D. Tinkle, and C. M. Surko. Measurements of positron-annihilation rates on molecules. *Physical Review A*, 51:473–87, 1995.

[42] Koji Iwata, R. G. Greaves, and C. M. Surko. γ-ray annihilation spectra from positron-molecule interactions. *Physical Review A*, 55:3586–3604, 1997.

[43] Koji Iwata, R. G. Greaves, and C. M. Surko. γ-ray annihilation spectra from positron-molecule interactions. *Physical Review A*, 55:3586–3604, 1997.

[44] Koji Iwata, G. F. Gribakin, R. G. Greaves, C. Kurz, and C. M. Surko. Positron annihilation on large molecules. *Physical Review A*, A61:022719, 2000.

[45] Koji Iwata, G. F. Gribakin, R. G. Greaves, and C. M. Surko. Positron annihilation with inner-shell electrons in noble gas atoms. *Physical Review Letters*, 79:39–42, 1997.

[46] Koji Iwata, G. F. Gribakin, R. G. Greaves, and C. M. Surko. Positron annihilation on large molecules. *Physical Review A*, A61:022719, 2000.

[47] J. H. Kin, G. Yang, S. Yang, and A. H. Weiss. A pulsed positronium beam. *Materials Science Forum*, 105-110:1915–18, 1992.

[48] R. Krause-Rehberg, F. Borner, and F. Redmann. Positron beam studies of defects in semiconductors. *Material Science Forum*, 363-365:404–408, 2001.

[49] C. Kurz, R. G. Greaves, and C. M. Surko. Temperature dependence of positron annihilation rates in noble gases. *Physical Review Letters*, 77:2929–32, 1996.

[50] G. Laricchia and C. Wilkin. Semiempirical approach to positron annihilation in molecules. *Physical Review Letters*, 79:2241–2244, 1997.

[51] G. Laricchia and C. Wilkin. On the annihilation of positrons in binary encounters with molecules. *Nuclear Instruments and Methods in Physics Research, Section B*, 143:135–139, 1998.

[52] M. Leventhal, A. Passner, and C. M. Surko. Positron-molecule bound states and positive ion production. In R. J. Drachman, editor, *Annihilation in Gases and Galaxies*, pages 272–283. National Aeronautics and Space Administration, Washington, DC, 1990.

[53] Marco A. P. Lima, Luiz M. Brescansin, Antônion J. R. da Silva, Carl Winstead, and Vincent McKoy. Applications of the schwinger multichannel method to electron-molecule collisions. *Physical Review A*, 41:327–332, 1990.

[54] Jorge L. S. Lino, José S. E. Germano, Euclimar P. da Silva, and Marco A. P. Lima. Elastic cross sections and annihilation parameter for e^+-h_2 scattering using the schwinger multichannel method. *Physical Review A*, 58:3502–3506, 1998.

[55] John Ludlow. *Many-body theory of positron-atom interactions*. PhD thesis, Queen's Univerisity, Belfast, U. K., 2003.

[56] A. C. Mao and D. A. L. Paul. Positron annihilation in methane. *Canadian Journal of Physics*, 55:235–9, 1977.

[57] J. P. Marler, L. D. Barnes, S. J. Gilbert, J. P. Sullivan, J. A. Young, and C. M. Surko. Experimental studies of the interaction of low-energy positrons with atoms and molecules. *Nuclear Instruments and Methods in Physics Research B*, 221:84, 2004.

[58] R. P. McEachran, A. G. Ryman, and A. D. Stauffer. Positron scattering from argon. *Journal of Physics B*, 12:1031–31, 1979.

[59] J. D. McNutt, V. B. Summerour, A. D. Ray, and P. H. Huang. Complex dependence of the positron annihilation rate on methane gas density and temperature. *Journal of Chemical Physics*, 62:1777, 1975.

[60] David Mehl, A. R. Koymen, Kjeld O. Jensen, Fred Gotwald, and Alex Weiss. Sensitivity of positron-annihilation-induced auger-electron spectroscopy to the top surface layer. *Physical Review B*, 41:799–802, 1990.

[61] A. P. Mills, Jr. Positronium-molecule formation. bose-einstein condensation and stimulated annihilation. *Nuclear Instruments and Methods in Physics Research B*, 197:107–116, 2002.

[62] A. P. Mills, Jr. and E. M. Gullikson. Solid neon moderator for producing slow positrons. *Applied Physics Letters*, 49:1121–3, 1986.

[63] J. Mitroy, M. W. J. Bromley, and G. Ryzhikh. Positron binding to a model alkali atom. *Journal of Physics B*, 32:2203, 1999.

[64] J. Mitroy, M W J Bromley, and G G Ryzhikh. Positron and positronium binding to atoms. *Journal of Physics B*, 35:R81, 2002.

[65] J. Mitroy and I. A. Ivanov. Semiempirical model of positron scattering and annihilation. *Physical Review A*, 65:042705, 2002.

[66] T. J. Murphy and C. M. Surko. Annihilation of positrons on organic molecules. *Physical Review Letters*, 67:2954–7, 1991.

[67] T. Nishimura and F.A. Gianturco. Vibrational excitation of methane by positron impact: Computed quantum dynamics and sensitivty tests. *Physical Review A*, 65:062703(11), 2002.

[68] T. Nishimura and F.A. Gianturco. Virtual-state formation in positron scattering from vibrating molecules; a gateway to annihilation enhancement. *Physical Review Letters*, 90:183201, 2003.

[69] A. Occhigrossi and F. A. Gianturco. Low-energy positron dynamics in small hydrocarbon gases. *Journal of Physics B*, 36:1383–1395, 2003.

[70] D. A. L. Paul and L. Saint-Pierre. Rapid annihilation of positrons in polyatomic gases. *Physical Review Letters*, 11:493, 1963.

[71] R. Ramaty, M. Leventhal, K. W. Chan, and R. E. Lingenfelter. On the origin of variable 511 kev line emission from the galactic center region. *Astrophysical Journal, Letters*, 392:L63–6, 1992.

[72] G. G. Ryzhikh and J. Mitroy. Positronic lithium, an electronically stable li-e^+ ground state. *Physical Review Letters*, 79:4124–4126, 1997.

[73] M. W. Schmidt, K. K Baldridge, J. A. Boatz, S. T. Elbert, M. S. Gordon, J. H. Jensen, S. Koseki, N. Matsunaga, K. A. Nguyen, S. J. Su, T. L. Windus, M. Dupuis, and J. A. Montgomery, Jr. General atomic and molecular electronic structure system. *Journal of Compuational Chemistry*, 14:1347–1363, 1993.

[74] A. Schramm, I. I. Fabrikant, J. M. Weber, E. Leber, M. W. Ruf, and H. Hotop. Vibrational resonance and threshold effects in inelastic electron collisions with methyl iodide molecules. *Journal of Physics B*, 32:2153–2171, 1999.

[75] J. W. Shearer and M. Deutsch. The lifetime of positronium in matter. *Physical Review*, 76:462, 1949.

[76] T. Shimanouchi. *Tables of Molecular Vibrational Frequencies Consolidated I.* National Bureau of Standards, Washington, 1972.

[77] P. M. Smith and D. A. L. Paul. Positron annihilation in methane gas. *Canadian Journal of Physics*, 48:2984–2990, 1970.

[78] J. P. Sullivan, S. J. Gilbert, J. P. Marler, R. G. Greaves, S. J. Buckman, and C. M. Surko. Positron scattering from atoms and molecules using a magnetized beam. *Physical Review A*, 66:042708, 2002.

[79] J. N. Sun, Y. F. Hu, W. E. Frieze, and D. W. Gidley. Characterizing porosity in nanoporous thin films using positron annihilation lifetime spectroscopy. *Radiation Physics and Chemistry*, 68:345, 2003.

[80] C. M. Surko, M. Leventhal, W. S. Crane, A. Passner, and F. Wysocki. Use of positrons to study transport in tokamak plasmas. *Review of Scientific Instruments*, 57:1862–7, 1986.

[81] C. M. Surko, A. Passner, M. Leventhal, and F. J. Wysocki. Bound states of positrons and large molecules. *Physical Review Letters*, 61:1831–4, 1988.

[82] Masanori Tachikawa, Robert J. Buenker, and Mineo Kimura. Bound states of positron with urea and acteone molecules using configuration interaction *ab initio* molecular orbital approach. *Journal of Chemical Physics*, 119:5005–5009, 2003.

[83] S. Tang, M. D. Tinkle, R. G. Greaves, and C. M. Surko. Annihilation gamma-ray spectra from positron-molecule interactions. *Physical Review Letters*, 68:3793–6, 1992.

[84] A. Weiss, R. Mayer, M. Jibaly, C. Lei, D. Mehl, and K. G. Lynn. Auger-electron emission resulting from the annihilation of core electrons with low-energy positrons. *Physical Review Letters*, 61:2245–8, 1988.

[85] E. Bright Jr. Wilson, J. C. Decius, and Paul C. Cross. *Molecular Vibrations*. Dover Publications, Inc., New York, 1980.

[86] G. L. Wright, M. Charlton, T. C. Griffith, and G. R. Heyland. The annihilation of positrons and positronium formation in gaseous Kr and Xe. *Journal of Physics B*, 18:4327–4347, 1985.

[87] Ta-You Wu and Takashi Okumura. *Quantum Theory of Scattering*. Prentice-Hall, Inc., Englewood Cliffs, N. J., 1962.